NEW CHLORIDE AND PROTON LIGHT-DRIVEN PUMPS: FUNCTIONAL CHARACTERIZATION AND CRYSTALLIZATION

From the Faculty of Georesources and Materials Engineering of the
RWTH Aachen University

Submitted by

Dmytro Volkov MSc

from Kiev, Ukraine

in respect of the academic degree of

Doctor of Natural Sciences

approved thesis

Advisors: **Prof. Dr. Valentin Gordeliy**
Prof. Dr. Georg Büldt
Prof. Dr. Martin Engelhard
Prof. Dr. Ernst Bamberg

Date of the oral examination: 24.11.2017

This thesis is available in electronic format on the university library's website

Table of contents

NEW CHLORIDE AND PROTON LIGHT-DRIVEN PUMPS: FUNCTIONAL CHARACTERIZATION AND CRYSTALLIZATION 1

Dmytro Volkov MSc 1

Table of contents 3

List of Abbreviations 5

Introduction 7

Main results 10

1. Literature overview 11

1.1. Membrane proteins study 11

1.2. Microbial rhodopsins early study 12

1.3. Optogenetic applications of rhodopsins 14

1.3.1. Microbial channel rhodopsins in neuroscience 15

1.3.2. Microbial pumping rhodopsins 18

1.4. Structural insights 19

1.4.1. *H.salinarium* bacteriorhodopsin bR 19

1.4.2. Anion pumps (HsHR, NpHR) 23

1.4.3. *K.eikastus* KR2 sodium pump 29

1.4.4. Light-gated channels structures 31

1.4.5. Active centre motifs of rhodopsin pumps 34

1.5. Conclusion 35

2. Materials and methods 37

2.1. Materials 37

2.1.1. Organisms 37

2.1.2. Vectors 37

2.1.3. Oligonucleotides used in this work 40

2.1.4. Chemicals 40

2.2. Methods 40

2.2.1. Molecular biology methods 40

2.2.2. *E.coli* culture and overexpression 43

2.2.3. LEXSY culture and overexpression 45

2.2.4. Biochemical methods 45

2.2.5. Protein purification 47
2.2.6. Characterization 51
3. Results and discussion 55
3.1. Protein selection 55
3.1.1. RNA secondary structure optimisation 56
3.2. Polarella glacialis PGr1 rhodopsin (UNP F6K461) 58
3.2.1. Expression and purification of PGr1 58
3.2.2. Functional tests and characterization of PGr1 65
3.2.3. Crystallisation of PGr1 71
3.3. Phycisphaera mikurensis PMr1 and PMr2 rhodopsins (UNP I0IBH0 and I0IGJ9) 74
3.3.1. Expression and purification of PMr1 and PMr2 74
3.3.2. Functional test of PMr1 and PMr2 81
3.3.3. Crystallisation of PMr2 88
References 90
Appendix 98
Acknowledgements 102

List of Abbreviations

6AHA	amino hexanoic acid
A8-35	amphipol A8-35
AcP	acetyl phosphate, potassium salt
AIM	auto induction media
APS	ammonium persulfate
bR	bacteriorhodopsin
Brij	nonionic polyoxyethylene surfactant
BSA	bovine serum albumin
CMC	critical micelle concentration
DDM	n-Dodecyl-β-D-Maltopyranoside
DM	n-Decyl-β-D-Maltopyranoside
DMSO	dimethyl sulfoxide
DTT	dithiothreitol
EDTA	ethylenediaminetetraacetic acid
Fos	n-Dodecylphosphocholine
GPCR	G protein coupled receptor
IPTG	Isopropyl β-D-1-thiogalactopyranoside
MTAB	myristyltrimethylammonium bromide
NLS	sodium lauroyl sarcosinate
OG	octyl-β-glucopyranoside
PCR	polymerase chain reaction
PEG	polyethylene glycol
PEP	phosphoenol-pyruvic-acid, mono-potassium salt
RNasin	RNase inhibitor
SDS	sodium dodecyl sulphate
SDS PAGE	sodium dodecyl sulphate polyacrylamide gel (electrophoresis)
TEMED	tetramethylethylenediamine
WB	Western blot
OD_{600}	Optical density at 600 nm wavelength
GPCR	G protein-coupled receptor
NMR	nuclear magnetic resonance
MW	molecular weight
CCCP	Carbonyl cyanide m-chlorophenyl hydrazone
TPP	Tetraphenylphosphonium bromide
MO	monoolein, $C_{21}H_{40}O_4$, 2,3-Dihydroxypropyl oleate
TM	transmembrane
UNP	UniProt protein database ID

Introduction

The discovery of microorganisms by Antonie van Leeuwenhoek and the observations of plant "cells" by Robert Hooke led scientists to understanding that life is much more complicated than it was thought before and the investigations of cells' mechanisms proceed till these days. The significant methodology improvements since that time allowed scientists to make lots of discoveries and shifted the cells' mechanisms investigations from microscopic (10^{-6} m) to angstrom (10^{-10} m) scale.

In eighteenth century the distinct class of biological molecules was recognized. In the very beginning they were erroneously believed to consist of one type of big molecule but latter their polypeptide structure was found. And the logical question of how few dozens of "building bricks" can lead to such diversity in functions appeared. The scientists figured out that the structure of the protein being built of these "bricks" is the key to "understanding" the protein. Since then the long journey of proteins characterization studies begun and proceeds till nowadays.

The proteins can be divided into two major types in terms of cell localization: membrane proteins and non-membrane proteins. Membrane proteins typically constitute about third of all proteins that cell expresses in a given moment [1] and play important role in cell's life. So, the membrane protein receptors mediate information flow from the environment into the cell thus modulating the cell mechanisms in response to environmental changes. Another type of membrane proteins - transport proteins - allow cells to communicate by means of signaling molecules and receive necessary nutrients from the environment.

The cell is the smallest generally accepted unit of life. But cells consist of non-living molecules. The way these molecules organize into the living cell (allowing the emergence of life in general and human consciousness in particular) is yet not clear. In search for an answer to this question along with more practical efforts in finding the efficient drugs and methods to cure various diseases, scientists came to the anatomical studies and discovered the nervous system the core of which is the brain. The brain is an extremely complicated structure and even now with modern level of technologies and things that were only a hundred years (only two generations) ago believed to be impossible (like the controlled flying), we still don't know much about it.

The vast studies led to a new method being named the optogenetics. This new approach utilizes the light to control the cells in a living tissue. The key elements of this method are the light sensitive proteins that work as a "function switches" under control of scientists. And the

majority of such "switches" belongs to the rhodopsins. Unlike direct neuron excitation methods via the electrodes, the optogenetic approach is less invasive. The rhodopsin gene is injected into the cell allowing latter to express the rhodopsin and embed it into the membrane in the same way as its endogenous proteins. After injection cell becomes light-sensitive and can be manipulated just with the visible light impulses.

The rhodopsins themselves are known already for a while and estimated to consist of two major types: microbial rhodopsins (type I) and mammalian rhodopsins (type II). Despite the common name (rhodopsin, derived from Greek for "rose" and "sight"), mammalian rhodopsins significantly differ from those in microorganisms - they belong to a large class of proteins called G protein-coupled receptors (GPCRs), while their microbial analogues aren't. Due to the differences in the mechanisms of function, microbial rhodopsins are simpler thus are more convenient to use in the neuroscience.

The optogenetics uses rhodopsins to investigate the cells' mechanisms and their interaction within the tissue. But each protein has its own characteristics and there isn't any ideal "instrument" for all the applications – each experiment requires for the specific "tools" (rhodopsins) with different properties for optogenetic investigations. So, one experiment requires fast quenching of the neuronal cells signaling thus having no particular requirements to a long-term behavior of the protein, while in the other experiment investigator may use rhodopsins with slow kinetics, but requires the moderately high steady-state signal during the long-term illumination. The large diversity of possible optogenetic applications requires the expansion of a "tool-kit", which in turn leads to a characterization of new rhodopsins – the purpose this work.

The most abundantly used rhodopsins in optogenetics are channels (ChRs, derived from channel rhodopsins). These channels provide a light-modulated passive transport of ions along the gradient, which leads to a neuron membrane depolarization. Since the characterization of the two ChR1 and ChR2 from *Chlamydomonas reinhardtii* in the beginning of the century [2][3], the vast list of mutated variants of these proteins emerged (along with discovery of others, like VChR from *Volvox carteri*), improving the characteristics of these channels in terms of neuroscience.

The other proteins type being applied is microbial pumping rhodopsins (the sensory rhodopsins despite being reported to be successfully applied[4] need further characterization). Since the discovery of proton pump bacteriorhodosin and anion pumping halorhodopsin from *Halobacterium halobium (Halobacterium salinarum)* in early 70th, microbial pumps were

believed not to be able to pump cations other than proton (due to a proposed mechanism of functioning). The recent discovery of KR2 [5]–[7], non-selective sodium pumping rhodopsin from *Krokinobacter eikastus*, demonstrated that type I rhodopsins are able to cover pumping activity of both types of charged molecules. Thus, the microbial pumping rhodopsins now can be divided into 2 major groups: cation pumps and anion pumps. The first includes so called sodium pumps and proton pumps. The optogenetic application of latter is still disputed due to their ability to directly change the pH, while first posses low selectivity/overall poor performance. Thus, halorhodopsin (anion pumping rhodopsins, HRs), despite the debates on their ability to hyperpolarize membrane "far beyond the physiological levels" are the most common rhodopsins that are used for cell membrane repolarization.

Despite being known for forty years, halorhodopsins are much less understood in compare to proton pumps (particularly, bacteriorhodopsin). The structures of few HRs were obtained with high resolution [8]–[10], which made possible to suggest a functioning model and thus modify their properties in a controlled way. Despite that, all the halorhodopsins with known structure available now possess the red-shifted absorption spectra with maxima at 570-590nm. This implies limitations on their use in neuroscience in pair with depolarization tools due to possible interference of the signals.

Although it might seem that microbial rhodopsins are already being well investigated, the new questions and hypothesis arise [8][10]–[13] that concern the base of our knowledge - the proton transport based model of rhodopsins function. Apparently additional studies on rhodopsins needed to clarify whether those intriguing hypothesis are true.

Taking into account the above, the aim of this work was to find and characterize the new rhodopsins that might be useful for optogenetic implications.

Main results

The three genes of non-characterised before rhodopsins were optimised and expressed in *E.coli* expression system. The positive results of expression trials of membrane proteins were obtained for relatively new LEXSY expression system.

The two rhodopsin proteins were characterised from kinetic point of view and the model of unidirectional transitions cycle was proposed to consist of four and five spectrally distinguishable intermediates for PGr1 and PMr2 rhodopsins respectively. The pumping activity of a putative proton-pumping rhodopsin was demonstrated *in vivo*. The functional activity of anion pump with significantly shifted into blue light region (in compare to those were reported) was demonstrated with three methods (spectroscopic, BLM and light induced pH changes by proteoliposomes). The FRET energy transfer demonstrated to occur not only in archaeal rhodopsins, but also in proteorhodpsins.

Along with functional characterisation, the importance of few structural features of novel anion pump was shown, while crystals of proton pump were obtained. The crystallisation trials for both of the two new rhodopsins are still going.

1. Literature overview

1.1. Membrane proteins study

Membrane proteins typically constitute approximately 30% of all proteins that cell expresses in a given moment [1]. This type of proteins play crucial role in cell life. By means of membrane receptors cell can receives information about its environment and modify internal processes in response. Membrane transport proteins provide cell with a route, using which cells communicate to each other and get nutrients.

Due to the role they play, membrane proteins, specifically GPCRs, nuclear receptors and ion channels, constantly attract attention of pharmacy industry [14]. Recent analysis of DrugBank and FDA data for 2007-2010 (US Food and Drug Administration) shows that 44% of all human FDA approved drugs target receptors, 42% of which constitute GPCRs (19% of overall targets). Moreover, stunning 36% of drugs approved by FDA (Food and Drug Administration) target GPCRs [15].

There are two major types of drug design: ligand-based and structure-based. Ligand based drug design relies on knowledge of already discovered and characterized ligands. On the other hand, structure-based methodrequires three dimensional structure of a drug target protein [16]. But in both cases drug design requires deep understanding of target functioning mechanism. In order to pick or create the ligand for a specific protein one have not only to know dynamics of the ligand molecule but also conformational changes that this particular ligand causes in the target protein.

NMR-spectroscopy is one of major techniques for obtaining information about biological molecules. NMR-spectroscopy utilizes intrinsic ability of all isotopes having nonzero spin to absorb and re-emit electromagnetic radiation. To the moment various techniques were developed which significantly extended applicability of NMR for protein 3D structure determination. Nevertheless, high resolution experiments still struggle to overcome restriction by size of protein in question (proteins/fragments up to 100 residues [17]). According to Pfam-A database the average length of eukaryotic protein is 419 residues (306 aa for bacterial ones; hereafter aa corresponds to amino acids). Structural/functional domains average are 185 aa and 188 aa for human and bacterial proteins respectively [18]. This means that only a small fraction of proteins in their native states can be investigated and characterized by NMR methods.

Electron microscopy (EM), as another alternative, was successfully applied to a problem described previously. According to a RCSB PDB statistics the number of structures solved with EM methods was growing exponentially in the past two decades [19]. In the past few years several structures of complexes were resolved with resolution ranging 2.8-4.5 Å with molecular masses greater than 465 kDa. Alberto Bartesaghi at el. (2015) resolved structure of *E.coli* complex β-Gal–PETG with resolution of 2.2 Å [20]. Nevertheless, molecular mass of the complex needed to resolve the structure of β-galactosidase was 465 kDa. This means that molecular mass limitations of EM specimens, even though significantly improved, but isn't overtaken yet.

Crystallography is the third method to resolve protein structure and mechanism. Despite the limitations, such as difficulties in obtaining sufficient amounts of highly purified protein and optimal crystallisation conditions finding, this method allows to get almost atomic resolution structures for a broad range of membrane protein sizes, closing the molecular weight gap between two previously described methods.

In recent years more and more attention is paid to the method being called optogenetics. This relatively new method made a gigantic leap from the start of the new millennium. Being the method of the year 2010 by Nature Methods [21] and one of the biggest breaks through of the decade by Science [22], the optogenetics uses a long time known ability of some microorganisms to use light as a source of energy. But, unlike that in plants, the microbial optical system is simpler is more convenient to use in order to control and investigate nervous activity. The proteins responsible for such a function in microorganisms are called rhodopsin.

1.2. Microbial rhodopsins early study

Microbial rhodopsins are transmembrane proteins possessing the common for GPCRs topology. They consist of 7 transmembrane α-helices (here and after, TMH) and covalently bound to vitamin A derivative chromophore retinal. The chromophore in these proteins absorbs light and isomerises from all-trans to 11-cis conformation (unlike of rhodopsins in vertebrates) and starts a series of conformational changes of whole rhodopsin molecule called photocycle. The first step to this knowledge was done in early 70th while scientists were trying to characterise bacteria *Halobacterium halobium (Halobacterium salinarum)*. Its membrane was found to have specific purple colour due to a retinal and 26 kDa protein in ratio 1:1 [23],[24]. The protein from *H.halobium* later was named bacteriorhodopsin (bR) due to its origin – it was the first known retinal binding light sensitive protein from prokaryotes.

Since its discovery in 1971 and till the end of 70th lots of efforts were applied to characterise bacteriorhodopsin. So, the relative orientation of the protein within a cell membrane was determined to be an inside-out – N-terminus of bR is on the outer side of a cell membrane [25],[26]. In 1975 the first three-dimensional structure (electron microscopy model with 7 Å resolution) was obtained and determined to consist of 7TM helices [27]. In the same period bR's millisecond photocycle with its letter-labelled intermediates was established along with their correlation with proton translocation steps [28], [29],[30].

Most of studies were performed on membrane mixture (vesicles) or *H.salinarum* culture cells. This approach soon misled scientist first to conclusion about two possible roles of bR [31] and a bit later to a statement that there is a second sodium pumping light sensitive protein[32], [33]. Later the situation was clarified and what was first in 70th an additional functionality of bR at the beginning of 80th became a second light driven chloride pump known as halorhodopsin (HR) [34], [35]. Soon after that, two more light sensitive proteins were discovered in *H.salinarum*. Due to their functionality they were called sensory rhodopsins I (sRI) [36], [37] sensory rhodopsins II (sRII) [38].

The end of a previous century became another waypoint in rhodopsins history. The resolution of bR structure was significantly improved during 90th and at the end of a decade reached roughly 1.5 Å [39], providing even more details to bR's functioning models. Along with structural studies new microbial rhodopsins were found. Some were like discovered before, whereas others were of a new class known now as a channel rhodopsins [40], [41], [42]. But due to few obstacles, only 18 years latter these proteins were properly characterised [2], [3].

Due to a rapid growth of gene techniques a new method of direct characterisation of rhodopsins appeared without need of purifying the protein. Gene of protein was expressed in non native host of scientist choice. This allowed to determine the exact voltage dependence of light activated proteins. First it was done for proton pumping rhodopsin, anion pump and relatively soon after that for channel rhodopsins I and II (ChR1 and ChR2). After shoving the ability of ChR2 to depolarise the membrane of *Xenopus* oocytes and some other mammalian cells, scientists started to widen this application of rhodopsin for other cell types (including mouse brain cells slices). This was the beginning of optogenetic [43]. In parallel to the development of optogenetics, total genome sequencing projects in combination with permanently improved computational methods influenced the optogenetic development process. Scientists now can choose among the verity of tools (rhodopsins) the most appropriate ones for each application.

1.3. Optogenetic applications of rhodopsins

Rhodopsins are light sensitive proteins. They can be divided into two superfamilies: opsins of type I (microbial) and type II (animal). It's hard to exaggerate their role in nature. For humans they are main components of photoreceptor cells responsible for visual phototransduction. As for unicellular organisms, rhodopsins responsible for a variety of functions, such as maintenance of osmotic pressure level, phototaxis, etc.

In terms of optogenetics greater role play Type I microbial rhodopsins. Unlike those from animals, microbial represent self-sufficient system that perform function without the need of multicomponent cascades (like those for restoration of its cofactor retinal after each photocycle). In addition, rhodopsins of vertebrate are GPCRs, whereas microbial rhodopsins aren't – they can produce photoresponse by themselves by changing the concentration of ions. These concentration changes may lead to the membrane potential changes and, when being expressed in neuronal cells, to the "firing up" or quenching currents in neuronal circuits.

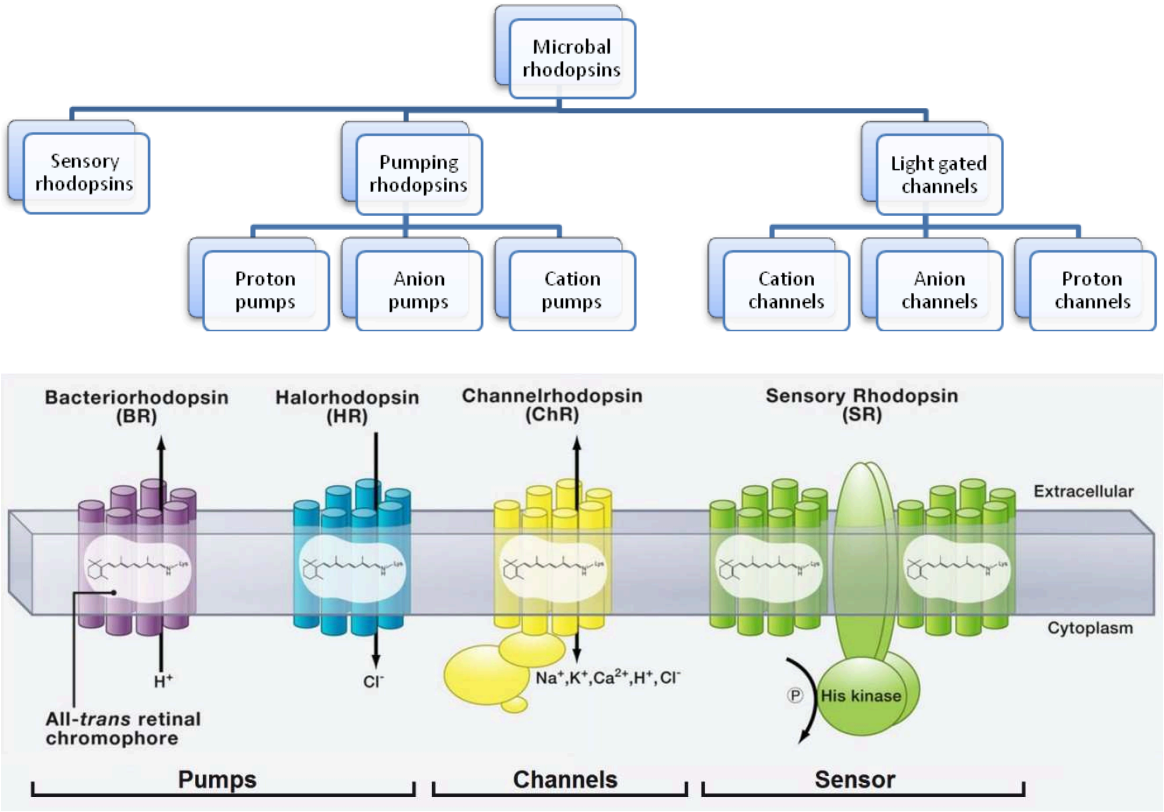


Figure 1.1 Microbial rhodopsins diversity tree (**top**) and schematic representation of functionality (**bottom**, adopted from [44]). Pumps hyperpolarize membrane while channels conduct cations/anions both ways along electrochemical gradient.

By the functioning mechanism microbial opsins can be divided into three major groups (see Figure 1.1).

Even though the study of the sensory rhodopsins proceeds, this class of microbial rhodopsins didn't became widely spread among optogenetic. The resent study on cyclase rhodopsins (being named "CyclOps" = "cyclase opsins") demonstrated them to enable rapid light-triggered cGMP increase in heterogeneous cells[4]. But not much statistics available to the moment for these proteins to be used in neuroscience. In opposite, pumps and channels are permanently modified and applied. The cation/anion pumps and channels are more common rather than proton pumps. Nevertheless, proton pumps are also of persistent interest for scientists.

The optogenetic palette being used by scientists contains tools of four categories: fast excitation, fast inhibition, bistable modulation, control of intracellular biochemical signalling.

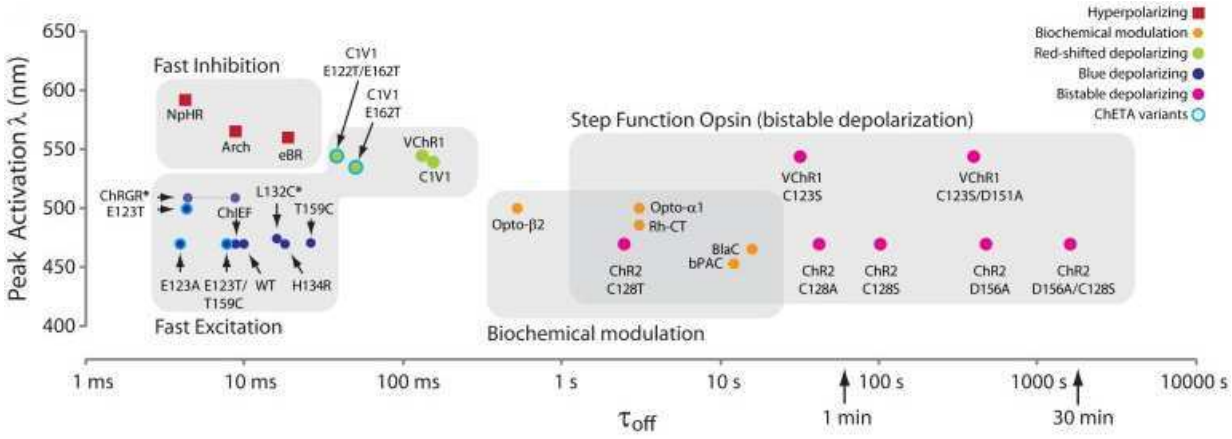


Figure 1.2 Four categories of tools along with their spectral and kinetic characteristics (adopted from [45]).

Even though there's a correlation between rhodopsins functions and application categories (pumping rhodopsins utilised in tests where the fast inhibition needed) we'll proceed with characterisation according to rhodopsin type described before.

1.3.1. Microbial channel rhodopsins in neuroscience

Among all microbial rhodopsins the most attention of optogenetic society was paid to channels, specifically cation channels. Recently discovered ChR1 and ChR2 [2][3] from *Chlamydomonas reinhardtii* since the moment of discovery were used to depolarize numbers of mammalian tissues. The variety of functional mutants and chimeras were produced despite the lack of structural information. The pure ChR2 structure is currently available with 6 Å resolution, providing general information on protein helices topology but not details on a cofactor cavity[46]. The structure for chimeric C1C2 cation channel protein with higher

resolution (2.3 Å; C1C2 chimeric protein based on truncated ChR1 proton channel with TM6 and TM7 swapped to those from ChR2 cation channel) is also obtained [47]. C1C2 demonstrates cation channel functionality, but the amount of modifications done to the base protein can't be neglected in relation to the structure. Recent work have showed that C1C2 chimera and native ChR2 undergo distinctive light-induced structural changes during their photocycles [48].

Nevertheless, light-gated ion channels and their mutants/chimeras even without precise structural information (and sometimes even without ion translocation characterisation of the protein [49]) found their way to neuroscience.

This difference in "necessary" amount of rhodopsins characteristics for each optogenetic lab makes it difficult to directly compare all the instruments found and being used. Apparently, since the whole method is relatively young more time is needed to establish the list of key optogenetic features requested from its instruments and to set a limited classification list of purposes for which each protein might be applicable. But first attempts in the information structuring were made [50], [51].

Channel	**Spectral peak, peak/steady state**	**Desensitization level, $I_{steady\text{-}state}/I_{peak}$**	**Light sensitivity, peak/steady state, EC_{50}, $mW \times mm^{-2}$**	**Opening rate/ closing rate@19.8 $mW \times mm^{-2}$ intensity**
ChR2	470 nm/450 nm	~0.22 @ 470 nm	~1.10/~1.05	~1.21/~13.5
VChR1	570 nm/550 nm	~0.48 @ 570 nm	–	~2.8 @15$mW \times mm^{-2}$ />90ms
ChR2 H134R	450 nm/450 nm	~0.39 @ 470 nm	~1.07/~0.98	~1.92/~17.9
ChETA (ChR2 E123T)	490 nm/–	~0.24 @ 470 nm	~5.02/~0.62	~0.86/7.9-8.5
ChD	450 nm/450 nm	~0.31 @ 470 nm	~3.23/~1.02	~1.49/~7.82
ChEF (ChR1 and ChR2 chimera)	470 nm/490 nm	~0.70 @ 470 nm	~0.72/~0.46	~1.56/~24.9
ChIEF (ChEF I170V)	450 nm/450 nm	~0.80 @ 470 nm	~1.65/~1.38	~1.62/~12.0

Table 1.1 List of few directly compared light-gated channels and their modifications [50].

Below is the list of kinetic characteristics of most abundant in optogenetics opsins [50],[45]:

- ChR2 – **peak 470 nm, τ_{off} ~10 ms**; high desensitisation level (~80% current reduction under physiological pH), aggregates at high expression rates in cells, the conductance 50-250fS;

- ChR2 H134R – **peak 470 nm, τ_{off} 18 ms;** (in compare to ChR2) reduced desensitisation, sensitivity increase, slower channel closing; has no advantages over ChEF/ChIEF;
- ChR1 has low conductance at pH close to physiological (pH 7)
- VChR2 is in many ways close to ChR2 but has slower kinetics and thus no obvious advantages over ChR2
- ChR2 C128X (X-T/A/S), ChR2 D156A – (in comparison to ChR2) higher sensitivity, 2-100 times slower kinetics, lower photocurrent; τ_{off} might be reduced with orange light; fits for prolonged depolarisation experiments
- ChETA (ChR2 E123T) – **peak 490 nm, τ_{off} 8 ms;** (in comparison to ChR2) faster kinetics; lower photocurrent amplitude; high desensitisation level; lower light sensitivity;
- VChR1 – **peak 545 nm, τ_{off} 133 ms;** red-shifted spectral response (but strongly excited ~400 nm);slow kinetics; incomplete recovery after desensitisation; in compare to VChR1 the mutant VChR1 E123T seems to have improved kinetics;
- ChEF (ChR1 and ChR2 chimera) and ChIEF (ChEF I170V) – **ChIEF peak 450 nm, τ_{off}~10 ms;** (in comparison to ChR2) have increased steady-state phase response; comparable kinetics (ChIEF is faster than ChEF); ChIEF has reduced light sensitivity; incomplete recovery after desensitisation (might be improved with 570 nm illumination); both are better in trafficking to membrane
- ChD (ChR1 and ChR2 chimera) – has comparable to ChETA kinetics but better membrane trafficking;
- ChR2 E123A – **peak 470 nm, τ_{off} 4 ms;**
- ChR2 T159C – **peak 470 nm, τ_{off} 26 ms;**
- C1V1 (ChR1 and VChR1 chimera) – **peak 540 nm, τ_{off} 156 ms;**
- C1V1 E162T – **peak 530 nm, τ_{off} 58 ms.**

Till recently, optogenetics predominantly used cation channels and chloride/proton pumps for reversible optogenetic inhibition. But the high-resolution structure of chloride channel C1C2 made it possible to construct a series of structure based mutants with improved properties (C1C2 (ChR1+ChR2 chimera), iC1C2 (chloride channel, 9x mutant of C1C2) and SwiChRs (iC1C2 derivative) [52], iC++ (10× mutant of C1C2) [53]) and to test them in living tissue. These tests

demonstrated a better inhibitory performance of iC++ chloride channel on acute slices of pyramidal cells in compare to eNpHR3.0 construct (chloride pumping rhodopsin), while behaviour modifying tests in freely moving animals demonstrated equity of rhodopsins tested (iC++ vs. eNpHR3.0 vs. eArch3.0) [53].

The recent studies revealed two more cation channels named Chrimson (CnChR1 from the *Chlamydomonas noctigama*, NCBI KF992060) and Chronsos (CnChR1 from the *Stigeoclonium helveticum*, NCBI KF992040). These two proteins with absorption peaks at ~600 and 500nm (for Chrimson and Chronos respectively) and fast kinetics of the Chronos were successfully applied in experiments on independent excitation of neurons without any detectable cross-talk among them [49].

Another unique type of channel rhodopsins was described in 2016. Unlike previously reported natural variants of ChRs, these light gated channels permit anions and were used to repolarize the cell membrane [54]. The GtACR1 and GtACR2 (*Guillardia theta* anion channel rhodopsins 1 and 2) selective permeability was demonstrated along with ion permeability sequence to be established $NO3^- > I^- > Br^- > Cl^- > F^- > SO4_2^-$ (where $SO4_2^-$ corresponds to zero permeability) The amplitudes of both anion channels' photocurrents was similar, but the kinetics of GtACR2 was faster than that of GtACR1.

1.3.2. Microbial pumping rhodopsins

Proton pumping rhodopsins are known for more than four decades. These rhodopsins were believed to be outward proton pumps that make H^+ gradient utilized for synthesis of ATP in halophilic bacteria. Recent studies revealed new pumping rhodopsins possessing the feature that long time was believed impossible to exist – inward proton pumping (PoXeR from *Parvularcula oceani* [55]) and sodium pumping (KR2 from *Krokinobacter eikastus* [56], [57]).

Even though the number of known pumps is by far greater than that of channels, only small number was utilized in living cells and tissue tests.

Pump name	Type	Peak λ, nm	Off kinetics, ms
eNpHR3.0	Chloride pump	578 (589 [58])	4.2
eArch3.0/eArchT3.0 /eMac3.0	Proton pumps	552[59]/566(~570 [60])/470-500[58]	~9/-
eBR	Proton pump	540	19

Table 1.2 The list of most abundantly used ion pumping rhodopsins constructs in neuroscience.

In first tissue tests the anion pumping rhodopsins HR from *H.salinarium* demonstrated excessive desensitisation while *N.pharaonis* NpHR gave rise to hyperpolarising currents. But only recently the inhibition tool properties of NpHR were proved on the intact mammals. Next generation of this anion pump was named NpHR2.0 and was mainly called to overcome poor membrane trafficking of native NpHR by addition of ER motif from Kir2.1 potassium channel. Further modifications leaded to addition to rhodopsin version 2.0 of neurite trafficking sequence from the Kir2.1. The version NpHR3.0 has even more improved photocurrents and thus increased sensitivity of cells to the light (light with wavelength up to 680 nm might be used to drive inhibition).

Approximately at the same time the robust efficacy of proton pumps Mac, Arch and eBR was shown. But the long-term application consequences on mammalian neurons of proton gradient producing optogenetic tools is still unclear [45].

Most scientists' scepticism concerning the use of anion pumping opsins in mammalian tissues is connected with main difference between channels and pumps – the ion conductance mechanism. Firs, pumps (unlike channels) perform ion gradient production during continuous illumination, while the channels being demonstrated to stay opened after irradiance for up to 30 minutes. This pushes scientists to decrease light intensity which in response requires to improve membrane trafficking of opsins in order to maintain the same level of photocurrents [45]. Another argument is pumps' independency of ion gradients, that might lead to the cell membrane hyperpolarisation far beyond the physiological levels [53].

1.4. Structural insights

1.4.1. *H.salinarium* bacteriorhodopsin bR

Among all rhodopsins bacteriorhodopsin from *H.salinarium* (hereafter bR) is the most studied and often used as a template for comparison of not only novel proton pump structures but all microbial rhodopsins. Its 1.55 Å X-ray structure is one of the most resolved membrane protein structures [39]. Thus it's better to start the rhodopsins structure analysis from bR description.

The proton pump bR is a relatively small (26 kDa) membrane protein consisting of opsin part and chromophore. The opsin is composed of 7TMH, short interhelical loops and extramembrane N- and C-termini (extra- and intracellular respectively). The chromophore retinal – (2*E*,4*E*,6*E*,8*E*)-3,7-Dimethyl-9-(2,6,6-trimethylcyclohexen-1-yl)nona-2,4,6,8-tetraenal – is

bound via Schiff-base to conservative amino acid Lys216. The B-C interhelical loop forms an anti-parallel β-sheet, stabilised with hydrogen bonds.

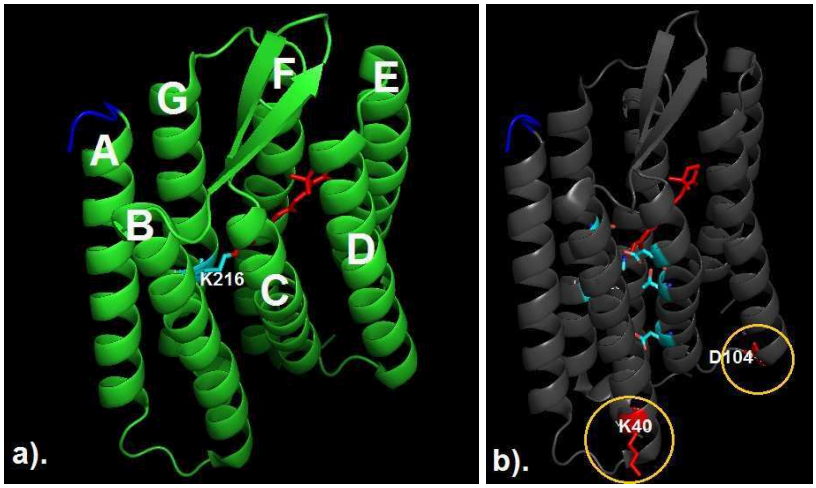


Figure 1.3 The overall structure of bR. **a)** 7TMH (in green) named A to G starting from extracellular N-terminus (depicted in blue), Lys216 depicted in light blue and all-trans retinal depicted in red. **b)** Lys40 and Asp104 (red) emphasized with yellow circles

Helices	**Hydrogen bonds between**
A–B	Arg7 (NH2) and Leu61 (O), Arg7 (NH2) and Met60 (O)
B–C	Thr46 (OG1) and Asp96 (OD2), Tyr57 (OH) and Arg82 (NH1) via water 407
C–D	Leu87 (O) and Asp115 (OD1) via water 511, Thr90 (OG1) and Asp115 (OD1)
D–E	Met118 (O) and Ser141 (OG), Ala126 (O) and Arg134 (NH1), Thr128 (O) and Arg134 (NH1)
E–F	Trp138 (NE) and Pro186 (O), Arg134 (NE) and Glu194 (O), Arg134 (NH2) and Glu194 (O), Leu152 (O) and Arg175 (NH1)
F–G	Trp182 (NE) and Ala215 (O) via water 501, Tyr185 (OH) and Asp212 (OD1), Ser193 (OG) and Glu204 (OE1), Ser193 (N) and Glu204 (OE1), Glu194 (OE1) and Glu204 (OE2)
G–A	Leu224 (O) and Lys30 (NZ)
A–C	Arg7 (NH1) and Tyr79 (OH), Glu9 (OE1) and Tyr79 (OH)
B–F	Tyr57 (OH) and Asp212 (OD2)
B–G	Ty57 (OH) and Thr205 (O) via water 407
C–F	Tyr79 (N) and Glu194 (OE1) via water 404, Tyr83 (OH) and Trp189 (NE1)
C–G	Thr46 (O) and Lys216 (O) via water 502, Tyr79 (O) and Glu204 (OE2) via water 405, Arg82 (NH1) and Thr205 (O) via water 407, Arg82 (NH2) and Thr205 (O) via water 407, Asp85 (OD2) and Asp212 (OD1) via water 402, Asp85 (OD2) and Lys216 (NZ) via water 402

Table 1.3 The list of hydrogen bonds formed between neighboring helices (A to G naming) and amino acids involved [39].

The bR forms a very tight trimeric unit stabilized by helix-helix interactions that includes salt bridge between K40 on helix B of one molecule and D104 on helix D of its neighbor (see Figure 1.3b). The barrel-like rigid structure of bR is due to extensive net of hydrogen bonds between each pair of neighboring helices (see Table 1.3).

The chromophore pocket is built of Trp86, Thr89, Thr90, Met118, Trp138, Ser141, Thr142, Met145, Trp182, Tyr185, Trp189, and Asp212 amino acid side chains that are within 3.6Å from retinal. Many of these residues were shown to influence absorption maximum or thermal isomerisation rate, while Leu93 demonstrated to influences the rate of retinal 13-*cis* to all-*trans* re-isomerisation [61][39].

The hydrogen-bonded network, which comprises the positively charged Schiff base, the three water molecules W401, W402, and W406, as well as Asp85 and Asp212, stabilizes the separated charges at the active site in the ground state[39]. The breaking of hydrogen bond between Asp85 and Thr89 upon retinal isomerisation proposed to increase the pKa of Asp85 and thus making it a proton acceptor.

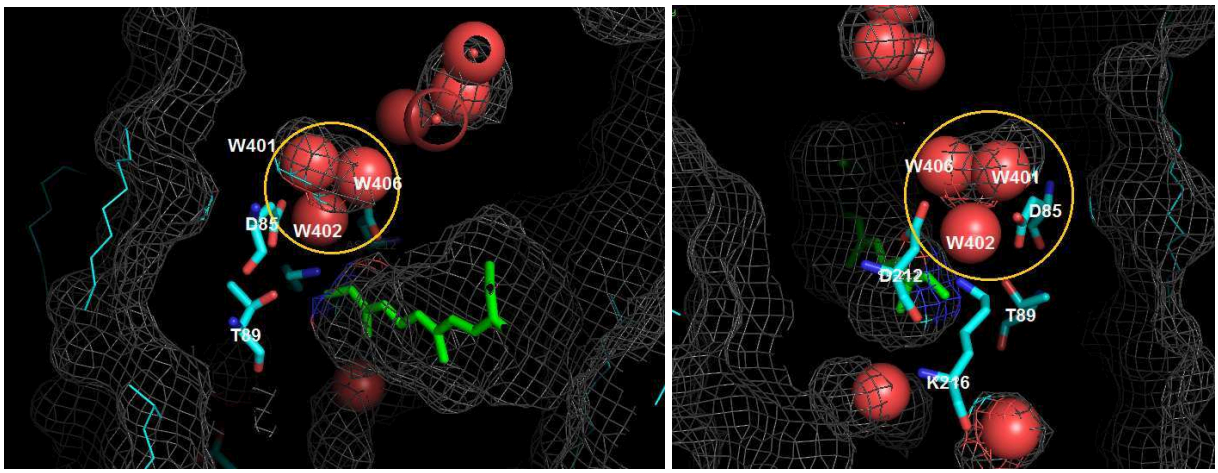


Figure 1.4 View from different perspectives of water molecules (red spheres, W401, W402 and W406 emphasized with yellow circle) near proton uptake side of Schiff base and D85/D212 residues. PDB structure 1C3W, 1.55 Å.

The analysis of bR kinetics reveals a spectrally distinguishable intermediates K, L, M, N and O. The ground state and O intermediate contain all-*trans* retinal, while in the others it's in 13-*cis*,15-*anti*. The generally accepted intermediates are depicted in Figure 1.5. The L and N state contain 13-*cis*,15-*anti* retinal and $RSBH^+$. Thus in order to take into account the vectoriality of proton transport multiple M states should be considered.

Despite the debates on some specific intermediates, there's a general agreement over the main steps of bR's photocycle [62]:

1. before the illumination the Schiff base is in protonated state and retinal is in all-*trans* conformation, the $RSBH^+$ accessible from cytoplasmic side (ground state of bR);
2. the photoisomerization of the retinal (K state) from all-*trans* to 13-*cis*,15-*anti*;
3. the $RSBH^+$ accessibility switch to extracellular side (L state);
4. the Schiff base proton is transferred to Asp85 located on the extracellular side (M_1);
5. the proton release to the bulk from a proton release site (presumably involves Glu194 and Glu204) near the surface, the RSB becomes accessible from cytoplasmic side (M_2);
6. reprotonation of Schiff base through a chain of water molecules (N);
7. and finally, reprotonation of Asp96 (O) and re-isomerisation of retinal (back to ground state).

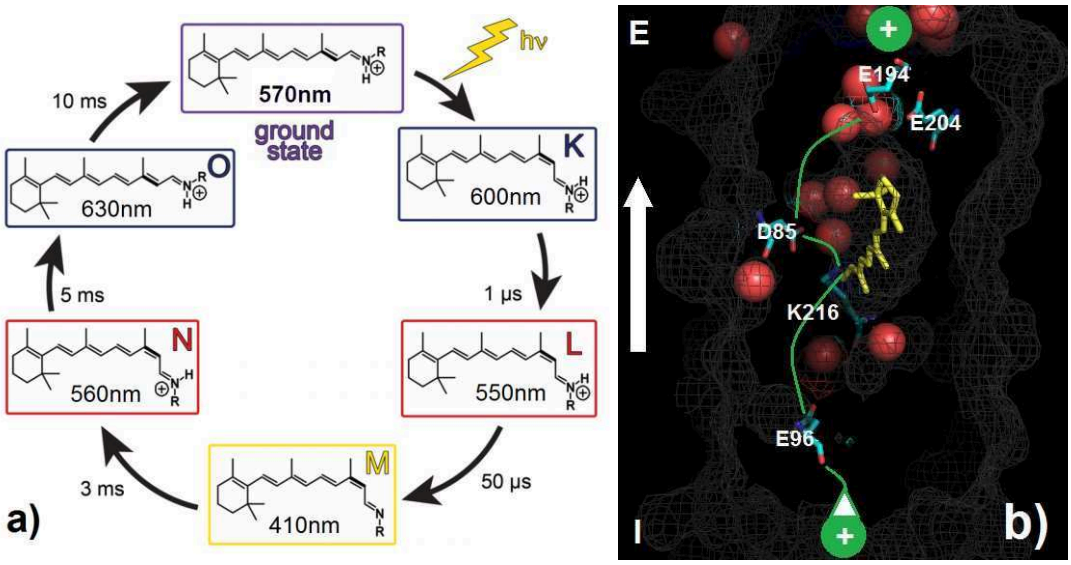


Figure 1.5 **a)** Schematic representation of bR's photocycle with color-depicted absorption maxima of intermediates (adopted from [62]), **b)** the proton (green circle) path (green line) from intracellular (I) to extracellular (E) space on the right.

All the diversity of proton-pumping rhodopsins can be classified into few major subtypes with substantial sequence similarities. The main subtypes are bacteriorhodopsins (mostly haloarchaeal), proteorhodopsins (PRs, mainly eubacterial but also were found in some Archaea), xanthorhodopsins (XRs) and fungal/algal proton pumps.

Spectrally PRs can be divided into green light absorbing (λ_{max} ~525 nm, presumably characteristic for marine bacteria living near the surface) and blue light absorbing PRs (λ_{max} ~490 nm, common for marine bacteria living in the deep sea). Many proteorhodopsin variants have slow photocycles and weak photocurrents. PRs are thought to be the most abundant microbial rhodopsin. Another subtype is XRs, whose distinctive feature is a second chromophore

(like carotenoid salinixanthin), works as a light harvesting antenna with efficiency ~40% of that for retinal (in XR from *Salinibacter ruber*). Structural studies of XR revealed significant difference from BR. Among those are one water molecule in RSB site, absence of proton release mechanism and β-stranded B-C loop on the extracellular side. Fungal proton pumps are similar to BR, but their physiological role is unclear. As for algae, recently determined (3.2 Å resolution) structure of algal proton pumping rhodopsin Ace2 from *Acetabularia acetabulum* revealed overall structure similarity to bR with the lack of proton release complex and the unique interaction of cytoplasmic proton donor with cysteine residue on helix G [62].

1.4.1.1. FRET studies of bR

The absorption UV-visible light ground state spectrum of bR contains 3 peaks. The 570 nm and ~400 nm peaks are due to retinal chromophore. The third peak with maximum at ~280 nm is superimposed mostly of absorptions of retinyl moiety (~10% of total extinction at 280 nm) and aromatic residues (tryptophans and tyrosines). Most studies of bR photocycle involved protein excitation in visible light range.

Soon after discovery of bR, it was shown that photocycle can be started indirectly. Excitation of bacteriorhodopsin with 265 nm laser pulses lead to the photocycle identical to that being started with visible light irradiation. The energy comes in this case not only from direct excitation of retinal, but also because of energy transfer (FRET phenomenon) from aromatic residues. The energy transfer with a quantum yield of 0.7-0.8 leads to a complete quenching of all tyrosine molecules, while one tryptophan is unquenched and one is quenched partially (~80%) [63]. Much later, with discovery of XR, another indirect energy gain was demonstrated, which involved external carotenoid molecule salinixanthin. It was suggested that carotenoid is functioning as a light-harvesting antenna in addition to retinal with ~40% energy transfer efficiency [64]. Taken together, these data suggest that aromatic residues in rhodopsins may function not only as structural elements, but also as additional light-harvesting antennas.

1.4.2. Anion pumps (HsHR, NpHR)

First discovered (and thus most structurally characterised) anion pumping rhodopsin was HsHR (*Halobacterium salinarum*, UNP B0R2U4). Nevertheless, it's not as well understood as proton pump bR.

Unlike bR, which pumps specifically proton, HsHR can transport various anions, such as chloride, bromide, iodide and nitrate into the cell against electrochemical gradient. The anion

selectivity of halorhodopsin is not very high. However, in biological systems the chloride ion is the only halide which is present in abundance [65]. The chromophore retinal is bound to the only lysine K242 residue on the helix G (bR naming). The absorption maximum of this protein is 578 nm.

The mutated T203V HsHR protein structure with 1.6 Å resolution was obtained [65], while the best known resolution obtained for wild type HsHR is 1.8 Å [9]. The B-C loop of wild type HsHR contacts ends of helices C-G and forms two antiparallel β-strands. The tip of this loop anchored by highly conserved histidine H95 (which is hydrogen bonded to V218 and G220; see Figure 1.6a). The N-terminal domain forms a short helix G', that is located almost parallel to the plane of membrane. Together with arginine A-B-helix intracellular residues (R52, R55, R58 and R60), the R258 forms a highly positively charged surface region (Figure 1.6b).

In the ground state of the wild type HsHR structure all-trans, 15-anti retinal is bound to K242. And, even though both the structural and spectroscopic studies imply presence of two chloride binding sites (CBSs), one well resolved Cl^- ion (Cl501) is present in the structure and is located close to RSB nitrogen atom but not in presumable CBS1(S115 [9]) or CBS2 (R24 and R103 [65]).

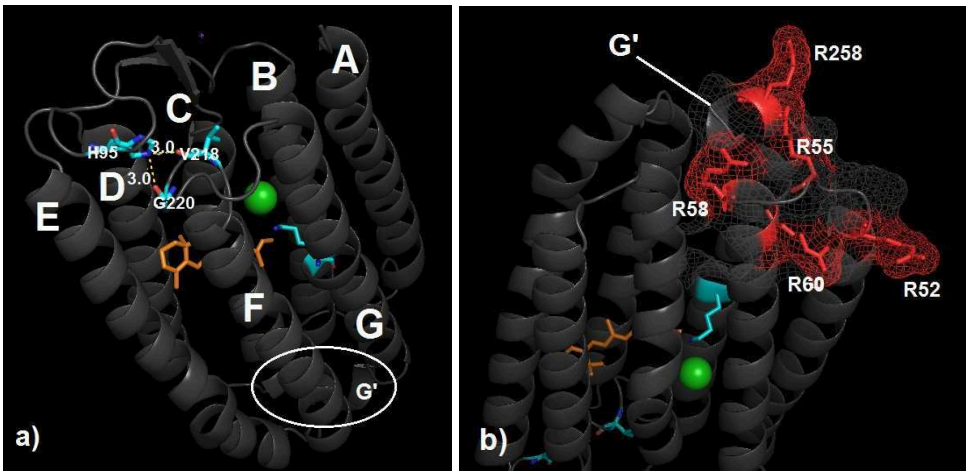


Figure 1.6 The HsHR (UNP B0R2U4, PDB structure entry 1E12) overall structure. **a)** The helices depicted with A-G letters, retinal is represented in orange and Cl^- ion is represented with green sphere. The distances between anchoring H95 and G220/V218 are around 3 Å. **b)** The positively charged C-terminal (intracellular) surface region.

The halide atom in RSB region is located in the cavity formed by 6 residues (V72, S73, S76 of B helix and T111, W112 and S115 of C helix) and water cluster comprising 3 molecules W505, W508 and W512. Despite close contact, RSB is unfavorably oriented to form hydrogen bond with Cl^- (see Figure 1.7).

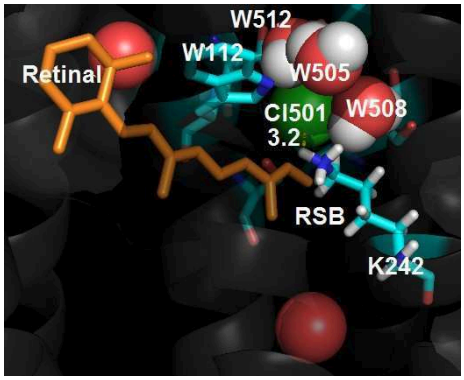


Figure 1.7 The RSB-Cl cavity. Cl501 ion lies close to RSB, but no direct RSB-Cl electrostatic interaction observed (PDB 1E12).

While wild-type ground state structure revealed only one chloride ion (near RSB [9], PDB ID 1E12), both the structure of L1 intermediate and ground state of the T203V mutant protein[a] showed the second anion binding site (without any water molecules near). The anion is found 14.3 Å from the anion in RSB region and being coordinated by Q105, R103 and R24 on the extracellular (N-terminal) side of rhodopsin [65].

The bR and HsHR in their initial states share few common for both proton and halide ion transport mechanisms traits. First, for both the translocating ion is the one either bound to RSB (proton in bR) or very closely located to RSB (Cl^- in HsHR). Second common feature is the complex counter ion charge distribution around RSB, which is almost identical as Cl501 virtually replaces the OD1 atom of D85 (D85, D212, and R82 of bR are replaced in HR by CL501, D238, and R108) [9]. And third, the D85→T or D85→S mutation converts bR to an inward chloride pump like HsHR [66].

Many studies were to characterize the photocycle of HsHR. Nevertheless, many details of it are unclear or even contradictory. The presence of intermediates and their time constants dependencies differ among studies (for instance, here named N→HsHR conformation transfer was found to depend on $[Cl^-]$[67], while these observations weren't confirmed in other works). But it became clear that due to HsHR being a chloride pump, it would have different photocycles in presence of Cl and without it. In addition to unclear Cl-dependent intermediates the so called light-adapted and dark-adapted states of HsHR (like for bR) are also present in the protein mixture, which makes the HsHR's kinetics characterization even more complicated.

[a] In latter paper [65] authors note that initially [9] these secondary chloride ions were mistakenly modelled as potassium ions but the later T203V structure and experiments with potassium bromide allowed them to clarify the uncertainty .

Due to the main topic of this work, the photocycle of HsHR will be mainly described in presence of chloride and under physiological conditions.

In presence of chloride the photocycle contains three spectrally deferrable intermediates K, L and N (sometimes named HR_{600}/K_{600}, HR_{520}/L_{520} and HR_{640}/O_{640} respectively). The proposed model of HsHR's photocycle differs from that of bR. The three spectrally distinguishable intermediates suggest the absence of M-state of HsHR in presence of 2 M NaCl. Thus the photocycle can be represented by HsHR→K↔(L_1↔L_2)↔N→HsHR transformations (see Figure 1.8), where L_1 and L_2 are spectrally indistinguishable [68].

The HsHR's photocycle in general is much faster than that of bR with 3 ms and 10 ms time limiting steps (N→HsHR and O→bR respectively).

Another anion pump NpHR from *Natronomonas pharaonis* was well studied and found an optogenetic application[b]. The two strains of this organism (DSM 2160 and DSM 3395) contain slightly mutated protein sequences (identity ~97%) with UNP P15647 and Q3ITX1 with difference in non-conservative regions (mostly in F and G helices; see Figure 1.9).

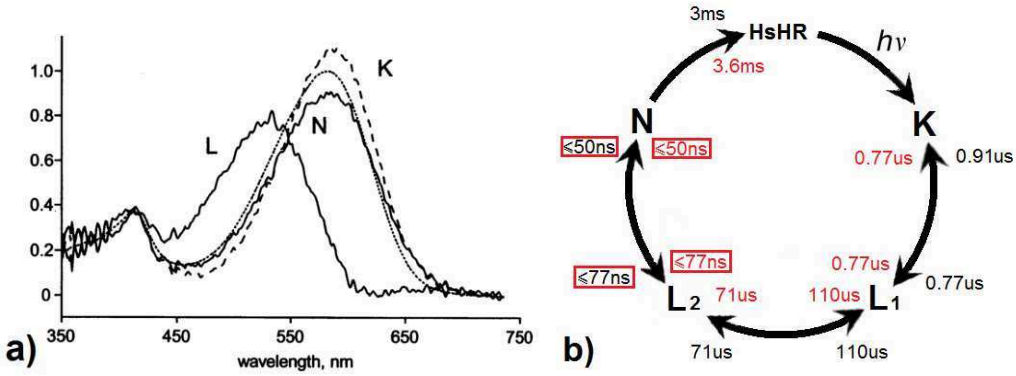


Figure 1.8 **a)** The HsHR kinetic intermediates and ground state spectra (in presence of 2 M NaCl). L and N states represented with solid lines, K state - with broken line, the ground state - with dotted line. **b)** The time rates of intermediates conversions in 100 mM NaCl (black font) and 2 M NaCl (red font). The rates in red rectangles are unclear [68]

Both NpHR variants differ from HsHR in few aspects. First, 2 Å-resolution ground state structure (UNP Q3ITX1, PDB 3A7K) revealed the carotenoid (bacterioruberin) binding site in the slit between two adjacent protein molecules within trimeric rhodopsin assembly. Second, unlike HsHR, *N.pharaonis* halorhodopsin has the N-terminal α-helix (A') that participates (together with B-C loop) in capping of the active center from extracellular side. [10][8].

[b]Despite small differences, optogenetic application found protein P15647 (DSM 3395), for which the construct being applied and named eNpHR3.0 [92].

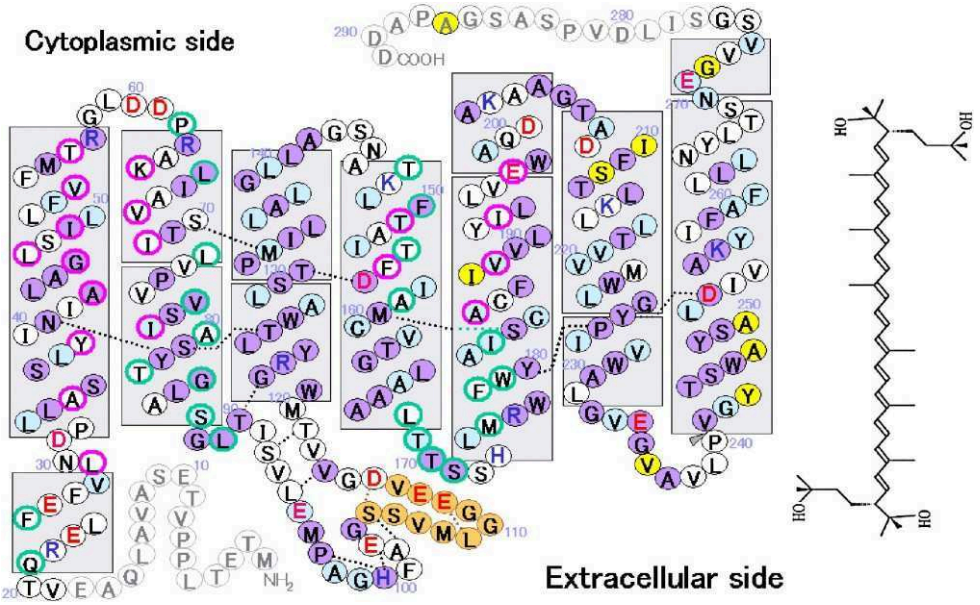


Figure 1.9 Schematic representation of NpHR topology. Residues contacting bacterioruberin framed magenta circles; residues participating in intra-trimer protein–protein interactions - green circles; violet and light blue circles represent residues conserved between NpHR and HsHR; orange circles show inserted residues found only in NpHR; residues conserved among all known HR homologs are marked with violet circles; yellow circles - residues that are not conserved between the two strains of *N.pharaonis* (DSM 2160^T and DSM 3395^T). Residues excluded from the structural model of NpHR are shown by grey letters. On the right is the chemical structure of bacterioruberin [10].

The positions of retinal and bacterioruberin seem non-optimal for energy transfer between these chromophores and thus latter was suggested to participate in protomers stabilization under natural conditions. Nevertheless, the observations that chloride binding causes the noticeable bacterioruberin vibronic band sharpening suggest the strong interaction between carotenoid and NpHR.

The HsHR possesses a secondary binding site of chloride that is surrounded by R24, R103 and Q105. The secondary binding site of NpHR is located at cytoplasmic membrane surface between two protomers. The second halide in this site is coordinated with K65 of the one subunit and N145[c] of another one. In addition to these two sites the two more sites were proposed to exist according to the analysis of differences in electron density maps of chloride- and bromide-bound forms of NpHR [8]. The anion in the binding site III is coordinated by V177, V118, V233 and V241 side chains (between BC and FG loops). The electron density of anion in site III was much lower than that for primary and secondary (I and II) sites. The occupancy of this site by bromide ions was estimated to be ~50%. The anion binding site IV was proposed to be near M96, but the occupancy was impossible to estimate due to the low affinity of bromide ion.

[c] The authors denote this residue as N147 despite the trhreonine residue to be present on the 147th position in the PDB 3QBK structure that was referred to in the paper.

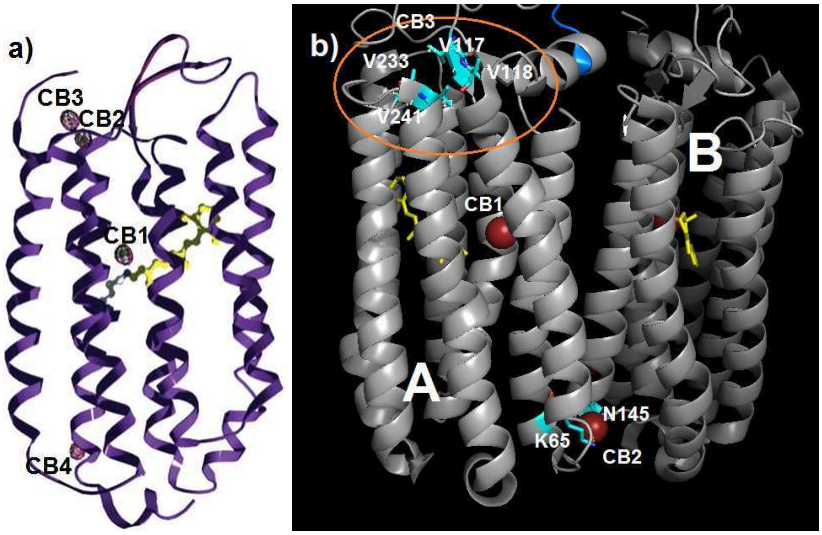


Figure 1.10 The anion binding sites of[d] (a) the T203V mutant of HsHR (adopted from [65]) and (b) NpHR (PDB 3QBK, [8]). The binding sites are denoted as CB1-4 (the region of CB3 and presumable CB4 in NpHR is denoted in orange). The two protomers (in the structure of protein trimers) of NpHR denoted with A and B.

The structure of the third anion pump ClR from *Nonlabens marinus* (UID W8VZW3) was recently solved [69]. The unique property of this protein is its active center motif – it is represented by N98, T102 and Q109 (unlike TSA and in HsHR and NpHR, see Figure 1.11). The overall structure of ClR is similar to both the NpHR and the HsHR, but at the it has common conservative regions with KR2 (see 1.4.3).

The investigations of the T102D ClR mutant revealed complete loss of pumping activity, while the T102N protein remained 70% of it. The structure of the T102D mutant demonstrated, that the newly introduced D102 forms hydrogen bonds with both protonated RSB and N98. In contrast, the Asn102 in T102N mutant interacts with Cl^- ion in the same way as T102 does in the wild type protein structure, which explains the remained pumping activity in the T102N mutant and the loss of it in the T102D[69].

```
P02945 BACR_HALSA          89   NPIYWARYADWLFTTPLLLLDLALLVDADQGTI-----LALVGADGIMIGTGLVGALTK-
N0DKS8 N0DKS8_9FLAO       103   LFNNGYRYLNWLIDVPMLLFQILFVVSLTTSK-FSSVRNQFWFSGAMMIITGYIGQFYEV
B0R2U4 BACH_HALS3         102   VRSQWGRYLTWALSTPMILLALGLLADVDLGSL-----FTVIAADIGMCVTGLAAAMTTS
P15647 BACH_NATPH         117   VVTMWGRYLTWALSTPMILLALGLLAGSNATKL-----FTAITFDIAMCVTGLAAALTTS
W8VZW3 W8VZW3_9FLAO        89   TFSNGYRYVNWMATIPCLLLQLLIVLNLKGKE-LFSTATWLILAAWGMIITGYVGQLYEV
I0IGJ9 I0IGJ9_PHYMF       106   MYSNGYRYVNWAITVPLLLMTLMVVIPLAHAAKRQKAARRLVIFGVSMVFCSWVGGFFEA
```

Figure 1.11 The amino acids sequence alignment of bR (P02945), KR2 (N0DKS8), HsHR (B0R2U4), NpHR (P15647), ClR (W8VZW3) and putative chloride pump PMr2 (I0IGJ9 from this work). The similarity level of

[d] While the authors describe[8] four anion binding sites in the paper, the uploaded structure with PDB 3QBK contains only two bromide atoms corresponding to binding sites I and II (CB1 and CB2 on image). The same situation is true for the T203V HsHR mutant structure, where authors mention the evidences of existence of four anion binding sites. While CB2 of NpHR was found on the intracellular side of the protein, the CB2 of T203V HsHR mutant is found on the outer side.

residues depicted with shades of grey, the positively charged residues - with green, negatively charged residues - with red, the helical regions of bR, HsHR and NpHR - with pink. The blue boxes emphasize the residues correspondent to those in NDQ motif in KR2 (DTE in bR).

1.4.3. *K.eikastus* KR2 sodium pump

In 2013 another new and promising type of rhodopsins was found [5]. *K.eikastus* (reclassified recently to *Dokdonia eikasta* [70]) KR2 protein is the first known Na^+ pumping rhodopsin, that long time was believed not to exist. The reasons are clear and based on the known rhodopsins (BR, PR and HR) – the retinal is bound to the Schiff base, which most of the time is in protonated state and cations, other than proton, are not stable in RSB region due to an electrostatic repulsion[71]. The key difference lies in RSB region amino acids. So, proton acceptor and donor of bR (D96 and D85 respectively) substituted with polar uncharged N112 and Q123 amino acids in KR2. In addition to that, T89, which is not much involved in the proton transport in bR, is replaced with D116. Therefore, the distinguishing feature of proton pumps is the DTD (DTE in case of proteorhodopsin) motif, whereas KR2 possesses NDQ motif[56].

Structural studies of KR2 confirmed this theory, revealing the protein structure in monomeric and pentameric states with up to 1.45 Å resolution [6][7]. This protein shares common to other rhodopsins 7TM (A to G naming) structure with intracellular C-terminus while the chromophore is bound to K255 residue. Differences begin from N-terminal α-helix that capping the inside cavities of the protein and is unique feature among other microbial rhodopsins. Along with it, B-C intrahelical β-hairpin loop notably extended and involved in β-sheet interaction with N-terminal α-helix to opsin A helix linker [72]. Crystals grown contained both monomeric and pentameric KR2, and while cytoplasmic part of protein molecules in pentameric packing is similar to monomers, the extracellular side undergoes slight rearrangement mostly in extracellular side of helix C (residues 107-116). Also, the positions of N112 and D116 and their environment differ within the different protomers in pentamers of KR2 (see Figure 1.12b).

On both (extra- and intracellular) sides from retinal the two tryptophan amino acids (W113 and W215) are hydrogen bonded to two water molecules (W419 and W404 respectively; W419 is also coordinated by D251; see Figure 1.12a). The distance from RSB nitrogen to W419 exceeds 4 Å (Figure 1.12b).

Due to the absence of structural information on KR2 photocycle intermediates, the mechanism of sodium ions transport stays unclear and might be disputed. The ground spectrum

of KR2 doesn't exert significant shifts in present of NaCl and without it (maximum at 523.7 nm and 522.6 nm respectively).

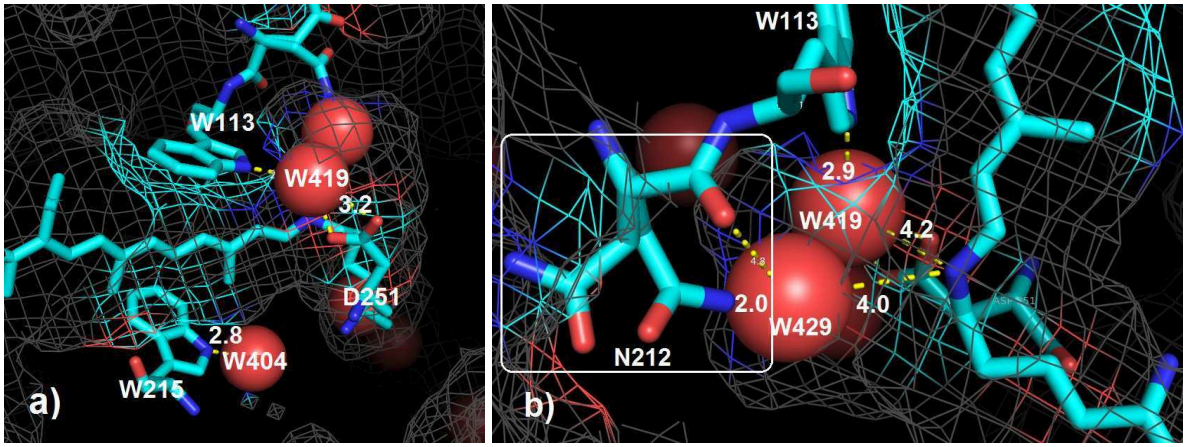


Figure 1.12 Retinal binding pocket of KR2 (PDB ID 4XTN, 2.2 Å, dodecamer). **a)** The coordination of W404 and W419 water molecules. **b)** The two entities of N112 (emphasized with white rectangle) within the crystal pentamers (decamers) and W419 and W429 molecules coordination.

The initial characterization of photocycle suggested that in presence of NaCl red-shifted K blue-shifted L(505 nm)↔M(400 nm) and red-shifted O intermediates appeared sequentially in the photocycle and, unlike for bR, L and M appear simultaneously (see Figure 1.13) [5]. But in terms of bR naming of intermediates (K-L-M-N-O), M state represents deprotonated RSB, while key difference of O intermediate is reprotonation of proton donor residue. The reprotonation of RSB in bR occurs during N state formation, and thus N intermediate can't be missing (in bR-like photocycle), which implies that O state can be formed during the N decay. Since L and N intermediates possess close spectra (in bR 550 nm and 560 nm respectively), they might not be clearly distinguished in absence of M or be represented by new I_{LN} state, that differs from both bR-like L and N intermediates.

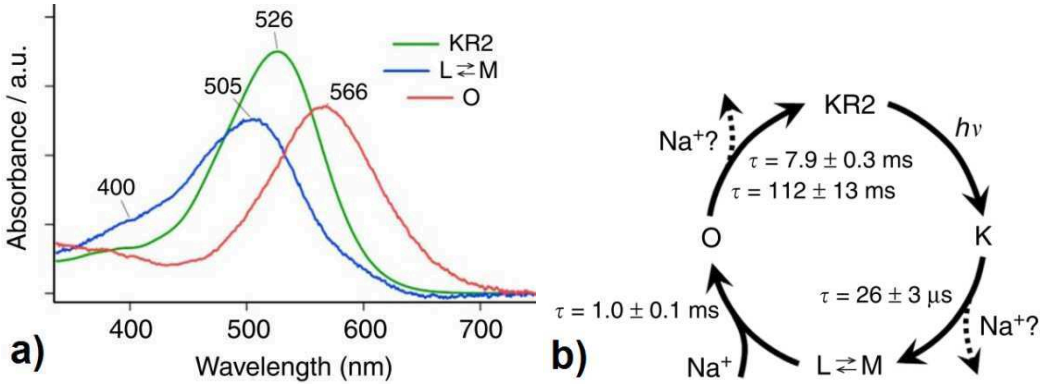


Figure 1.13 **a)** KR2 photointermediates spectra and **b)** photocycle scheme with time constants in presence of NaCl being proposed in [5].

Another detail is the non-100% selectivity of KR2 even in presence of sodium ions. This means, that in protein sample some portion of protein is pumping a proton and the M-like intermediate observed may only be a trace of H^+-photocycle, while in "pure" Na^+-photocycle proton never lives the RSB, and thus total loss of N-state.

Taken together, all this suggests that the KR2 photocycle can't be described in terms of only one photocycle model and it should be split into two models (see Figure 1.14).

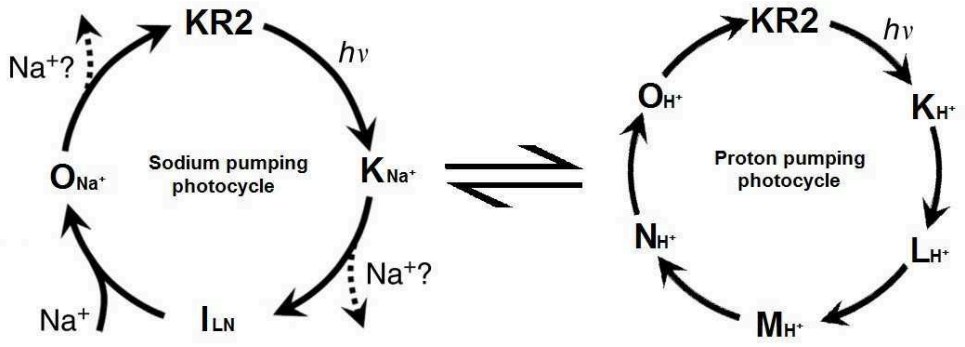


Figure 1.14 The proposed model of KR2 photocycle.

In our proposed model K_H^+ and O_H^+ aren't identical to K_{Na}^+ and O_{Na}^+. In addition, structural changes exerted by KR2 during K-L-M-N-O transformations should not be referred to as direct correspondence to those of bR (especially M and O states due to significant difference in proton uptake by RSB in bR and KR2) and are named so only due to similar absorption maxima shifts.

The rise of intermediate O accelerates along with the sodium concentration, which may be explained that Na ion uptake occurs during the O state formation. The sodium release is expected to occur upon decay of K or O intermediates [56].

1.4.4. Light-gated channels structures

The main and unique feature of ChRs among other rhodopsins is their channel activity. These proteins function as a light-gated ion channels and, unlike pumps, mediate passive ion transport activity through membrane only along the gradient. It was shown that this activity is directly connected to a photocycle, during which ChR2, for instance, functions as a proton pump as well, transporting one proton per cycle, i.e. ChR2 has a dual (pumping and channel) activity [73].

The photocycle of ChR2 represented on Figure 1.15. Deprotonation of active state P500 (transition 1 to P390) to the extracellular side and reprotonation (transition 2) from the cytoplasmic side (reprotonated state P520) leads to the pumping of one proton per photocycle.

During the lifetime of P520, the channel is opened and allows permeation of protons and cations M^+ (red arrow). Upon closing (transition 3), ChR2 reaches the light-adapted state P480. Recovery to the ground state takes seconds in the dark and is accelerated by a second light reaction under continuous illumination.

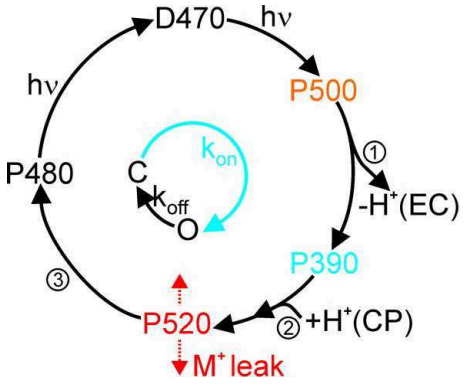


Figure 1.15 Dual activity ChR2 photocycle model. The inner circle represents the channel activity, while outer represents the photocycle with its intermediates connected with proton pumping activity (adapted from [73]).

Not so much structural information available regarding microbial channel opsins to the day. Channel rhodopsins ChR1 and ChR2 from *C.reinhardtii* consist of 712 and 737 amino acids each, but only N-terminal core ~300 aa are needed for their photocurrent functionality [2], [3].

The 3D structure prediction models built by homology demonstrated the 7TM pattern (as in other microbial opsins) while sequence alignment revealed high homology in ChR2's predicted TMHs 3,6 and 7. The bR's retinal-binding lysine K216 in TMH7 represented by K257 in ChR2.

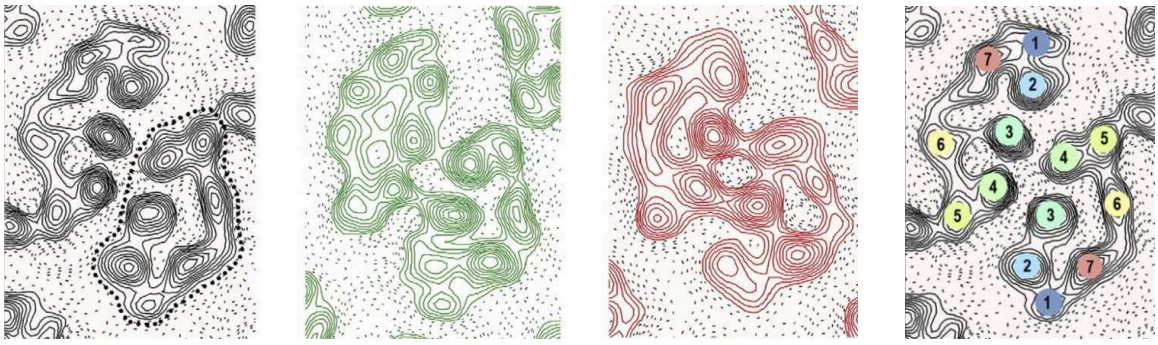


Figure 1.16 ChR2 C128T EM densities of A, B and C types of crystals and numbered helix assignment corresponding to bR A-G helices.

First insight into ChR2 structure was obtained in 2011 [46]. Three types of ChR2 2D crystals were grown in presence of 1,2-dimyristoyl-sn- glycero-3-phosphocholine (DMPC) and *Escherichia coli* lipids, and investigated with electron microscopy (ChR2 C128T mutant protein was expressed in *Pichia pastoris*). Two types of crystals grew in DMPC with LPR 1.25 and 8.75 for type A and C respectively and one in *E.coli* lipids with LPR 1.25 with the same space group

$p22_12_1$. Rectangular unit cell dimensions were 111.8 Å×77.6 Å for type A, 114.8 Å×77.2 Å for type B and 112.5 Å×76.1 Å for type C. The SDS-PAGE of protein before and after crystallisation contained two bands (weaker at ~35 kDa and stronger at <65 kDa) and no traces of proteolysis.

All three types of crystals were formed with ChR2 dimer with no significant difference between separate dimers' projections of all three crystal types (two different lipids). Which was unusual, since, for instance, bR and HR formed crystals of monomers and trimers (bR) ant tetramers (HR), while functional in monomeric state. Taken all together these facts might suggest that ChR2 functional unit is dimeric. Further structure investigation revealed 7 well resolved densities corresponding to predicted 7 transmembrane helices with 3 TMs near dimer interface seem to be perpendicular to membrane plane, while other 4 being tilted (more like bR's).

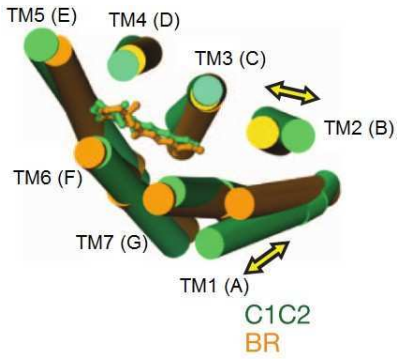


Figure 1.17 Superimposed C1C2 and bR (PDB 1IW6) structures transmembrane domains and retinal (RSB) position (adopted from [47]).

Another structural study of ChRs was reported. The crystal structure of closed C1C2 channel (sometimes being called $ChR_{5/2}$; chimera between ChR1 and ChR2 from *Chlamydomonas reinhardtii*) was obtained with 2.3 Å resolution. Overall structure of C1C2 superimposed better to bR than to bovine rhodopsin bRh. The TM3-6 are very similar to bR, as well as conserved RSB position. But despite moderate level of similarity, C1C2 possesses some distinctive features. First, the two terminal domains. The N-terminal domain contributes to a dimerization of rhodopsin monomers and C-terminal domain presumably is involved in subcellular localisation. Next, TM7 is protruding into the intracellular space for ~18 Å, while the function of this part of TM7 remains unknown. And last, is a high tilt of TM1 and TM2 outward of monomer C1C2 central axis in compare to bR [47].

The retinal in its all-trans conformation is bound to K296, and, as in bR, located in the hydrophobic pocket formed by aromatic residues (W163, F217, W262, F265 and F269).

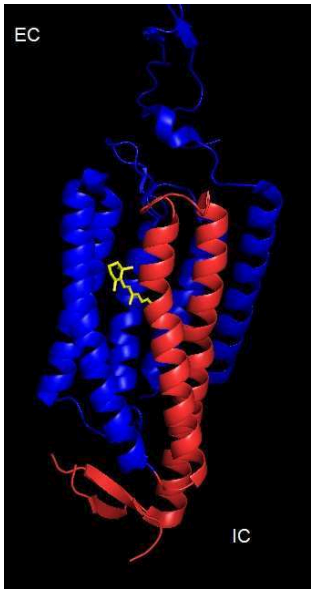


Figure 1.18 C1C2 chimera structure. Parts of chimera belonging to ChR1 and ChR2 colored with blue and red respectively. All-trans retinal is depicted in yellow. Extracellular side (EC) and intracellular side (IC) depicted as well.

Recent spectroscopic studies on C1C2 (as well as ChR1 and ChR2) demonstrated that the light induced conformational changes of C1C2 differ from ChR2. The protonation state of a glutamate residue E129 (E90 by ChR2 numbering) in chimeras C1C2 ($ChR_{5/2}$) and $ChR_{2/5}$ isn't changed as much as in ChR2 wild type channel. Taken this facts together with differences in major photocycle intermediates between chimeras and wild type ChR2 indicates different gating mechanisms of chimeras and ChR1/ChR2 [48] and, thus, further structural studies of ChR1/ChR2 natural channels are needed.

1.4.5. Active centre motifs of rhodopsin pumps

From mechanism point of view, rhodopsins have only few key amino acid residues that seem to predetermine their function. So, D96 and D85 directly involved in proton translocation to and from RSB in bR, being donor and acceptor of proton respectively. The sodium pump KR2 have N112, D116 and Q123 (D85, T89 and D96 in bR), where D116 interacts with protonated Schiff base and presumably plays role of accessibility switch or proton donor upon formation of a red-shifted O state. [13].

The presence of active center residues in corresponding to those in bR positions suggests, that rhodopsin pumps might be categorized by their functions by considering these key residues (are called rhodopsins motifs) and their functions might be predicted by their motifs.

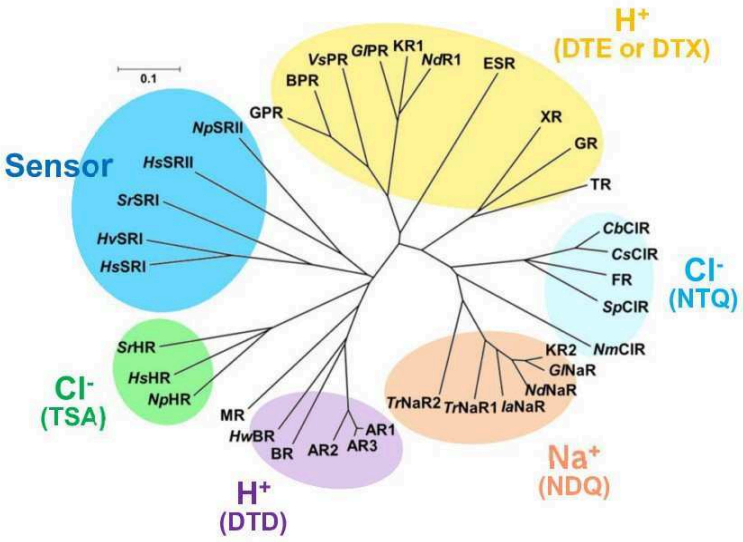


Figure 1.19 Phylogenetic tree of microbial rhodopsins with corresponding active center motifs (adopted from [13]). Marine bacteria rhodopsins represented by yellow, orange and cyan clouds; archaeal pumps depicted in blue, light blue and green. The scale bar represents the number of substitutions per site (evolutionary "proximity" of rhodopsins).

The mutational studies of bR revealed its ability to pump chloride with only one point D85T mutation [66], transforming it to TTD motif protein. Thus it seems that more of proteins with already known functions (such as sodium pumping) but different motifs are naturally available.

1.5. Conclusion

Despite overall success in rhodopsins structural studies and characterization, many of the aspects are still missing. So, the photocycle and mechanism model of recently discovered sodium pump need to be further investigated. About fifteen years ago the debates on the mechanism of rhodopsins function emerged [12][11] and proceed even these days [10][8]. The simplicity of conversion bR into anion pump with only one D85T mutation leaded to a hypothesis of bR to be not he invard H^+ pump but outward OH^- transport, while HRs are HCl/proton antiporters. The fact of existence of alternative models alone describes the modern understanding of rhodopsins.

Even more dramatic situation evolved concerning ChRs. While they became generally accepted and broadly used optogenetic tools, the lack of structural information doesn't allow the production of even more efficient mutants.

While the list of hyperpolarizing tools, even though consisting mostly of ChRs, is more than extensive, depolarization is still the bottleneck of efficient neuronal optogenetic control. Only few rhodopsins and their derivatives are used currently in bidirectional experiments. The use of

proton pumps in this context is still disputed. Which makes anion pumps the most preferable option. But the choice is quite narrow.

2. Materials and methods

2.1. Materials

2.1.1. Organisms

Used organisms are listed in the **Table 2.1** below.

Strain	Relevant genotype	Source
Escherichia coli TOP10	F- mcrA Δ(mrr-hsdRMS-mcrBC) φ80lacZΔM15 ΔlacX74 nupG recA1 araD139 Δ(ara-leu)7697 galE15 galK16 rpsL(StrR) endA1 λ-	Invitrogen
Escherichia coli BL21 (DE3)	fhuA2 [lon] ompT gal (λ DE3) [dcm] ΔhsdS λ DE3 = λ sBamHIo ΔEcoRI-B int::(lacI::PlacUV5::T7 gene1) i21 Δnin5	New England BioLabs
Escherichia coli C41 (DE3)	F - ompT gal dcm hsdSB (rB- mB-) (DE3)	Lucigen
Escherichia coli C43 (DE3)	F - ompT gal dcm hsdSB (rB- mB-) (DE3)	Lucigen
Escherichia coli SE1	F-, CmR, ompT, lon, hsdSB (restriction-, modification-), gal, dcm, DE3 (lacI, T7polymerase under the control of the PlacUV5 promoter), ccdB+.	Delphi genetics
Escherichia coli SHuffle	F′ *lac*, *pro*, $lacI^{Q}$/*Δ(ara-leu)7697 araD139 fhuA2 lacZ::T7 gene1 Δ(phoA) PvuII phoR ahpC* galE (or U) galK λatt*::pNEB3-r1-*cDsbC* ($Spec^{R}$, $lacI^{q}$) *ΔtrxB rpsL150*(Str^{R}) *Δgor Δ(malF)3*	NEB
Leishmania tarentolae T7-TR	T7polymerase and TET repressor	Jena Bioscience

Table 2.1 The list of organisms being used in this work.

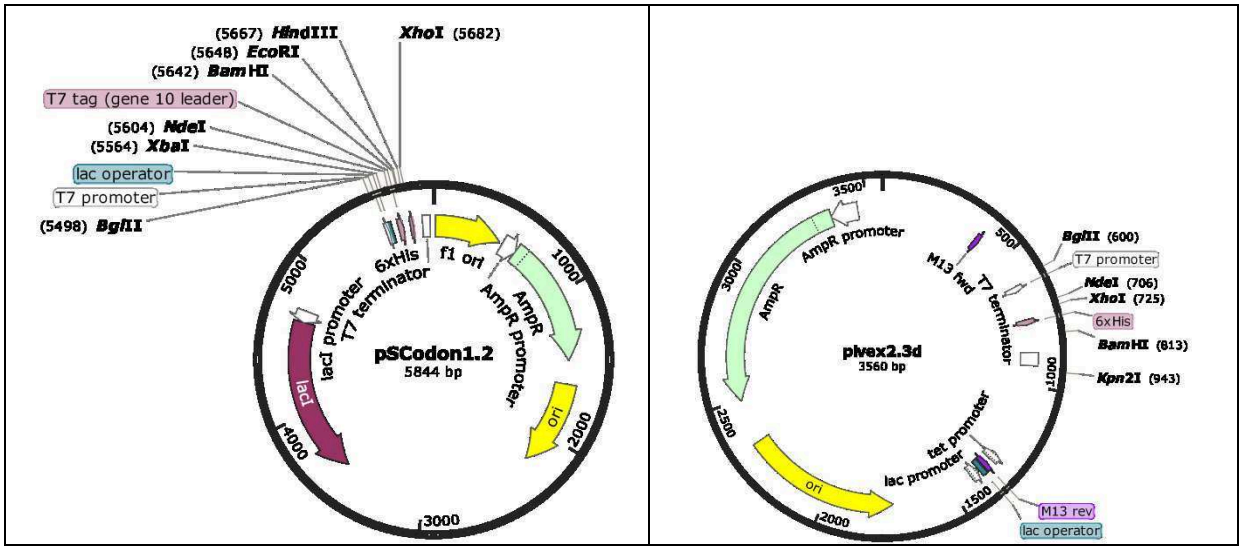
2.1.2. Vectors

Used vectors with main features are listed in **Table 2.2**. On the **Figure 2.1** you can find their maps.

Vectors	Relevant features	Source
pSCodon1.2	T7 promoter, His C-terminal tag, ccdA, Amp resistance, lacI repressor	Delphi genetics
pivex2.3d	T7 promoter, His C-terminal tag, high copy number, Amp resistance	5 Prime

pivs	T7 promoter, His C-terminal tag, high copy number, Amp resistance (modified pivex2.3d)	5 Prime
Vectors	**Relevant features**	**Source**
pRK603	tetO promoter, TEV protease S219D mutant, Kn resistance, 30 copies per cell	Addgene
pEKT7Rmin	Modified pEKT7 plasmid (T7 promoter, His C-terminal tag, lacI repressor, Kn resistance) with eliminated lacI repressor gene	Dr. Taras Balandin
pEX-K, pEX-K4, pEX-A2	proprietary gene delivery plasmids with Kn (pEX-K, pEX-K4) or Amp (pEX-A2) resistance	Eurofins
pLEXSY_IE_blecherry4	Episomal inducible LEXSY expression vector with the blecherry marker and reporter gene consisting of bleomycin resistance gene (*S. hindustans*) and cherry fluorescence gene, enabling selection of recombinant LEXSY strains with the antibiotic LEXSY Bleo	Jena Bioscience GmbH
pLEXSY_I-blecherry3	Inducible LEXSY expression vector with the blecherry marker and reporter gene consisting of bleomycin resistance gene (*S. hindustans*) and cherry fluorescence gene, enabling selection of recombinant LEXSY strains with the antibiotic LEXSY Bleo.	Jena Bioscience GmbH

Table 2.2 List of plasmid vectors with main features used.



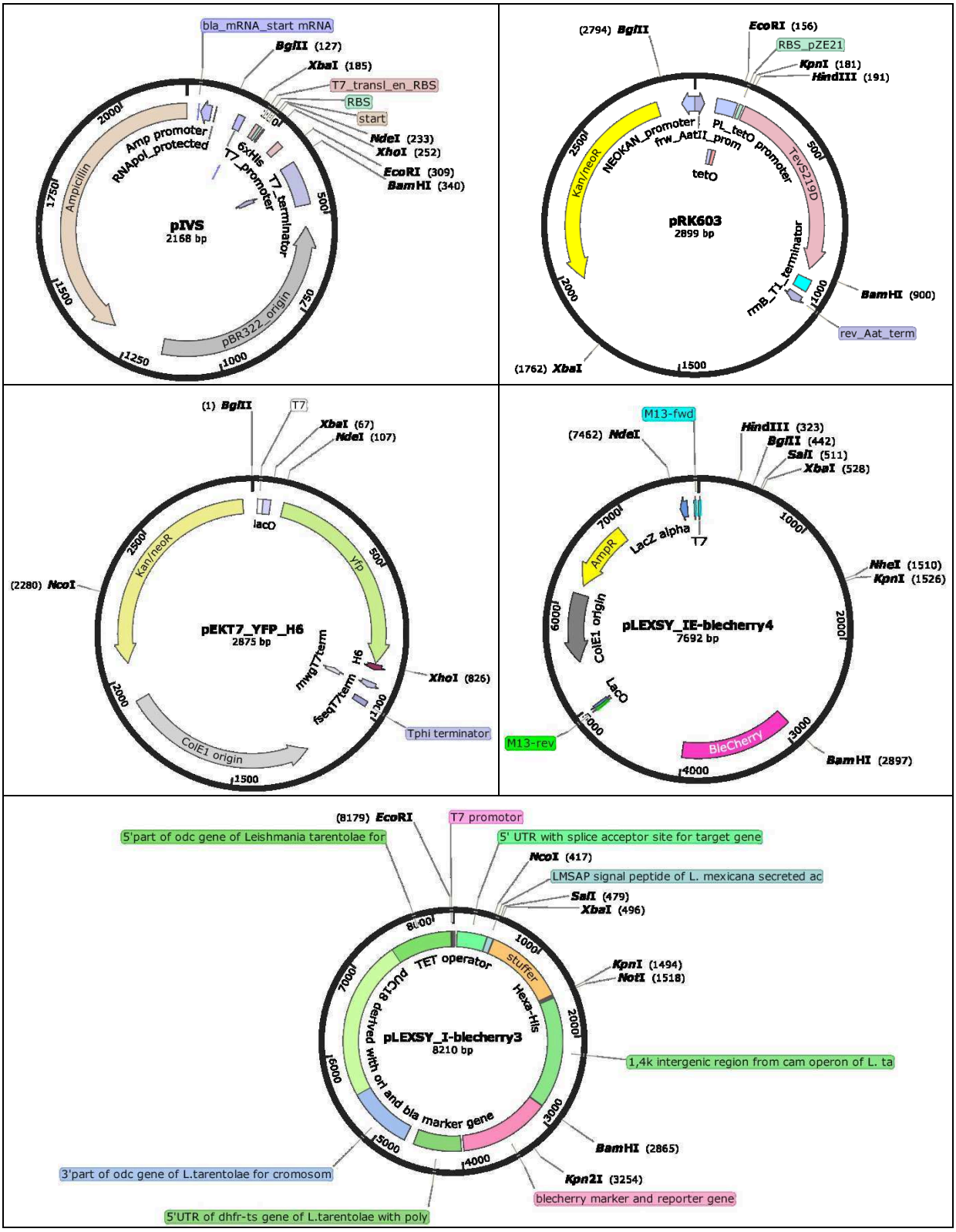


Figure 2.1 The maps of vectors with common features.

2.1.3. Oligonucleotides used in this work

Optimized I0IBH0, I0IGJ9 and F6K461 genes for *E.coli* expression were synthesized by MWG, Ebersberg, Germany. The following primers were used to generate constructions used in this work:

Name	Sequence
f16PMr2	5'-ccaccagatctgccatgaatatggaaaacttttcagctatacaccgg-3'
f18PMr2pivs	5'-atggaaaacttttcagctatacac-3'
f27PMr1	5'-accagatctgccatgcacatggcaaattggtttgcatatacccc-3'
f29PMr1pivs	5'-atggcaaattggtttgcatatacc-3'
fpmr20.5Tr	5'-cgcggcagcggcctcgagcgagctccc-3'
Fpmr2trh6(1-273)	5'-gagggcctggtgccgcgcggc-3'
fpSC0.5TrGH	5'-cgcggcagcggccaccaccaccaccacc-3'
fw_18PMr2_e24	5'-ttcgaaagctatacaccgggtcagcattttgc-3'
r0.5Trpivs	5'-cggcaccaggccctctgccggtgcttcattacg-3'
rPMr1_KpnI	5'-ggtgggtacctgcttcggcatgtgccggttcac-3'
rPMr2_KpnI	5'-ggtgggtacctgccggtgcttcattacggg-3'
Rpmr2trh6(1-273)	5'-aacacgaacggccagacgacccatcagaatgcc-3'
Rpmr2trh6(1-274)	5'-ggcaacacgaacggccagacgacccatc-3'
rpSC0.5TrGPMr2w	5'-cggcaccaggccctcgagtgccggtgc-3'
rvF6K461_W155	5'-ccaacgaacgctcagatcttcttgaatttcaccc-3'
rvF6K461_WtoI155	5'-aatacgaacgctcagatcttcttgaatttcacccgg-3'
rvpivs18PMr2_e22	5'-ttcaaagttttccatatgtgccatggtatatctccttcttaaag-3'

Table 2.3 The list of oligonucleotides used.

2.1.4. Chemicals

Non-organic salts and acids were bought from Sigma-Aldrich, Applichem and Merck. Detergents and lipids – from Sigma-Aldrich, Affimetrix and Avanti Polar Lipids. Components of cell free expression system – from Sigma-Aldrich, Roth and Roche. DNA modifying enzymes – from Thermo. Factor Xa protease – from Qiagen, enterokinase – from New England Biolabs, thrombin – from Sigma-Aldrich.

2.2. Methods

2.2.1. Molecular biology methods

2.2.1.1. Transformation of plasmids into *E.coli* cells

Competent cells were prepared as described earlier [74]. Briefly TOP10 *E.coli* cells were grown in 50 ml of LB medium (1% Trypton, 0.5% Yeast extract, 1% NaCl, pH 7.0) in 500 ml

flask at 37°C with vigorous shaking to the early exponential phase (OD_{600} 0.3-0.4). Then the cells were pelleted by centrifugation at 1000×g for 10 min at 4°C and resuspended at one-tenth of their original volume in ice-cold TSS solution (LB broth with 10% PEG8000, 5% DMSO, 50 mM $MgCl_2$, pH6.5). 0.1-ml aliquots of the cells were transferred into cold polypropylene tubes and frozen in liquid nitrogen. The frozen competent cells were stored at -80°C.

For transformation a plasmid solution (5 µl) or ligation mixture (50 µl) were added to 0.1-ml aliquot of competent cells and kept on ice for 1 h. Then the heat pulse was applied at 42°C for 1min with gentle stirring. After that the cells were incubated on ice for additional 10-15 min. Next, 0.5 ml of LB broth was added, and the cells were grown at 37°C with shaking (120 rpm) for 1 h to allow expression of the antibiotic-resistance gene. The bacteria were stroke on agar plate containing appropriate antibiotics (1% Trypton, 1% Yeast extract, 0.9% NaCl, up to 2% glucose, 1.5% agar, pH7.0 and appropriate antibiotic). The plate was incubated overnight at 37°C.

2.2.1.2. Plasmid DNA isolation

For plasmid DNA isolation the separate colony was grown overnight in 20 ml of LB medium in 100 ml flask at 37°C with shaking (120 rpm). The bacteria were pelleted by centrifugation at 5000×g for 10 min at 4°C and resuspended in 0.5 ml RNAse A containing Buffer A1 from commercial NucleoSpin® Plasmid purification kit (Macherey-Nagel, Dueren, Germany). Next, the bacteria were processed by SDS/alkaline lysis (addition of 0.5 ml Buffer A2). High-salt Buffer A3 (0.5 ml) was added to neutralize the lysate and to create appropriate conditions for DNA binding to the silica membrane. After centrifugation at 10000×g for 10 min at 4°C the clear supernatant was loaded onto a NucleoSpin® Plasmid spin column. After that additional washing with 0.6ml Buffer AW was done. Contaminations like salts and macromolecular cellular components were removed by simple washing with 0.6ml ethanol-containing Buffer A4. The plasmid DNA was eluted in 50 µl slightly alkaline Buffer AE (5 mM Tris-HCl, pH 8.5) and stored at -20°C.

2.2.1.3. Plasmid DNA purification for cell free protein synthesis

For *in vitro* protein expression high quantity of pure plasmid matrix is needed. That is why the special protocol was used. Briefly, the separate colony was grown overnight in 35 ml of LB medium in 500 ml flask at 37°C with shaking (180 rpm). The bacteria were pelleted by centrifugation at 5000×g for 10 min at 4°C and resuspended in 4 ml Buffer P1 from commercial

Qiagen® Plasmid Plus Midi Kit (Qiagen, Hilden, Germany). Next, 4 ml of lysis Buffer P2 was added and the mixture was incubated for 3 min at room temperature. High-salt Buffer S3 (4 ml) was added to neutralize the lysate and to create appropriate conditions for DNA binding to the silica membrane. The mixture again was incubated for 10 min at room temperature and then filtered through QIAfilter Cartridge. 2 ml of Buffer BB was added to the clear lysate. The mixture was loaded onto Qiagen Plasmid Plus spin column. To wash the DNA 0.7 ml Buffer ETR and 0.7 ml Buffer PE were used. The pure plasmid DNA was eluted in 100 µl Buffer EB and stored at -20°C.

2.2.1.4. Amplification of genes.

DNA fragments were amplified by PCR. 50 µl of the reaction mixture contained 5 ng of DNA matrix, 1 pmol of each primer, 20 nmol of each dNTP's, 0.5 U Phusion Hot Start II DNA Polymerase (Thermo, USA) and 10 µl of Phusion HF Buffer or Phusion GC Buffer. In case of whole plasmid PCR, additives were used – 2% DMSO and 50 nmol $MgCl_2$ (final concentration of 1 mM).

Depending on a reaction, the amplification of DNA in the thermocycler was done in either:

- single step (for introduction of short mutations to a gene/vector, "cutting out" reactions)

1. 2' at 98°C
2. 20" at 98°C
3. 30" at primers' melting temperature (steps 2-4 repeat 35-40 times)
4. 40" at 72°C
5. 10' at 72°C
6. Stay at 4°C

- two-step manner (for introduction of extended inserts)

1. 2' at 98°C
2. 20" at 98°C
3. 30" at primers' melting temperature minus 3-5°C (steps 2-4 repeat 5-10 times)
4. 40" at 72°C
5. 20" at 98°C
6. 30" at primers' melting temperature (steps 5-7 repeat 30-40 times)
7. 40" at 72°C
8. 10' at 72°C
9. Stay at 4°C

In case of whole plasmid PCR elongation time at 72°C was increased according to DNA polymerase manufacturer recommendations.

2.2.1.5. PCR products analysis and purification

The PCR products were analyzed by horizontal agarose gel-electrophoresis. DNA probes, mixed with DNA loading buffer (Thermo, USA) in 1:5 dilution, were loaded onto 0.7-1.5% agarose gels running in TAE buffer (40 mM Tris-base, 1 mM EDTA, acetic acid till pH reaches 8.0). Staining of DNA bands was done by adding Midori Green Advance (Biozym) in 1:20000 dilution to TAE buffer. The DNA fragments were separated by applying 6 V/cm voltage to the gel. The bands of interest were cut out and NucleoSpin® Gel and PCR Clean-up kit (Macherey-Nagel, Dueren, Germany) was used for DNA extraction. Briefly, the agarose gel slice was dissolved in high-salt Buffer NT and applied to a NucleoSpin® Gel and PCR Clean-up Column followed by centrifugation and a subsequent washing step with ethanol-containing Buffer NT3. The pure DNA was eluted under low ionic strength conditions with slightly alkaline Buffer NE (5 mM Tris-HCl, pH 8.5).

2.2.1.6. DNA restriction and plasmids linearization

PCR products and plasmids were cut with corresponding restriction enzymes by 1 h incubation at 37°C. Usually FastDigest® restriction enzymes (Thermo) were used together with FastDigest Green® buffer. Restriction enzymes were heat-inactivated according to a manufacturer recommendations.

Plasmids, used further for ligation, were incubated with 1 U Thermosensitive Alkaline Phosphatase (Thermo, USA) for 30 min at 37°C after restriction enzymes inactivation.

2.2.1.7. Ligation of DNA

For ligation of the DNA fragments T4 DNA Ligase (Thermo, USA) was used. 100 ng of recipient vector DNA were mixed with excess amount of insert DNA (5-10 times excess) and 1 U of T4 DNA Ligase in ligase buffer. The ligation mixture was incubated overnight at 20°C and then used for transformation or stored at -20°C.

2.2.2. *E.coli* culture and overexpression

Overexpression in *E.coli* was done using either auto induction media [75] or standard IPTG-induction. In both cases preculture was prepared in the same manner. One colony of *E.coli*

from fresh agar plate was incubated at 37°C in 20 ml of LB broth containing 1% glucose and appropriate antibiotic in 100 ml flask until OD_{600}=0.8. 1 ml of culture was incubated again in the same conditions (at 37°C, in 20 ml of LB + 1% glucose and antibiotic, vigorous shaking till OD_{600}=0.8). All 20 ml of culture were transferred to 500 ml of ZY broth (1% Trypton, 0.5% Yeast extract) containing NPS, 0.4% glucose, 1 mM $MgCl_2$ and antibiotic, and cultivated at 37°C 120 rpm until OD_{600}=1.0.

2.2.2.1. Protein overexpression with *E.coli* in AIM

The procedure is adopted from [75] but slightly modified. The 6 L of AIM with appropriate antibiotic were inoculated with fresh preculture (starting OD_{600}~0.2). The bacteria were cultured in 2 L Erlenmeyer flasks at 37°C with vigorous shaking (120 rpm). Glucose level in media was controlled by commercial glucose tests (Merckoquant®). When glucose was depleted (OD_{600}~0.9), antibiotic containing solubilised all-trans Retinal mixture was added and culture was either cooled to 20°C for overnight incubation or left at 37°C for 5-7 h. The cells were harvested by centrifugation at 5000×g for 1 h at 4°C and then either immediately resuspended for further protein purification or frozen in liquid nitrogen and stored at -80°C.

For 1 L of AIM were mixed 930 ml of ZY broth (1% Trypton, 0.5% Yeast extract), 2 ml of 1 M $MgSO_4$ stock, 20 ml of 50×5052 stock (25% glycerol, 2.5% glucose, 10% α-lactose), 50 ml of 20×NPS stock (0.5 M $(NH_4)_2SO_4$, 1 M KH_2PO_4, 1 M Na_2HPO_4). ZY broth and NPS stock were autoclaved; the $MgSO_4$ and 5052 stocks were sterilized by filtering. Antibiotic containing Retinal concentrate mixture was prepared from stock solutions (20% Triton X-100, 50 mM all-trans Retinal dissolved in EtOH, 200 mg/ml Ampicillin); corresponding final concentrations in flasks are: 20 μM all-trans Retinal, 0.05% Triton X-100, appropriate concentration of antibiotic (usually 200 μg/ml Ampicillin).

2.2.2.2. Protein overexpression with IPTG-induced *E.coli*

The 6 L (0.5 L per flask) of 1Y1T (1% Yeast extract, 1% Trypton) with 0.4% glucose and appropriate antibiotic were inoculated with fresh preculture (starting OD_{600}~0.05). The bacteria were cultured in 2 L flasks at 37°C with vigorous shaking (120 rpm). When OD_{600} reached 1.1 (if not stated different) protein expression was induced with Retinal containing induction mixture. Next, the antibiotic concentration was renewed each hour for 6h (i.e. six times). After that, new portions of antibiotic were added each ~2 h till the end of expression period (12 h).

The cells were then harvested by centrifugation at 5000×g for 1 h at 4°C and then either immediately resuspended for further protein purification or frozen in liquid nitrogen and stored at -80°C.

Retinal containing induction mixture (Antibiotic-IPTG containing Retinal concentrate mixture) was prepared from stock solutions (20% Triton X-100, 50 mM all-trans Retinal dissolved in EtOH, 20 0mg/ml Ampicillin, 1M IPTG); corresponding the final concentration of each component in culture: 1 mM IPTG, 20 µM all-trans Retinal, 0.05% Triton X-100, appropriate concentration of antibiotic (usually 200 µg/ml Ampicillin).

2.2.3. LEXSY culture and overexpression

The genes in fusion with C-terminal polyhistidine tag (6×His) was introduced into the integrative inducible expression vector pLEXSY_I-blecherry3 (Jena Bioscience, Germany) via BglII and NotI restriction sites.

Leishmania tarentolae cells of strain LEXSY host T7-TR (Jena Bioscience) were transformed with the rhodopsins expression plasmid linearized by SwaI restriction enzyme. Transformed clones were further grown and induced in 24-well plate and the fluorescence of induction marker protein Cherry was measured.

2.2.4. Biochemical methods

2.2.4.1. Gel electrophoresis – denaturing SDS-PAGE

The separation of denaturated proteins with sodium dodecyl sulphate (SDS) was performed using linear gradient gels. These gels have two considerable advantages over uniform concentration gels: they fractionate proteins over a wider range of molecular weights than any uniform concentration gel; the gradient in pore size causes significant sharpening of protein bands during migration [76]. The solutions used for gel preparation are given in **Table 2.4**.

The separation gel was casted by mixing “heavy” and “light” gels using the gradient mixer (Bio-Rad, Germany) as described previously [76]. A thin layer of isopropanol was overlaid, to fasten the polymerization by avoiding contact with oxygen. The separation gel polymerized overnight in the gel-casting chamber. Next morning after rinsing with deionized water, the stacking gel was poured and polymerized for 3 h.

For protein samples preparation the loading buffer was added (25 mM Tris-HCl, 50% Glycerol, 500 mM DTT, 10% SDS, 0.1% bromophenol blue, pH 6.8) in sample:buffer ratio 5:1. Mixture was incubated for 15 min at room temperature and loaded onto acrylamide gel.

Compound	16.2% "heavy" gel, ml	7.8% "light" gel, ml	4% stacking gel, ml
Sucrose	6 g	-	-
AA/BAA* 30%/0.8%	16	6.5	3
Water	4	15	14.5
3 M Tris pH 8.8	3.125	3,125	-
1 M Tris pH 6.8	-	-	2.5
SDS 10%	0.250	0.250	0.200
Total	26	25	20
TEMED 100%	4 µl	8 µl	20 µl
APS 20%	8 µl	16 µl	40 µl

Table 2.4 Resolving gel mixture for gradient gels.

* - mixture of 30% Acrylamide and 0.8% Bisacrylamide

The separation was carried out by applying an external voltage of 150 V (6 V/cm) for 1 h. Anode and cathode buffer: 25 mM Tris-base, 200 mM Glycine, 0.1% SDS.

2.2.4.2. TCA protein precipitation

Protein precipitation by TCA is widely used to concentrate samples for gel analysis in a polyacrylamide gel and to remove detergents and lipids, which can have negative influence on protein's migration in the SDS PAGE [77]. Brief procedure: to the protein containing sample 100% trichloroacetic acid (TCA) was added in ratio 1:10 (protein solution:TCA), to get a 10% final concentration. The mixture was incubated for 15 min at –20ºC or 30 min on ice. Then the sample was centrifuged for 15 min at 16000×g and 4°C. The supernatant was carefully discarded; the pellet was retained and resuspended in 50-100 µl 0.1 M NaOH. The gel-loading buffer was added (as described before) and sample was further analyzed by acrylamide gel.

2.2.4.3. Staining of proteins in gels

The protein bands were visualized by staining the gel with Coomassie Brilliant Blue staining solution (0.12% Coomassie Brilliant Blue G250, 10% H_3PO_4, 10% $(NH_4)_2SO_4$, 20% methanol) for 2 h. For destaining 3% acetic acid was used.

2.2.4.4. Western-Blot analysis

Proteins were transferred from gel onto NC membrane (Macherey-Nagel, Dueren, Germany) in the blotting tank apparatus (Bio-Rad, Germany) for 1 h at 90 V. The transfer buffer (48 mM Tris-base, 38.6 mM Glycine, 0.04% SDS, 20% Methanol) was used to pre-treat the membrane, the gel and the filter paper. After transfer, the membrane was briefly rinsed with TBST buffer (20 mM Tris-HCl, 100 mM NaCl, 5% Glycerol, 0.05% Tween20, 0.02% NaN_3, pH 8.0), and afterwards incubated in TBST-milk buffer (20 mM Tris-HCl, 100 mM NaCl, 5% Glycerol, 0.05% Tween20, 0.02% NaN_3, 5% dry milk, pH 8.0) overnight. Next morning it was incubated for 1.5 h with the primary antibodies (PentaHis mouse lgG antibody, Qiagen), diluted (1:2000) in 8 ml TBST-milk buffer. After two 10-min washes with the same buffer the membrane was incubated with the alkaline phosphatase conjugated goat anti-mouse secondary antibodies (Sigma-Aldrich, Germany) in 8 ml TBST-milk buffer (with 1:2000 dilution). Finally, the membrane was washed two times with TBST buffer. Substrate NBT/BCIP solution (Thermo, USA) was used to elicit the signal by chemiluminescence, yielding an intense, insoluble black-purple precipitate when reacted with alkaline phosphatases.

2.2.5. Protein purification

2.2.5.1. Isolation of *E.coli* total membranes

Cell pellets were resuspended in ice-cold homogenization buffer 30 mM Tris-HCl, 300 mM NaCl, pH 8.0 (if not stated different), proteases inhibitor mixture cOmplete® (1 tablet per 50 ml of buffer; Sigma-Aldrich, Germany) in ratio 1:5 (1 g of cells per 5 ml of buffer). Deoxyribonuclease I from bovine pancreas (Sigma-Aldrich, Germany) was added to remove DNA from the cell suspension after lysis (5 mg of DNAse per 30 g of cells). Prior to cell lysis all-*trans* retinal in Triton X-100 (the total concentration is 5 μM of all-*trans* retinal,0.1% Triton X-100) was added and gently mixed to avoid foam formation. The cells were disrupted by passing six times through the precooled to 4°C microfluidizer (M110-P, Microfluidics, Newton, USA). The suspension was centrifuged for 1 h at 4°C in the fixed-angle rotor (70Ti, Beckmann, USA). After centrifugation membrane (insoluble) fractions were collected and either frozen in liquid nitrogen and stored at -80°C, or immediately processed through solubilisation procedure. The membranes were sedimented by centrifugation at 120000×g for 1 h at 4°C. The supernatant was discarded; the pellet was resuspended in the ice-cold solubilization buffer (30 mM Tris-HCl, 300 mM NaCl, cOmplete mixture, pH 8.0, if not stated different).

The produced thereby total membranes were contaminated with insoluble cell constituents of non-membrane origin.

2.2.5.2. Protein solubilization

Prior to the solubilisation, raw total membranes in solubilisation buffer were processed in glass Dounce tissue grinder (Wheaton, USA).

For "preparative scale" purification DDM was used. First 1% of DDM and 5 μM all-*trans* retinal were added to the membrane suspension. The mixture was incubated at 4°C overnight with moderate stirring. Insoluble proteins and lipids were separated by centrifugation at 120000×g for 1 h at 4°C. The supernatant was further used. In later experiments overnight membrane suspension was treated three extra times with the precooled to 4°C microfluidiser and being kept on a stirrer for 2 h at 4°C prior to the centrifugation.

2.2.5.3. Affinity chromatography

Ni^{2+}-NTA beads (Qiagen, Germany) were first washed with 5 column volumes (CV) of deionized water and then pre-equilibrated with the same volume of solubilization buffer containing 1×CMC of detergent.

The supernatant containing solubilised proteins was incubated with pre-equilibrated Ni^{2+}-NTA beads (Ni^{2+}-NTA volume (ml) to cells mass (g) ratio is 1:2 if not stated different) at 4°C for overnight under gentle rotation. Then resin was loaded onto chromatographic column (GE Healthcare, USA) in a certain way: on the bottom of the column (prior to loading the protein-containing resin) 0.5 ml of fresh "control" resin was loaded in order to confirm the absence of unbound protein. The column then was packed with protein-containing resin using gravity flow with flow restriction up to 0.5 ml/min for column 1 cm in diameter. If the control resin changed its blue colour to the intense colour of protein (rhodopsin) the column was packed and processed further and a flow-through was re-incubated at 4°C under gentle spinning for another 5 h with 1/10 volume of initially pre-equilibrated resin (i.e. Ni^{2+}-NTA volume (ml) to cells mass (g) ratio is 1:20). The "control" resin volume allows to visually determine the unbound protein by colour. When it is impossible to discrete visually the supernatant with and without protein in question just by colour the flow-through was analysed with WB.

After loading the resin was washed with 5×CV of washing buffer (30 mM Tris-HCl, 300 mM NaCl, 30 mM Imidazole, 0.2% DDM, pH 7.5 or 8.0 depending on a processed protein)

using cooled to 4°C AKTA purifier chromatographic system (GE Healthcare, USA). Bound protein was eluted in 2×CV of elution buffer (30 mM Tris-HCl, 300 mM NaCl, 300 mM Imidazole, 0.2% DDM, pH 7.5, if not stated different).

Different chromatography parameters were checked for optimization of the purification: the beads volume, the concentration of detergents, the concentration of imidazole at washing stage. All these trials were done using the analytical scale purification protocol (1g of cells).

2.2.5.4. Size-exclusion chromatography (gel-filtration)

In order to separate different oligomeric states and soluble aggregates of the protein and to remove imidazole size-exclusion chromatography was used. The protein suspension was concentrated using the centrifugal filter (Millipore, USA) with membrane cut-off 10 kDa to a concentration of 4 mg/ml. Insoluble aggregates were removed by centrifugation at 20000×g for 20 min. Supernatant was loaded in portions of 0.5 ml onto Superdex® 200i 24 ml column (GE Healthcare) pre-equilibrated with 39 ml of suitable buffer (30 mM Tris-HCl, 300 mM NaCl 0.2/0.1% DDM, pH 7.5/8.0). The column flow rate was adjusted to 0.5 ml/min (corresponding pressure is 2.5 MPa). The fractions corresponding to peeks on the chromatogram were pooled and further analysed by SDS-PAGE gel electrophoresis. The column calibration curves are shown on the **Figure 2.2**.

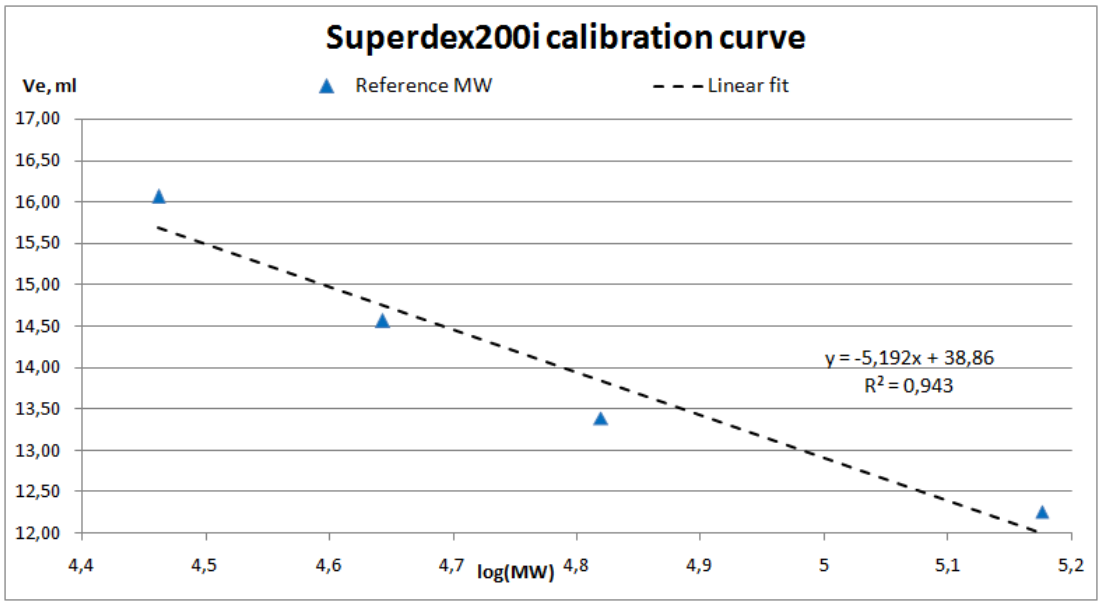


Figure 2.2 Calibration curves for Superdex 200i (GE Healthcare, USA) 24 ml column. Globular proteins were used for reference.

After SDS-PAAG analysis appropriate fractions were processed. Absorption spectra for each fraction was measured.

2.2.5.5. Anion-exchange chromatography

MonoQ™ 1 ml ion-exchange column (GE Healthcare, USA) was used (when needed) as an extra purification stage to separate rhodopsin from contamination.

Due to high cationic strength of MonoQ™ resin, the fractions from SEC were dialyzed (membrane cut-off 14 kDa) twice (once for 5 h and once overnight) at 4°C against 100-fold excess of column equilibration buffer (30 mM Tris-HCl, 0.2/0.1% DDM, pH 7.5/8.0). Next morning dialysis was terminated and the protein solution was centrifuged at 20000×g for 20 min at 4°C to remove aggregates. The clear supernatant was loaded with a flow rate of 0.1 ml/min onto pre-equilibrated with 5×CV of equilibration buffer MonoQ™ column (not exceeding the manufacturers recommendations for maximum amount 45 mg of total protein loaded). Protein was eluted by salt gradient (in equilibration buffer) up to 1 M NaCl in 20×CV at the same flow rate. Fractions were collected and further analyzed by SDS-PAGE and Western-blot.

In case of MonoS™ column the same protocol was used with deviations only in the equilibration buffer (30 mM Tris-HCl to 30 mM Na-HEPES).

2.2.5.6. Protein reconstitution into liposomes

The 1ml of 2% lipid in chloroform mixture was dried with nitrogen in a glass 15-ml tube to form a thin layer of lipid. The tube was left then for 1h at RT in a vacuum chamber to remove the chloroform completely. After, the lipid was solubilised in 1ml of 2% Sodium cholate (or 2% cholic acid) and was transferred to a sample tube.

All the further steps were done under the minimal illumination. The lipid-cholate mixture was briefly sonicated with minimum power and 1 ml of 2 mg/ml protein solution was added (gently hand-mixed to avoid foam formation). In order to remove the detergent from the sample amberlite (Amberlite XAD-2, Sigma-Aldrich, Germany) bids were added in next manner:

1. ~1/4 of volume, incubation for 1 h at appropriate temperature;
2. replaced with fresh amberlite ~1/2 of sample volume and incubated for a night;
3. replaced with fresh amberlite ~1/2 of sample volume and incubated for another 1 h.

Extra incubation stages with amberlite were added if necessary. The incubation temperature was set as low as possible, but 2-5°C above of the phase transition temperature of a lipid being used.

After incubation the proteoliposomes mixture was extruded through the polycarbonate membrane filter with the pores diameter 0.2 μm.

2.2.5.7. Protein reconstitution into nanodisks

The reconstitution of protein into MSP nanodisks was done similar to [78]. Brief procedure is next. Solubilised protein was mixed with expressed in *E.coli* His-tagged MSP protein (MSP1E3D1, MSP1D1 or MSP1) and lipid (DMPC or POPC) in ratio 147:1:0.5 (as an example is molar ratio of DMPC:MSP1E3D1:PGr1, i.e. 294 DMPC molecules and one PGr1 molecule tightened with two molecules of MSP1E3D1). If other lipids, MSP variants or protein being used the initial construction mixture should be recalculated considering the inner surface area of nanodisk, each lipid molecule and oligomeric state of protein to reconstitute.

The mixture was then briefly sonicated at lowest power possible and amberlite bids were added in the similar manner as in the liposome reconstitution protocol:

1. ~1/4 of volume, incubation for 1 h at appropriate temperature;
2. replaced with fresh amberlite ~1/2 of sample volume and incubated for a night;
3. replaced with fresh amberlite ~1/2 of sample volume and incubated for another 1 h.

The sample then was applied to SEC and the fraction corresponding to Nanodisks with rhodopsin were taken. The small portion of nanodisks was analysed on SDS-PAGE and/or WB.

The surface area values of different lipids and empty nanodisks being formed by different variants of MSP protein were taken from [78], while number for protomers being in nanodisks should be estimated empirically due to the different oligomeric states of protein in SEC and nanodisks.

2.2.6. Characterization

2.2.6.1. Time-resolved Laser Spectroscopy

Time-resolved laser spectroscopy measurements were performed on a solubilised rhodopsins and rhodopsins reconstituted into liposomes/nanodisks in the Hannover Medical School, Institute of Biophysical Chemistry by Dr. Igor Chizhov.

For measurements of the detergent solubilized protein, the concentration of protein was adjusted to approximately 0.5 mg/ml. Concentration was picked up for each sample individually so the retinal absorption spectrum maximum of rhodopsin was 0.6-0.7 AU.

The 1%POPC/DMPC liposomes containing rhodopsin (0.5-0.7 mg/ml of functional protein) were prepared as described before.

2.2.6.2. Dynamic light scattering to study samples monodispersity

The measurements were carried out using Dyna Pro-E-20-660 devise (Proterion corp., USA) in quartz cuvettes with 57 µl volume (Helma, z=8.5 mm, path length=3 mm).

2.2.6.3. Protein *In vivo* functional activity

The rhodopsins' functional activity was tested using *E.coli* grown under the same protocol as for overexpression procedure. During further sample preparation and measurements cells exposure to light was minimised Then, cells were harvested from 50 ml of fresh culture via centrifugation at 4°C 4000 g for 10 min. Transparent growing media was eliminated from tube, cells were gently resuspended in cold 4°C salt solution (100 mM NaCl, 100 mM KCl, Na_2SO_4 or K_2SO_4; pH adjusted to 6.5-7.5 if needed) and incubated at 4°C for 10 min with gentle mixing on roller mixer in the dark. This washing procedure was repeated twice. On a third time cells were incubated overnight.

Next morning the salt solution was changed twice and OD_{600} was adjusted to 8, tubes were covered with a foil. Prior to measurements the ionophore (100 µM CCCP or/and 10 mM TPP) was added (if needed; culture samples both with and without ionophore were incubated for 1 h as described above). For each measurements 1.5 ml of culture was taken. Measurements were performed in a glass beaker (see **Figure 2.3**).

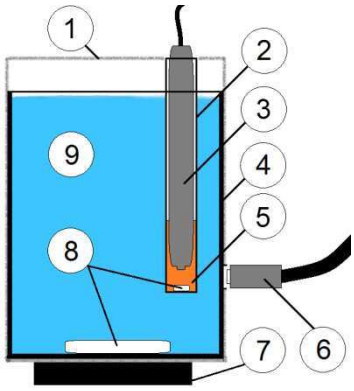


Figure 2.3 Schematic representation of setup made for *in vivo* activity measurements. 1 - aluminium foil, 2 - thin glass cylindrical tube, 3 - pH-meter electrode, 4 - thin-glass beaker, 5 - sample (depicted in orange), 6 - light guide from light source, 7 - magnetic stirrer, 8 - magnetic stirring bars, 9 - ice (mainly) and water.

Briefly, 500-ml glass beaker covered with aluminium foil was filled with an ice-water mixture (0°C to prevent sample from warming up) and placed on a magnetic stirrer in a dark

room. The 1.5-ml sample was loaded into the small diameter (2 mm wider than a pH electrode) glass tube dipped into the ice. The pH electrode was putted into the same tube and was left for 30 min under middle-speed stirring for equilibration. Both the tube and beaker are aligned in the way so both stirring bars were spinning and the tube was close to the beaker's wall (sample levelled with the hole in foil and light fiber). After, light source was turned on (Intralux 5000-1, Volpi, Switzerland; 150 W light bulb from Ushio, Japan) and the data from pH electrode was recorded via LabQuest Mini (Vernier, USA) interface.

2.2.6.4. *In vitro* functional activity

Freshly prepared 1% liposomes with final protein concentration of 1 mg/ml were dialysed three times against 200× volume of a salt solution (100 mM NaCl, 100 mM KCl, Na_2SO_4 or K_2SO_4; pH adjusted to 6.5-7.5 if needed) for 8 h/overnight at 4ºC under minimum illumination. Prior to the measurements the ionophore (100 μM CCCP or/and 10 mM TPP) was added and liposomes were incubated at 4°C for 1h on a roller mixer in the dark.

The measurement setup was used as described above.

2.2.6.5. Black lipid membrane (BLM) tests

The BLM measurements were performed in The Max Planck Institute for Biophysics, Frankfurt in similar to [57][79] way. Briefly, for measurements protein was reconstituted to 1% asolectin liposomes with 1mg/ml of protein. The electrolyte solution was 20 mM HEPES, pH 7.4, without any Na^+,K^+ or Cl^- ions. The system was illuminated with a mercury arc lamp (Osram HBO 100) at wavelengths >455 nm for up to 8 sec.

2.2.6.6. Crystallization

Fractions corresponding to a purified protein after size-exclusion chromatography were concentrated to final protein concentration 20-30 mg/ml using centrifugal filter with membrane cut-off 10 kDa. Protein concentration was controlled by NanoDrop spectrophotometer (Thermo, USA).

The detergent concentration was controlled by IR spectroscopy and the necessary amount of it was added if necessary. The protein solution was added to monooleoyl in a ratio 1:2 (vol:vol; if not indicated otherwise) and several passes through interconnected syringes for cubic phase preparation were performed. Cubic phase stored overnight at 22°C and was used in the proceeding morning.

Crystallization was carried out using robot for *in meso* membrane protein crystallization (NT 8 Crystallography, Formulatrix, USA). Crystallization probes were visualized and systematically scanned by automated system for imaging crystallization probes (Rock Imager 1000, Formulatrix, USA). The crystals were fished out with cryoloop (Hampton research, Aliso Viejo, USA) and flash frozen in liquid nitrogen. All crystallization experiments were done in the membrane protein crystallization platform of Institute of Structural Biology, Grenoble, France.

3. Results and discussion

3.1. Protein selection

The protein search was based on the primary structure of KR2 sodium pump (UNP N0DKS8), that was recently characterised. There were few main criteria of search that take into account the possible optogenetic application of proteins:

- active transport (pump) rhodopsin needed for membrane repolarisation;
- the probable cation specific pumping activity or non-characterised protein with new motif

Due to preselected choice of expression system (protein was supposed to be produced in *E.coli* since this system being generally accepted for protein production, including microbial rhodopsins), another criteria was the cysteine amino acid content, since cysteine bridges might be crucial for proper protein folding.

The initial BLAST[80] sequence search reviled the list of rhodopsins (along with presumable rhodopsins) with varying similarity and E-value indexes. The E-value less than 10^{-20} was considered as "stay" within rhodopsin proteins family. This threshold leaded to selection of 27 possible targets for further investigation.

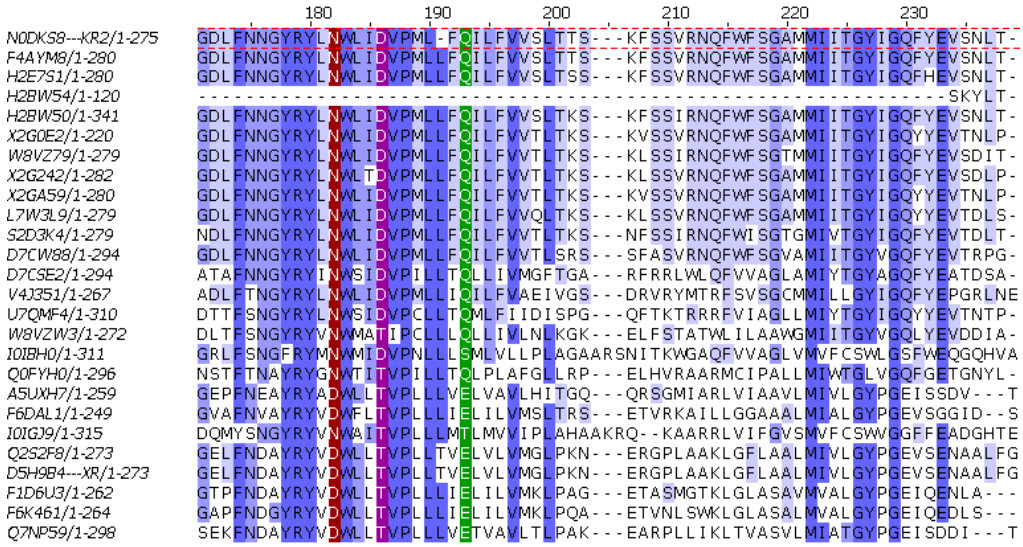


Figure 3.1 Sequence alignment of 27 picked targets in order of similarity decrease (E-value increase). The residues corresponding to D85 in bR (N112 in KR2) depicted in dark red, T89 (D116 in KR2) - purple, D96 (Q123 in KR2) - green. The identity of particular residue in each column depicted in shades of blue (the dark blue corresponds to >80% similarity, whereas non-colored - <40%). KR2 sequence emphasized with dashed red line.

These targets were aligned to KR2 in order to clarify the active center motif.

All the sequences contained conservative retinal-binding lysine residue. The transition from upper results batch (D7CW88 and higher) to a lower one is associated with rapid identity decrease (60.9% for D7CW88 and 47.8% D7CSE2) and E-value grow (2.3×10^{-109} for D7CW88 and 1.4×10^{-68} D7CSE2). Due to high identity (>60%), low E-value ($<10^{-100}$) and predicted TM3 helix similarity sequences upper batch was excluded from novel rhodopsins search. Another point is a rapid interest among scientific society to KR2-like proteins, thus selection of target proteins among those from upper batch might overlap with other groups targets.

Among proteins from batch 2 (lower one) our attention attracted two proteins from *Phycisphaera mikurensis* being recently isolated from marine algae [81]. The first view on the primary sequence of these two proteins (here and after named as PMr1 and PMr2; UNPs are I0IBH0 and I0IGJ9 respectively) revealed the unique NDS and NTT motifs which were not reported before and thus the function of these proteins was unclear.

It was shown before that radiation of bR with UV light triggers the photocycle of later, similar to that being started with visible light [63]. This raised the question if this feature is unique to bR only or inherent to other microbial rhodopsins as well. Among others we noticed eukaryotic rhodopsin (here and after named PGr1; UNP F6K461) from flagellate eukaryote *Polarella glacialis*. This protein along with a relatively high aromatic residues content (10%) is not characterized and has presumably (DTE motif) proton pumping functionality, which might be a good target to check the hypothesis as well as might be a good optogenetic tool replacing eArch protein.

3.1.1. RNA secondary structure optimisation

The protein characterization and crystallographic structural studies require relatively high amounts of purified protein. In our crystallization experiments we use 96-well crystallization plates. Each plate corresponds to ca. 30-40 µl of lipid phase with protein concentrations 20-40 mg/ml, i.e. more than 1 mg of protein might be needed for one sample plate. Thus, all the aspects of heteroexpression of proteins should be considered in the beginning of work to get most of the expression system capable of.

The first stage is the optimization of protein in question gene. It's know already for a while that different organisms might use different genetic code tables for translation (for instance, *M.pneumoniae* has codon CCG assigned to arginine [82], while *E.coli* - to proline). Moreover, different organisms, even thought might have the same codon-amino acid assignment, might have different frequency of occurrence of synonymous codons (this phenomenon called codon

usage bias) and thus corresponding tRNA occurrence frequency may influence the translation speed. To overcome these problems PGr1, PMr1 and PMr2 rhodopsin genes were optimized according to a target expression system codon usage. For this purpose, the GeneArt® service (ThermoFisher Scientific) was utilized. This service does both the mRNA secondary structure and codon usage optimizations. Nevertheless, the mRNA secondary structure of first 50 nucleotides of each gene was also manually optimized to avoid the mRNA "pin" formation on the gene starting region.

The two cloning sites NdeI and XhoI were chosen as most appropriate since they both uniquely present (1 site per plasmid) in preselected plasmid system (pIVS and pSCodon1.2) and are commonly used for cloning in other plasmids. Thus, during gene optimization the motifs of these sites (CATATG for NdeI, CTCGAG for XhoI) were avoided in genes. Sometimes it's difficult to avoid sites motifs without significant loss in corresponding codon host occurrence frequency.

The rhodopsins genes then were synthesised at Eurofins Genomics (Germany) and *E.coli* TOP10 strain was transformed with plasmids being received (pEX-A2-I0IBH0eo, pEX-A2-I0IGJ9eo and pEX-A2-F6K461eo, here and after "eo" in plasmid name denotes gene optimisation for *E.coli* expression systems) for plasmid amplification and stock purposes.

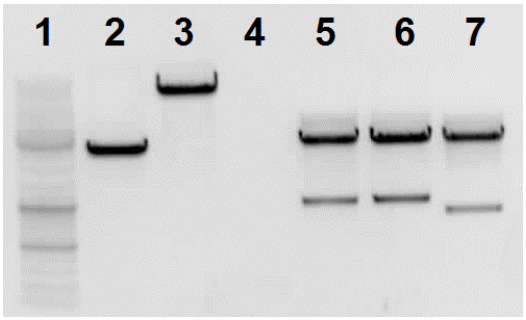


Figure 3.2 Agarose gel image of plasmids digested with NdeI and XhoI ferments: 1 - GeneRuler Mix, 2 - pIVS, 3 - pSCodon1.2, 4 - empty space, 5 - pEX-A2-I0IBH0eo, 6 - pEX-A2-I0IGJ9eo, 7 - pEX-A2-F6K461eo. Gene sizes (lower lines) in samples 5,6 and 7 are 936bp, 948bp and 795bp respectively.

Initially, the expression system based on *E.coli* SE1 strain with StabyCodon (pSCodon1.2 plasmid) plasmid was chosen due to reliable toxin/antitoxin stabilization, which improves the plasmid stability within the clones. For this purpose, both pEX-A2-F6K461eo and pSCodon1.2

plasmids were bi-digested with Fermentas® NdeI and XhoI cleavage enzymes. In addition plasmid pIVS was "cut" as well in order to make cloning plasmid pIVS-F6K461eo[e].

3.2. Polarella glacialis PGr1 rhodopsin (UNP F6K461)

The PGr1 protein is a putative eukaryotic proton pumping rhodopsin from *Polarella glacialis*. The protein disorder prediction tool confirmed expected 7TM helix secondary structure and absence of long disordered regions on both N- and C-termini. The closest E-value among known structures was 1.08×10^{-38} (PDB ID 5AZD, identity 38%).

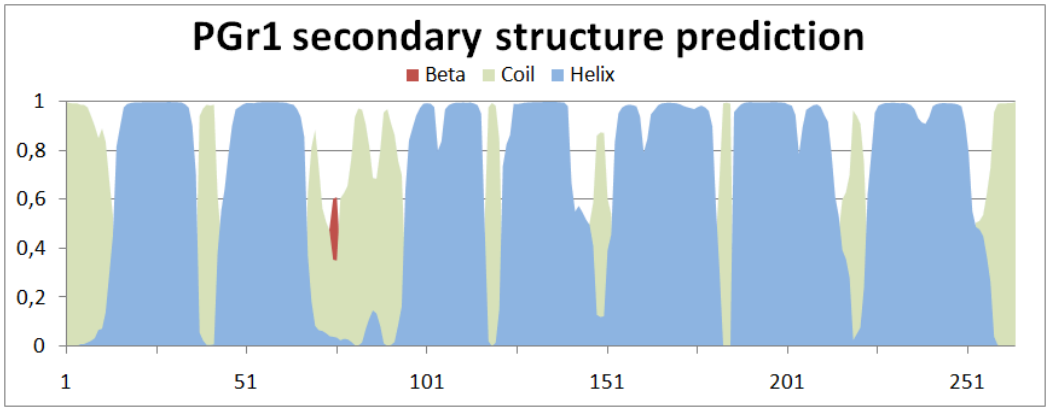


Figure 3.3 PGr1 rhodopsin secondary structure prediction results, made with RaptorX server [83]

Thus, we decided to start expression tests and trials with full-sized gene.

3.2.1. Expression and purification of PGr1

3.2.1.1. PGr1H6 expressing strain and plasmid

The first tests with SE1 strain being transformed with pSC-F6K461eoH6 revealed relatively high protein yields and thus this strain-plasmid combination was selected as a basis for further expression optimization tests. The plasmid schematic representation depicted on .

During the first tests with AIM-5052 the pelleted cells being observed to be "layered" – the more dense cells from the lower layer were less colored than those from the top layer (with less density). We assumed that this might be either due to inhomogeneous retinal absorption, or because of the presence of two cells populations in the media.

[e] The need of using separate plasmid for cloning and construction purposes (among other differences) lies in the significant difference of expression and cloning plasmid in sizes (the so called "minimal" plasmids pIVS and pSCodon1.2 are 2168 bp and 5837 bp respectively). The PCR ferment DNA polymerase stability significantly reduces upon amplification time extension and thus leading to improper PCR product.

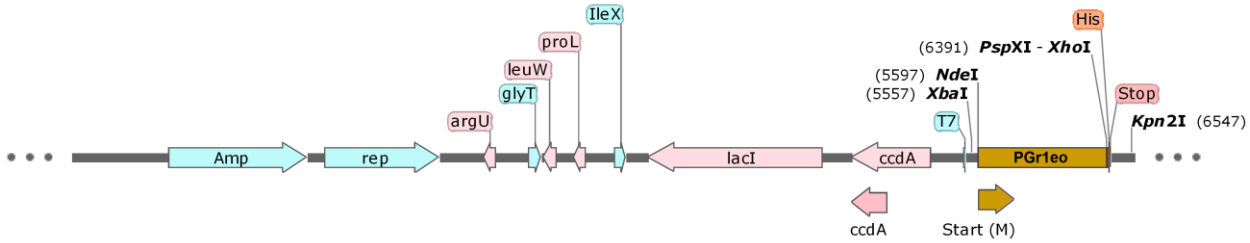


Figure 3.4 Linearized scheme of pSC-PGr1eoH6 plasmid with most relevant cleavage sites and features denoted.

The retinal solubility in water is approximately 50 µM, but this concentration isn't applicable for stock solution since its concentration in media is in micromolar range as well, and thus stock solution is typically prepared in ethanol. Upon addition of such solution into water-based media containing around 0.8-1.0 AU of cells retinal, due to its hydrophobic nature, seems to form a surface film and being fast absorbed by a small portion of cells in pre-surface media region leading to a cells differentiation on the other end. To eliminate this effect we pre-solubilized retinal in Triton X-100 detergent. This allowed to mix the retinal before it being absorbed by small portion of strain cells and thus significantly reduced the pelleted cells "layerization".

In order to improve overall protein yield (test yield varied among experiments thus expression parameters that had the most influence on protein amount must be specified) and to solve the cells population problem we decided to test for most appropriate induction time/way. It should be noted, that initial tests were done with AIM-5052 [75], which extends the induction time and thus might lead to a cells differentiation in short-termed induction experiments. The auto induction media AIM-5052 was preferred due to the convenience of whole method. Nevertheless, both AIM and IPTG induction being tested in order to achieve the sufficiently high yields of protein. To do this, the two separate but parallel experiments were set: with AIM and with 1Y1T IPTG media.

Since AIM-5052 media allows to vary only one parameter - the starting OD_{600} of the culture - we decided to find the induction moment for 5 different OD_{start}. The preculture was prepared as described in methods. Retinal was added after 6.5 h to all samples. The culture was vigorously shaking at 130 rpm, 37°C.

Despite different starting OD_{600}, it seems that induction appears in the same OD of 1 AU. The protein content of samples taken after 11.2 h and 24 h of expression start was then analyzed for (normalized to OD).

Time, h	OD_{600}=0.05	OD_{600}=0.1	OD_{600}=0.2	OD_{600}=0.4	OD_{600}=0.6
0,0	0,05	0,10	0,20	0,40	0,60
1,3	0,06	0,09	0,15	0,29	0,40
2,3	0,07	0,11	0,19	0,39	0,52
3,0	0,09	0,14	0,27	0,51	0,67
4,5	0,19	0,34	0,59	0,92	1,01
5,6	0,33	0,55	0,80	1,09	1,14
6,6	0,59	0,80	0,99	1,16	1,14
7,5	0,93	1,09	1,20	1,21	1,19
8,3	1,17	1,25	1,26	1,30	1,22
9,5	1,55	1,43	1,41	1,46	1,46
11,2	1,51	1,47	1,46	1,48	1,35
24,0	1,73	1,62	1,62	1,58	1,46

Table 3.1 The optical density dependence of AIM-5052 expression test with SE1 pSC-PGr1eoH6. Blue boxes depict depletion of glucose in media; yellow box - 250-500 mg/L glucose, red - >500 mg/L glucose.

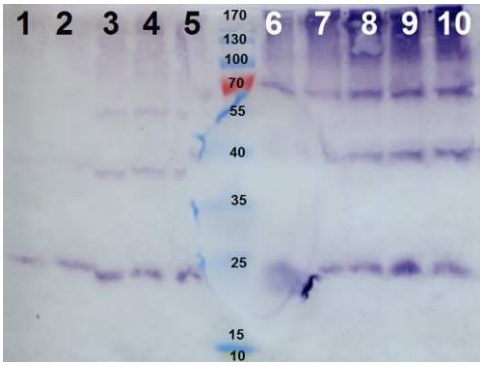


Figure 3.5 WB (PentaHis antibodies) of Samples taken after 11.2 h (1-5) and 24 h (6-10). 1 (and 6) - 0.05 AU, 2 (and 7) - 0.1 AU, 3 (and 8) - 0.2vAU, 4 (and 9) - 0.4 AU, 5 (and 10) - 0.6 AU. The PageRuler molecular weight marker was used (weight in kDa depicted).

Apparently, there's no significant difference among samples 8-10 and 6-7 in final protein concentration per cell. The difference in protein per cell quantity between two sample groups 8-10 and 6-7 seems to be due to overall difference in induction (expression) time (lower starting OD of culture leaded to a later induction and thus shorter expression time). But in terms of total protein yield samples 3/8 (starting OD_{600}=0.2 AU) conditions were preferred due to higher final OD and thus cells (protein) quantity.

Second expression test was done with IPTG induction of the same strain (*E.coli* SE1 containing pSC-PGr1eoH_6). This test was done to figure out the most appropriate induction OD of the culture and induction rapidness (IPTG concentration). The pre-culture was prepared as described in methods and starting dilution (OD_{600}) of the culture was 0.2 AU. The culture was vigorously aerated at 140 rpm, 37°C during the test. The induction occurred at different OD_{ind} 0.8, 1.0, 1.2, 1.5 and 2.5 AU. The data table is present in Appendix Table 1.

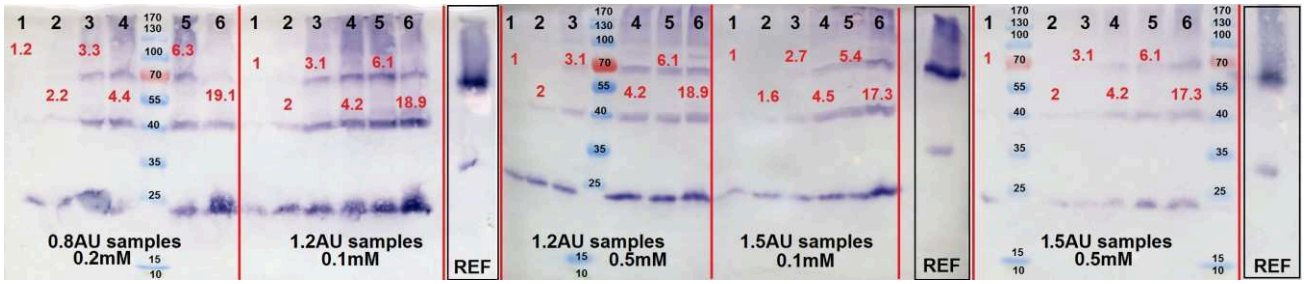


Figure 3.6 The WB (PentaHis antibodies) of IPTG induction expression test results analysis. Each separate box (red lined) represents samples with the same particular OD_{ind} and IPTG concentration used. Time in hours since induction depicted with red letters. The reference protein quantity is the same for all images. All samples normalized to a cell density of 1 AU and volume 1ml.

The samples corresponding to 0.8, 1.2 and 1.5 AU OD_{ind} and different C_{ind}(IPTG) being taken approximately each hour (see Figure 3.6). According to our estimation, the amount of protein per cell was highest if culture being gradually induced (low 0.1 mM IPTG concentration) at OD_{600}=1.2 AU. Since in AIM-5052 culture induced approx at 1.0 AU (corresponds to the absence of glucose in media), the additional 0.05% glucose were added to AIM (to the final concentration of 0.1%). This shifted induction to ~1.1-1.2 AU. The combination of both IPTG induction OD value with auto induction method leaded to steady expression levels of ~30 mg of purified solubilized protein from 6 L of culture (i.e. 5 mg/L).

The parameters of protein $PGr1H_6$ construct are:

- the isoelectric point 5.29
- MW(PGr1)=29.96 kDa
- PGR1 retinal absorption maximum 530 nm
- extinction coefficient at 280 nm 76100 $M^{-1}\times cm^{-1}$

In order to purify $PGr1H_6$, the total membranes were solubilized in buffer containing 30 mM Tris-Cl pH 7.5, 300 mM NaCl, 1% DDM, cOmplete® protease inhibitor, 5 µM all-*trans* retinal[f]. The protein was then purified with NiNTA affinity chromatography due to a presence of poly-His (6xHis residues) tag at C-terminus of $PGr1H_6$ construct.

[f] During the purification experiments we noticed that peak ratio (here and after PR=Abs(280 nm)/Abs(Retinal peak maximum); we use this value as indirect measure of rhodopsin protein quality) of purified protein can be reduced (reed improved; the smaller is better) with addition of extra 5 µM all-*trans* retinal to a total membrane solubilization mixture.

3.2.1.2. PGr1H6: affinity chromatography

The PGr1-containing solubilized protein mixture was applied to NiNTA pre-equilibrated resin. In order to visually control the PGr1 elution process from NiNTA resin, during the column packing 0.5 ml of fresh non-used and pre-equilibrated resin were extra added to form a layer of fresh NiNTA for comparison on top of the column. The color of this layer should be the same as the rest of the resin after protein elution. To remove the nonspecifically bound contamination from NiNTA column, the column was washed with washing buffer 30T7.5 (here and after, short designation of Tris-Cl buffers, where 30 represents millimolar concentration of buffer salt and 7.5 corresponds to pH), 300 mM NaCl, 30 mM Imidazole, 0.2% DDM. The lower detergent concentrations leaded to protein aggregation on resin. After washing, $PGr1H_6$ was eluted with elution buffer (30T7.5, 300 mM NaCl, 300 mM Imidazole, 0.5% DDM; the decrease of DDM concentration in elution buffer led to slow protein degradation and precipitation) and fractions corresponding to absorbance peaks were analyzed with SDS-PAGE and WB. The typical elution profile is on the Figure 3.7. On this figure, $PGr1H_6$ eluted at V_e 110-130 ml. The absorbance of first ~40 ml in visible light is due to presence of retinal in applied solubilized protein mixture and due to specific contaminant, that was co-solubilized with rhodopsin (visible light absorbance maximum of this protein is ~420 nm). The NiNTA fraction containing PGr1H6 (110-130 ml on Figure 3.7) were taken and total protein concentration was measured.

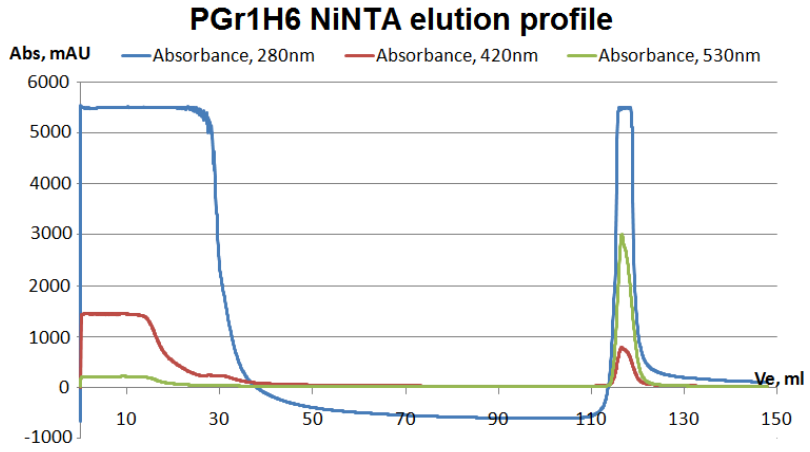


Figure 3.7 Typical $PGr1H_6$ NiNTA elution profile. The drop of absorbance at 280 nm to negative values is due to normalization to elution buffer, which contain imidazole (absorbing at 280 nm).

3.2.1.3. PGr1: size-exclusion (SEC) chromatography

Combined affinity chromatography fractions were divided to portions containing total up to 4mg of protein and these portions were applied to SEC. The SEC column was pre-equilibrated

with GF buffer 30T7.5, 300 mM NaCl, 0.5 mM EDTA, 2 mM 6AHA and 0.2% DDM. The typical SEC profile is on the Figure 3.8.

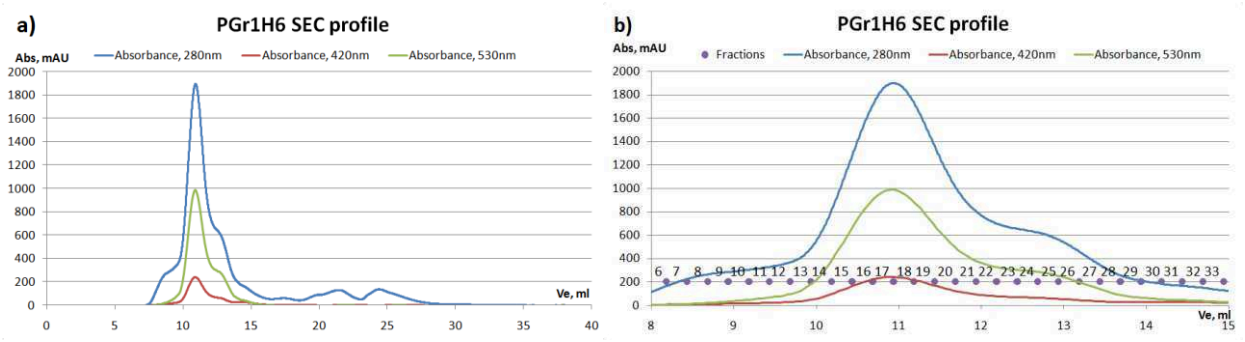


Figure 3.8 **a)** The typical PGr1H$_6$ SEC elution profile and **b)** enlarged rhodopsin containing segment (V_e 8-15 ml). The fractions starting point along with their numbers depicted with purple circles. Each fraction is 0.2 ml.

The SEC fraction corresponding to V_e 8-14 ml were analyzed with SDS-PAGE (see Figure 3.9). According to the SEC trace, the colored (functional) protein was in two oligomeric states (regions 10-12 ml and 12-14 ml, Figure 3.8b). The 8-10 ml region corresponds to high molecular weight aggregates without retinal (absorbance at 530 nm close to zero).

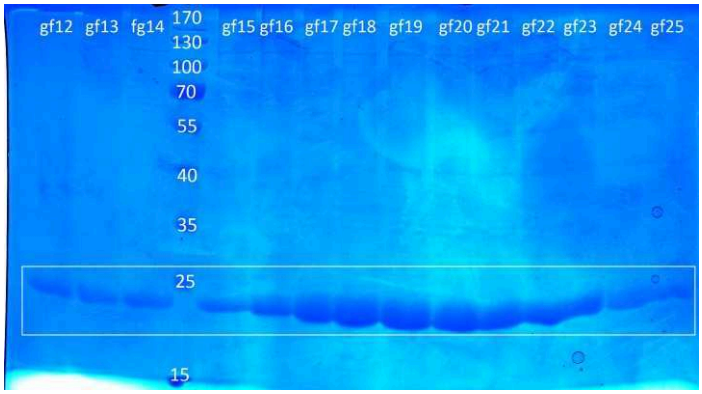


Figure 3.9 The SDS-PAGE gel of SEC fractions (gf12-25) of PGr1H$_6$ rhodopsin. MW marker Page Ruler being used (weights denoted in kDa).

Unfortunately, due to the nature of the SDS-PAGE method, gel revealed mostly the presence of protein in monomeric state. According to our SEC calibrations, the peak at V_e~11 ml (gf18) corresponds to a protein of particle ~200 kDa size. Thus, taking into account apparent DDM micelle size of 70 kDa, most probably protein forms a pentamers.

After SEC, the absorbance spectrum of each fraction was measured and fractions with PR=1.8 or less were taken for further characterization and crystallization.

3.2.1.4. PGr1 MonoQ anion exchange chromatography

In early experiments the SEC trace and proceeding WB/SDS-PAGE analysis revealed the presence of contaminant protein with MW~55 kDa absorbing at 420 nm (one of the reasons why we started to use additional 420 nm wavelength in our purification procedures; see Figure 3.10) and twining bands at ~35 kDa. In order to eliminate contaminant we decided to apply ion exchanging chromatography (more specific, MonoQ anion exchange column due to a negative charge of $PGr1H_6$ at pH 7.5).

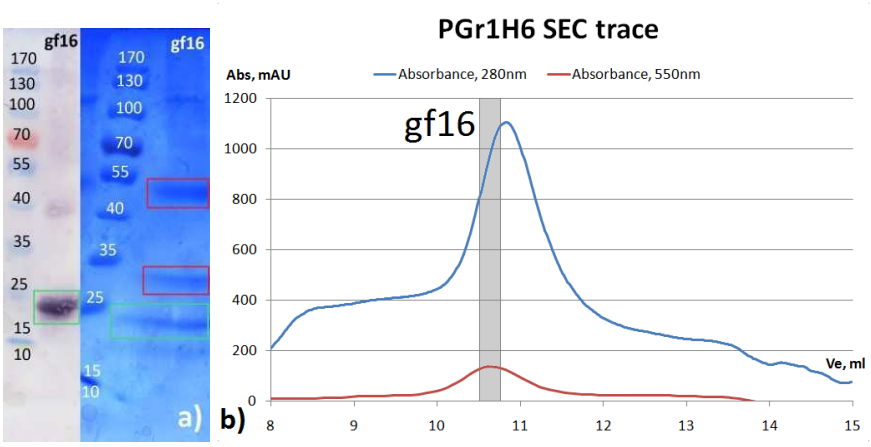
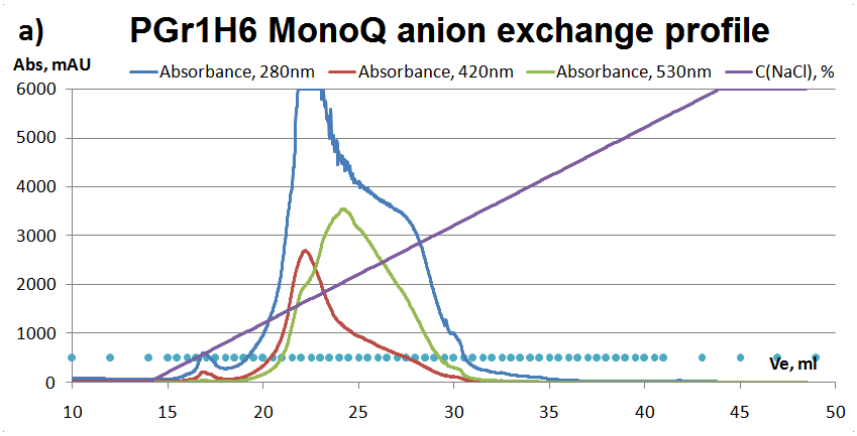


Figure 3.10 **a)** WB and gel of SEC fraction gf16 of early purification experiments; the green box depicts $PGr1H_6$, while the red box - contamination. **b)** Corresponding SEC trace; gf16 (10.5-10.75 ml) depicted with grey box.

In order to bind the rhodopsin to the MonoQ column resin, we dialyzed the protein corresponding SEC fraction against 30T7.5 buffer to eliminate the salt that might interfere with binding process[g]. The column then was washed and pre-equilibrated according to a manufacturer instructions manual with 30T7.5, 0.2% DDM buffer.



[g] After dialysis $PGr1H_6$ was kept at +4°C and remained stable for extended period of time.

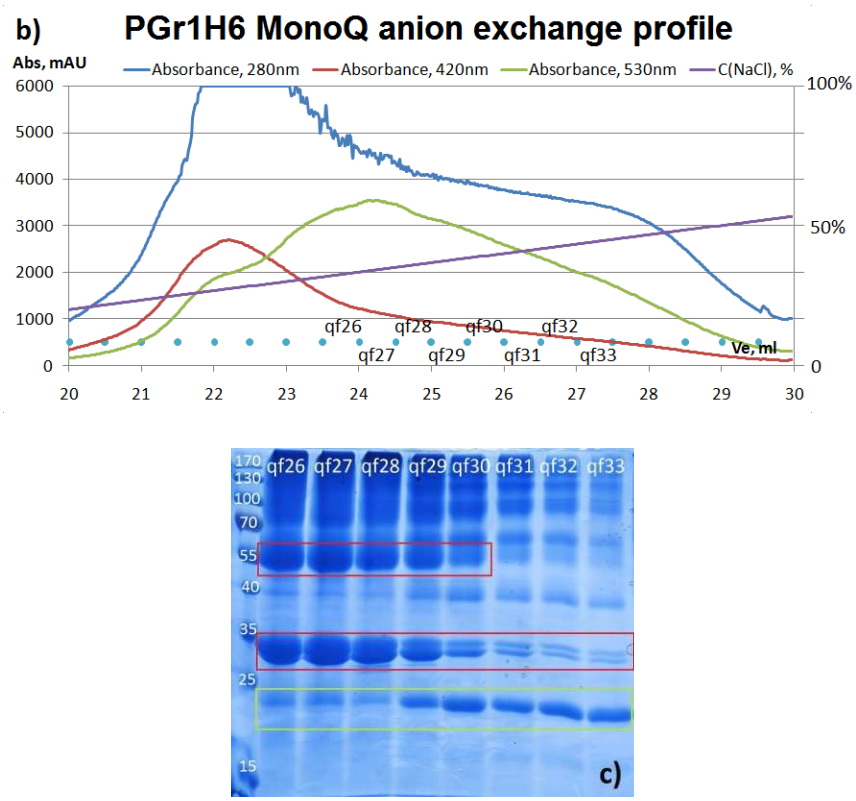


Figure 3.11 **a)** The PGr1H$_6$ anion exchange chromatography absorbance graphs overview and **b)** zone of interest. The numbered fractions represented with blue points. The 0% represents 30 mM NaCl concentration, while 100% corresponds to 0.5 M NaCl. **c)** The SDS-PAGE gel of fractions depicted on (b). PageRuler being used (numbers present on image represent weight in kDa). Contaminants depicted with red boxes, PGr1H$_6$ construct - green box.

The protein was eluted from MonoQ column with the salt gradient buffer 30T7.5, 0.2% DDM, 30-500 mM NaCl salt. This allowed decrease the contaminant content in rhodopsin sample.

This contamination problem was letter avoided during expression stage by increasing the shaking speed to 140 rpm.

3.2.2. Functional tests and characterization of PGr1

The purified protein absorbance spectrum, as was expected, contained 2 major absorption peaks, that correspond to mainly opsin part (280 nm) and retinal (527 nm; see Figure 3.12).

The additional non-zero absorbance in the 350-400 nm range apparently corresponds to a deprotonated RSB state[h].

[h] The sharp curve fluctuations around 450-475 nm are photometer detector artifacts, that were present in most of the spectra measured with the nanophotometer.

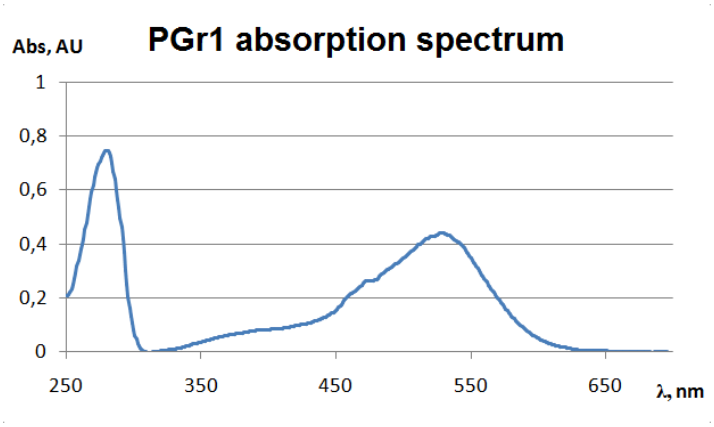


Figure 3.12 The refined PGr1 ($PGr1H_6$) UV-visible light absorption spectrum (blue line).

3.2.2.1. PGr1 peak ratio determination

In order to operate with PR values along purification procedure the "ideal" (corresponding to opsin:retinal = 1:1 ratio) PR should be estimated. To do so, the protein sample absorbance was measured in initial state and after addition of 2% SDS. Despite the rapid color change, retinal absorbance maximum didn't move to the ~390 nm (corresponding to non-bound retinal) but instead to ~450 nm. Apparently, the retinal remained bound to lysine. Thus we bleached it with permanent illumination. The two spectra of $PGr1H_6$ before denaturation and after SDS addition and bleaching are on Figure 3.13. Both spectra were taken against the reference buffer 30T7.5, 300 mM NaCl.

Since retinal and its isomers extinction coefficient may vary depending on the environment, the extinction coefficient of it should be measured in the same buffer as it is in the experiment. To find out the concentration of retinal being in the opsin initially, we measured the spectra of retinal with known concentration in the same buffer.

Taking into account that molar extinction coefficient of $PGr1H_6$=76100 $M^{-1}\times cm^{-1}$ and molecular weight 29.96 kDa (see Figure 3.13) we concluded that ideal PR value should be 0.81, i.e. for the protein being sampled in the test absorbance at ~530 nm should be 0.74 AU. Here we should though mention, that PR value doesn't take into account the fraction of the protein with deprotonated Schiff-base (non-zero absorbance at 370-400 nm region of the "blue" line on Figure 3.13). This fraction depends on pH of the buffer in which the spectrum was obtained.

For the given conditions, the opsin concentration is 7.8 µM, while the total retinal concentration protein is 6.3 µM, i.e. the retinal content is 81%.

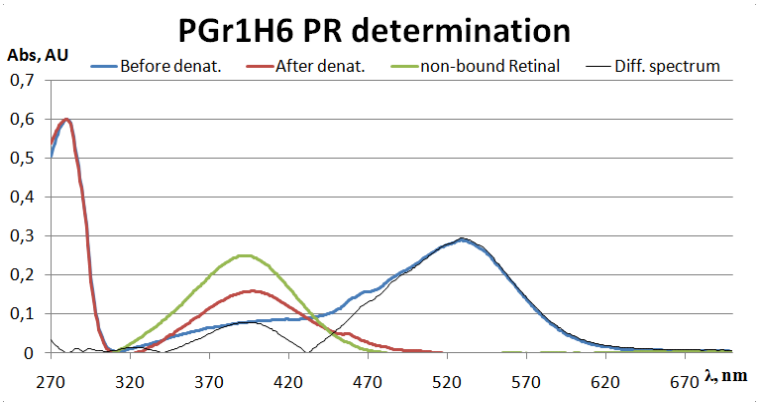


Figure 3.13 The absorbance spectra of protein sample before SDS treatment (blue), after addition of 2%SDS (red) and their difference spectrum (black). The spectrum of 10 μM retinal mixture (in the same buffer as protein) depicted in green. All spectra refined and normalized [84].

Assuming, that the retinal content doesn't influence the fraction of deprotonated RSB, we estimated the observable $PR_{7.5}$ (i.e. under considered conditions within the 30T7.5, 300 mM NaCl buffer) for protein containing 100% of retinal to be ~1.65 (i.e. ε_{530}=46100 $M^{-1}cm^{-1}$). Such a significant difference between ideal PR (0.81) value and our (1.65) is due to a large fraction (50.2%) of RSB in the sample at pH=7.5 is apparently in deprotonated state.

3.2.2.2. Functional activity test of PGr1 rhodopsin

The functional activity of $PGr1H_6$ was tested on the living culture. The *E.coli* strain C41 was transformed with pSC-$PGr1H_6$ plasmid and IPTG induced expression was performed. The test was performed as described in 2.2.6.3.

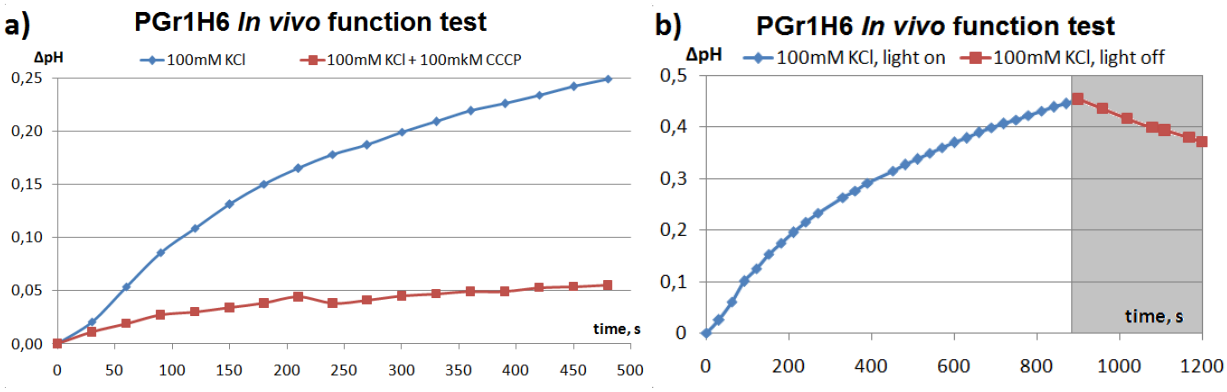


Figure 3.14 The PGr1 *In vivo* functional activity test. **a)** The absolute value of pH change upon culture illumination **b)** and the relaxation of the system. Gray box represents the absence of light. Tests were performed on ice at 2°C.

The obtained data presented on the Figure 3.14. The test was performed with two salts NaCl (data not shown; experiments didn't reveal any observable difference between NaCl and KCl salts with 100 mM concentrations) and KCl. The proton gradient formation speed and overall

ΔpH reduces upon addition of protonophore CCCP, which indicates that PGr1 pumps protons. During illumination pH of the testing culture decreased, thus proton was pumped out from the cells.

3.2.2.3. Flash photolysis of PGr1

The photocycle of PGr1 was measured in two types of environment: lipid nanodisks and detergent. The PGr1-nanodisk sample was prepared using POPC lipid along with MSP1E3D1 as described in [78]. The absorbance data sets (330 nm to 730 nm with step 10 nm) were obtained at 6 different temperature points 0, 10, 20, 30, 40 and 50°C and multi-exponential non-linear fit program MEXFIT was used the same way as in [85][84].

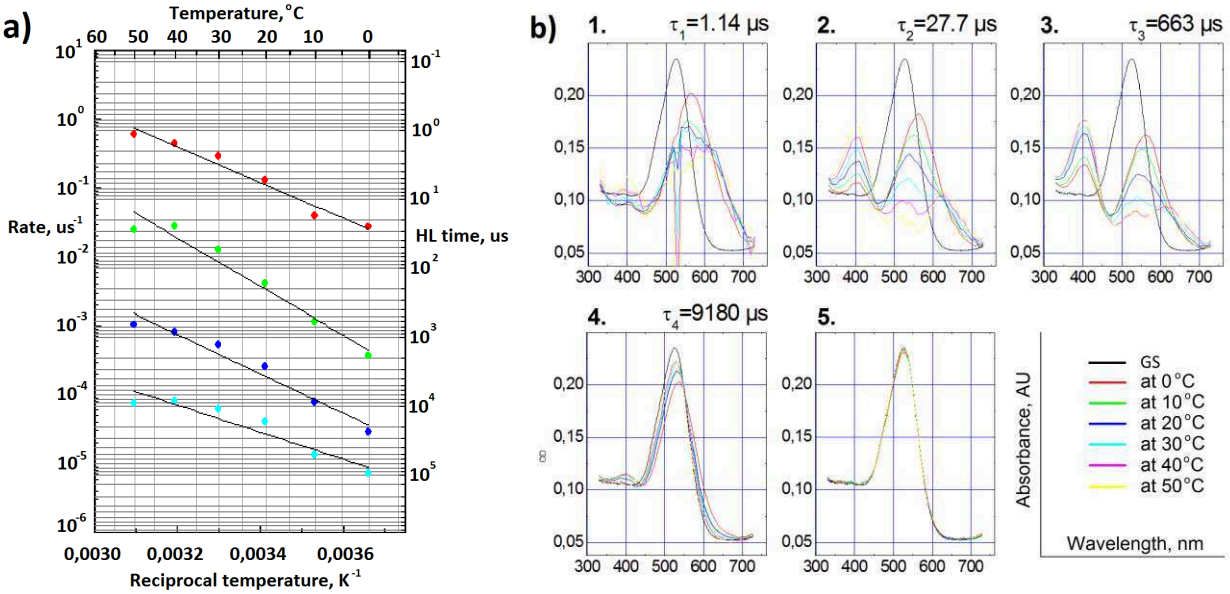


Figure 3.15 **a)** The Half-life time and rate constants of $PGr1H_6$ in POPC nanodisks at different temperatures. Red points correspond to K1, green - K2, blue - K3, light blue - K4. **b)** Reconstructed absorbance spectra of intermediates (1-4) at different temperatures. The intermediate 5 corresponds to a ground state (as well as black line on all intermediate spectra).

The number of exponents in fit was increased until no improvement in fit values was observed. Thus, the data for $PGR1H_6$ in both DDM and nanodisks are well described with 4 exponents. The half-life time constants for $PGr1H_6$ in nanodisks are present on the Figure 3.15a, while reconstructed absorbance spectra of corresponding intermediates at different temperatures are on the Figure 3.15b.

The direct comparison of rate constants for two samples demonstrates overall increase in time rate constants for DDM sample (i.e. slower kinetics/photocycle) at each temperature except

of K2. The absorbance spectra of intermediate 1 are poorly reconstructed due to residual noise from excitation laser.

Assuming the functioning mechanism similar to that of bR/PR (our PGr1H_6 protein possess motif of PR - DTE thus it should be closer to proteorhodopsins) the presence of more than 4 intermediates is most probable. Perhaps, further studies of this protein will allow resolving other states.

3.2.2.4. FRET in PGr1

In order to test whether this protein is capable to transfer energy to retinal from its aromatic residues the fluorescence life time was measured. To find out which residues are important for FRET in PGr1 we first performed a computer homology modeling of its structure. We found that the aromatic motif WFWW (W155, F156, W16, W158) is conserved in both PGr1 and bR (with a bit difference, in bR it is WFWY).

```
I0IGJ9 I0IGJ9_PHYMF  139   RQ--KAARRLVIFGVSMVFCSWVGGFFEADGHTEGGNLLGFWFSYLLGWVFYVL----LL 192
I0IBH0 I0IBH0_PHYMF  150   SNITKWGAQFVVAGLVMVFCSWLGSFWEQGQHVAGRGTFWFWVNYLIGWVAYVW----IL 205
F6K461 F6K461_POLGL  125   VN---LSWKLGLASALMVALGYPGEIQED--L----SVRWFWW-CL-SMIPFCY----VV 169
B0R2U4 BACH_HALS3    135   FT-------VIAADIGMCVTGLAAAMTTS-----ALLFRWAFY--AISCAFFVV----VL 176
P15647 BACH_NATPH    150   FT-------AITFDIAMCVTGLAAALTTS-----SHLMRWFWY--AISCACFLV----VL 191
B1YFV8 B1YFV8_EXIS2  109   RP---LLTKLVIADVIMIVGGYIGESSIN--IAGGFTQLGLWS-YLIGCFAWIY----II 158
N0DKS8 N0DKS8_9FLAO  136   ---SSVRNQFWFSGAMMIITGYIGQFYEVSNLTA----FLVWG--AISSAFFFH----IL 182
D5H9B4 D5H9B4_SALRM  120   GP---LAAKLGFLAALMIVLGYPGEVSEN--AA-LFGTRGLWG-FL-STIPFVW----IL 167
P02945 BACR_HALSA    122   LA-------LVGADGIMIGTGLVGALTK------VYSYRFVWW--AISTAAMLY----IL 162
Q8RUT8 Q8RUT8_CHLRE  147   RR----TMGLLVSDIGTIVWGATSAMATG-------YVKVIFF-----CLGLCYGA-NTF 189
K9G4Y0 K9G4Y0_PEND2  153   LI-------AIVAHLMMLVTALFGIFAG------HGRERWVWL--TLTCISYLV----VI 193
L1JET8 L1JET8_GUITH  123   FG-------AIVAVCILCAFM--ASVI-------PPPARYMWF--GMGITVFSAAWFNIL 164
```

Figure 3.16 The TM4 and TM5 (pink) regions according to bR, HsHR and NpHR, aligned to proteins in this work. The WFWW region in PGr1 depicted with green, while tryptophan residue W157 (PGr1) with high homology depicted in grey.

The Y210 in PGr1 corresponds to a retinal hydrophobic pocket forming W229 in bR. In the same time, the residues W158 and Y210 in PGr1, according to a model, located in the upper region between TM5 and TM6, which corresponds to a cavity in XR where salinixanthin carotenoid ring is located.

These considerations led to a hypothesis that the aromatic residues from this region in both bR and PGr1 might participate in the residue-to-retinal FRET energy transfer. To check this, we made the PGr1-F156I and PGr1-W155I-F156I mutants.

The readings of retinal fluorescence didn't reveal any difference between WT (wild type), F156I and W155I-F156I proteins. Moreover, the fluorescence was not detected due to the second harmonics signal to be much higher than possible fluorescence and in addition - in the same wavelength region (the residues were excited at 280 nm, while expected retinal fluorescence at

about 500 nm or higher; the observed high intensity noise was observed at 560 nm). Thus we moved to tryptophans fluorescence life time measurements.

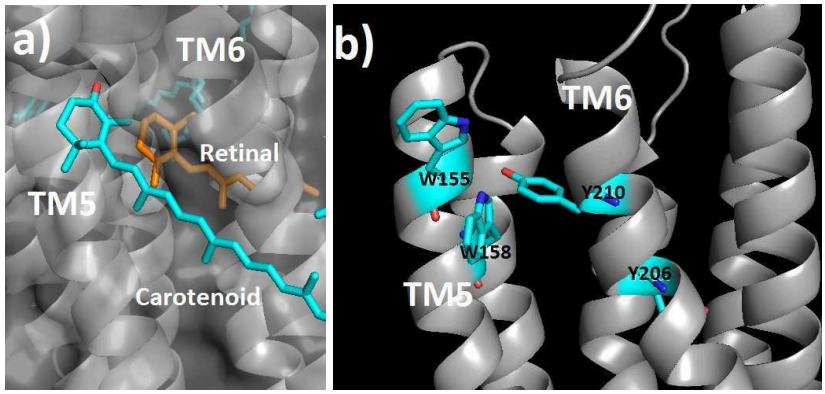


Figure 3.17 **a)** The carotenoid binding pocket in XR and its position corresponding to retinal. **b)** The PGr1 computer model of the same region.

While measuring the fluorescence of retinal we observed the high scattering - to eliminate the artificial component of possible readings we reconstituted proteins into DMPC liposomes, which in response, leaded to scattering. Despite this problem should not influence the tryptophans fluorescence life time measurements, we reconstituted the proteins into DMPC nanodisks with MSP1E3D1.

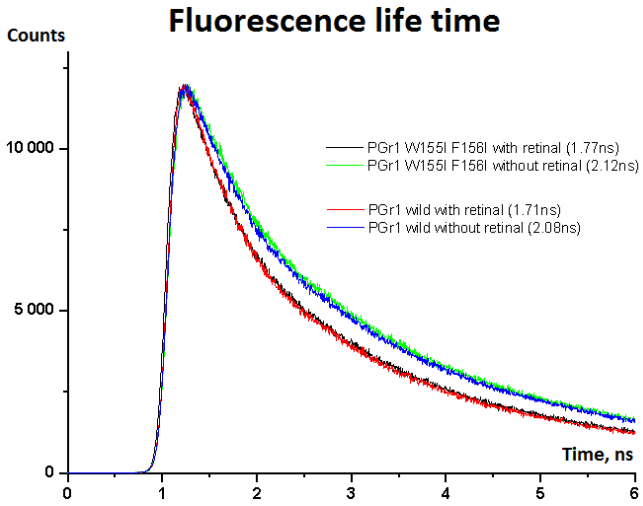


Figure 3.18 The tryptophans fluorescence life time measurements. The retinal content in protein samples with retinal brought to the same value (50%)[i].

In addition to that, we added extra negative control - the protein samples being expressed and purified without retinal (also being reconstituted to nanodisks). The data of fluorescence life

[i] During early experiments that life time strongly proportionally depended on the retinal content, i.e. the higher the retinal content - the greater the life time. Due to instability and poor yield of mutant proteins, the retinal content was significantly lower than that of WT. Thus we had to equilibrate content of WT to that of mutants.

time measurements are present on the Figure 3.18. From that data we can conclude that there is a FRET in the samples with retinal, since the addition of retinal to the system led to a 20% reduction of tryptophans fluorescence life. Despite that, we concluded that mutations we made didn't influence the energy transfer process to much - the deviations between readings for WT and mutant with and without retinal (1.71 ns vs. 1.77 ns and 2.08 ns vs. 2.12 ns correspondently) were within the measuring procedure error.

Thus, further investigations of this effect should be done to figure out the key residue responsible for energy transfer (if there's any).

3.2.3. Crystallisation of PGr1

Along with characterization experiments, the crystallization trials proceeded at IBS facilities in Grenoble, France.

Protein was crystallized *in meso* [86] using MO, similar to other our projects (for instance, [57]). The first screenings with commercially available Cubic Phase I and Cubic Phase II kits (Qiagen, USA) revealed that needle-shaped purple crystals 20-40 μm appeared in a broad range of conditions approximately two-three weeks after plate preparation. Few dozens of such crystals typically grow from few bundles within one plate well and reach up to 150 μm in length.

The main batch of needle shaped crystals seemed to grow within pH range 4.6-6.4 of Na/K Pi (0.2-1.2 M concentration; named PGr1K1 kit). Unfortunately, these crystals demonstrate the absence of diffraction.

Protein	$C_{protein}$ in phase, mg/ml	C_{DDM} came from protein, %	MO/protein volume ratio	Phase/Precipitate volumes, nl	Kit
$PGr1H_6$	20	5	1:1	100/400	CubicPhase I
$PGr1H_6$	20	4	1:2	100/400	CubicPhase I
$PGr1H_6$	20	5	1:1	100/400	CubicPhase II
$PGr1H_6$	20	4	1:2	100/400	CubicPhase II
$PGr1H_6$	18	7	1:2	300/600	PGr1K1
$PGr1H_6$	20	5	1:2	200/500	CubicPhase I
$PGr1H_6$	20	5	1:2	200/500	CubicPhase II

Table 3.2 The list of $PGr1H_6$ crystallization conditions.

Second type of $PGr1H_6$ crystals are thin rhomboids/triangles and rectangles. These crystals grow at moderately low pH (we noticed their presence at 5.8), in presence of high ammonium salts concentrations, and appear after ca. 2 months.

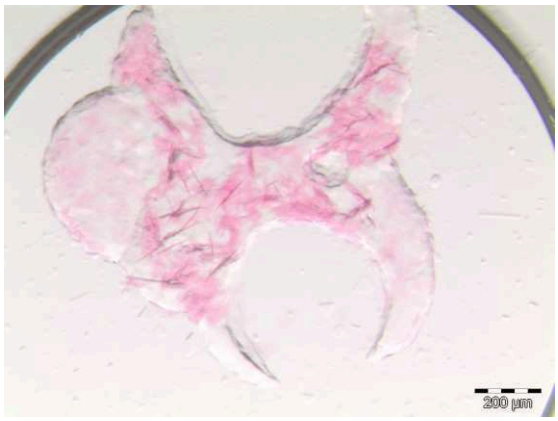


Figure 3.19 The photo of typical needle-shaped crystals that grow in a wide range of crystallization conditions. Image of Cubic Phase I, E5

These crystals reach up to few hundred micrometers, but are very thin and do not demonstrate sufficient diffraction.

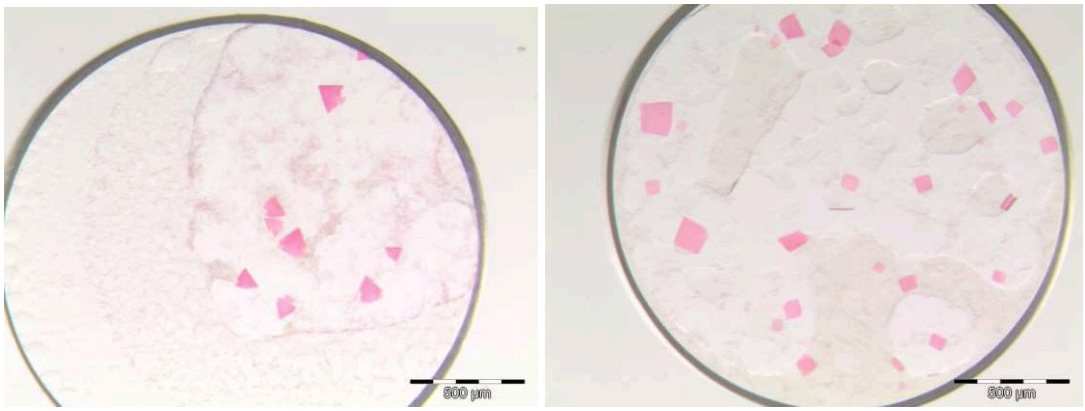


Figure 3.20 The triangular crystal (on the left, of Cubic Phase I, C8). The image in cross-polarised light taken 3 months after the plate preparation.

The third type of observed crystals is of non-determined shape. They are of a relatively small size (in compare to that of type two) of up to 50-60 µM and appeared after more than 3 moths. Interestingly, these crystals are the only found to grow in Cubic Phase II kit which main difference is presence of PEG with different MW.

The crystals of the third type were not tested yet.

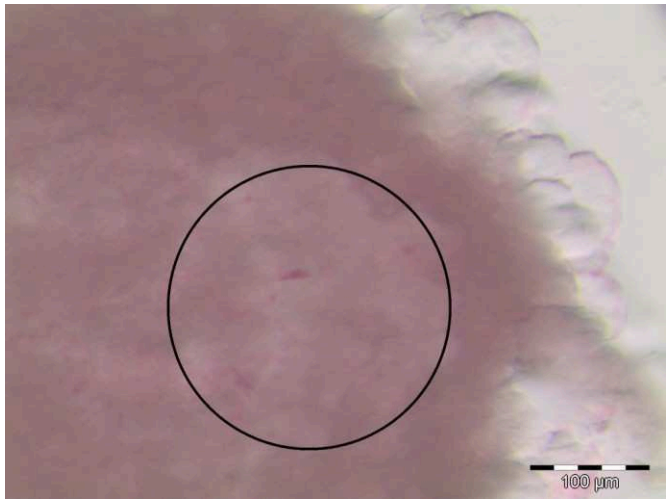


Figure 3.21 The image of non-determined shape crystals (emphasized with black circle). Cubic Phase II G5. Photo was made 3.5 months after plate preparation. The image corresponds to 0.1 M MES pHv5.8, 12% (w/v) PEG 6000, 0.2 M Sodium chloride (G5).

One of the possible reasons of poor crystals quality (and thus week diffraction) may be the interference of buffer within the protein sample with the crystallization salt solution - the high (30 mM) concentration may influence the crystals growing conditions leading to a shift of pH.

3.3. Phycisphaera mikurensis PMr1 and PMr2 rhodopsins (UNP I0IBH0 and I0IGJ9)

Unlike PGr1, the functionality of both PMr1 and PMr2 was unknown. Interestingly, the PMr1 homological BLAST (PMr1 like proteins were looked for) search revealed that the protein with highest identity of ~44% (E-value ~10^{-86}) is PMr2 (and the same situation with search for PMr2), i.e. the closest homologues are with 40% or lower identity. The protein disorder prediction service RaptorX revealed putative 7TMH structure with presumably ordered N- and C- termini.

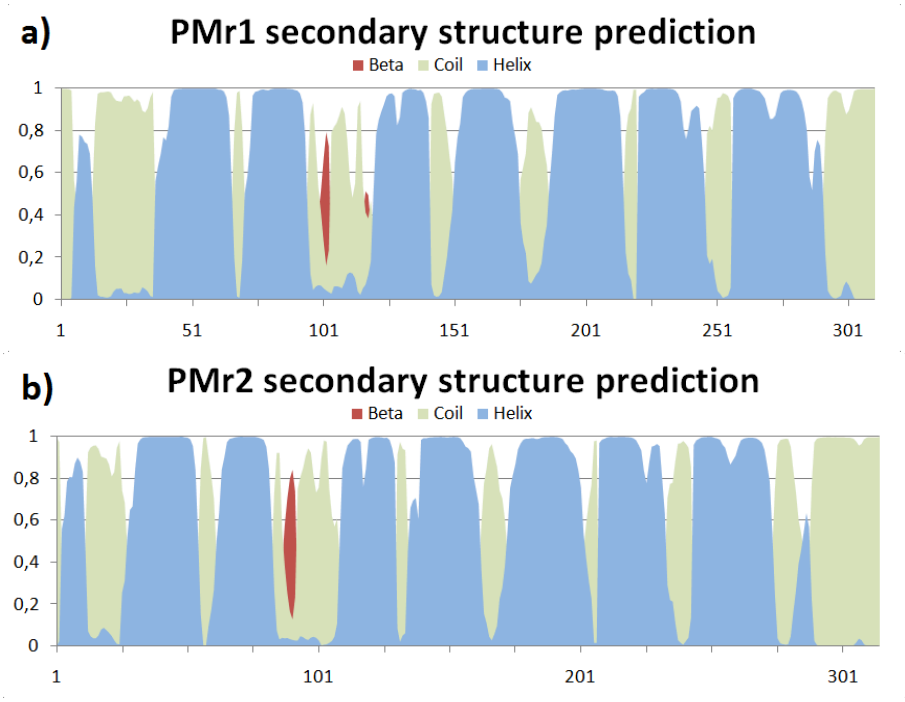


Figure 3.22 The disorder (secondary structure) prediction of **a)** PMr1 and **b)** PMr2 done using RaptorX server. The Overall 7TMH structure observed.

3.3.1. Expression and purification of PMr1 and PMr2

3.3.1.1. PMr1 and PMr2 expression

The first attempts in expression of these two proteins were done using *E.coli* strain SE1 transformed with pSC-PMr1eoH_6 and pSC-PMr2eoH_6 (see Figure 3.23) within AIM-5052 auto induction expression medium. The test samples were analyzed with WB and the presence of the both proteins were confirmed but with low yield (about 1mg per shaker, i.e. per 6 L of media).

This expression level we considered insufficient for further proteins characterisation experiments thus we proceeded with expression optimization. While analyzing the protein

primary structure (amino acid sequence) we noticed the methionine residues M29 and M18 in PMr1 and PMr2 respectively which might correspond to alternative translation starts.

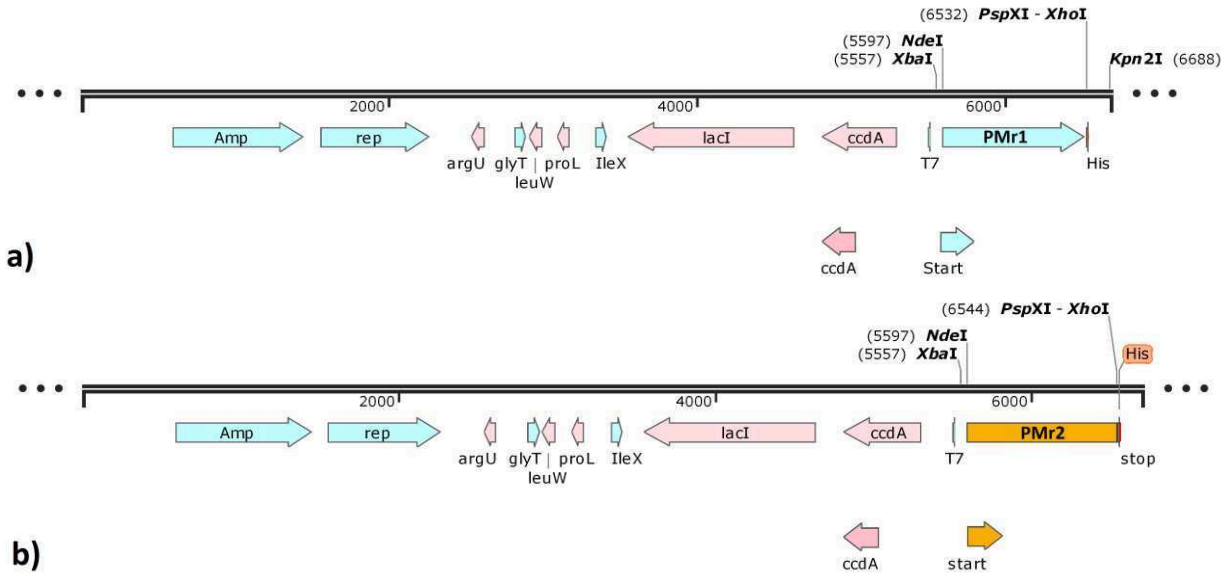


Figure 3.23 The **a)** pSC-PMr1eoH$_6$ and **b)** pSC-PMr2eoH$_6$ plasmid maps with relevant features and digestion sites depicted.

The SignalP [87] signal peptide prediction tool was used to analyze the N-terminal region of genes sequences of PMr1 and PMr2 and revealed no signal peptides neither from bacteria nor eukaryote domains. Thus, assuming that N-terminal regions do not influence protein functionality, we made two truncated mutants 18PMr2 and 29PMr1 (17 and 28 N-terminal residues truncated correspondingly). Along with *E.coli* expression we decided to estimate if proteins yields will be higher from LEXSY expression system. Even though it's an eukaryotic expression system, for first trials we decided to proceed without codon optimization for it and perform tests with *E.coli* optimized sequences to see if any noticeable difference in expression level will appear. To do this, we also constructed 2 plasmids pLEXSY_I-blecherry3_27PMr1 and pLEXSY_I-blecherry3_16PMr2[j] (see Figure 3.24).

To find the most appropriate strain/system we first tested *E.coli* SE1 proteins content (with PSCodon plasmid and in AIM) against LEXSY system. The test samples of cultures were analyzed with WB (hereafter, Western-blot analysis) stained with primary PentaHis antibodies. The WB images are on the Figure 3.25.

[j] In order to speed up the plasmid construction process we decided to use PCR primers that being available from our other projects. This leaded in 2 extra residues being left on each N-terminal region of both PMr1 and PMr2 and leaded to truncation of 16 aa and 27 aa instead of 17 aa and 28 aa (for PMr2 and PMr1 respectively).

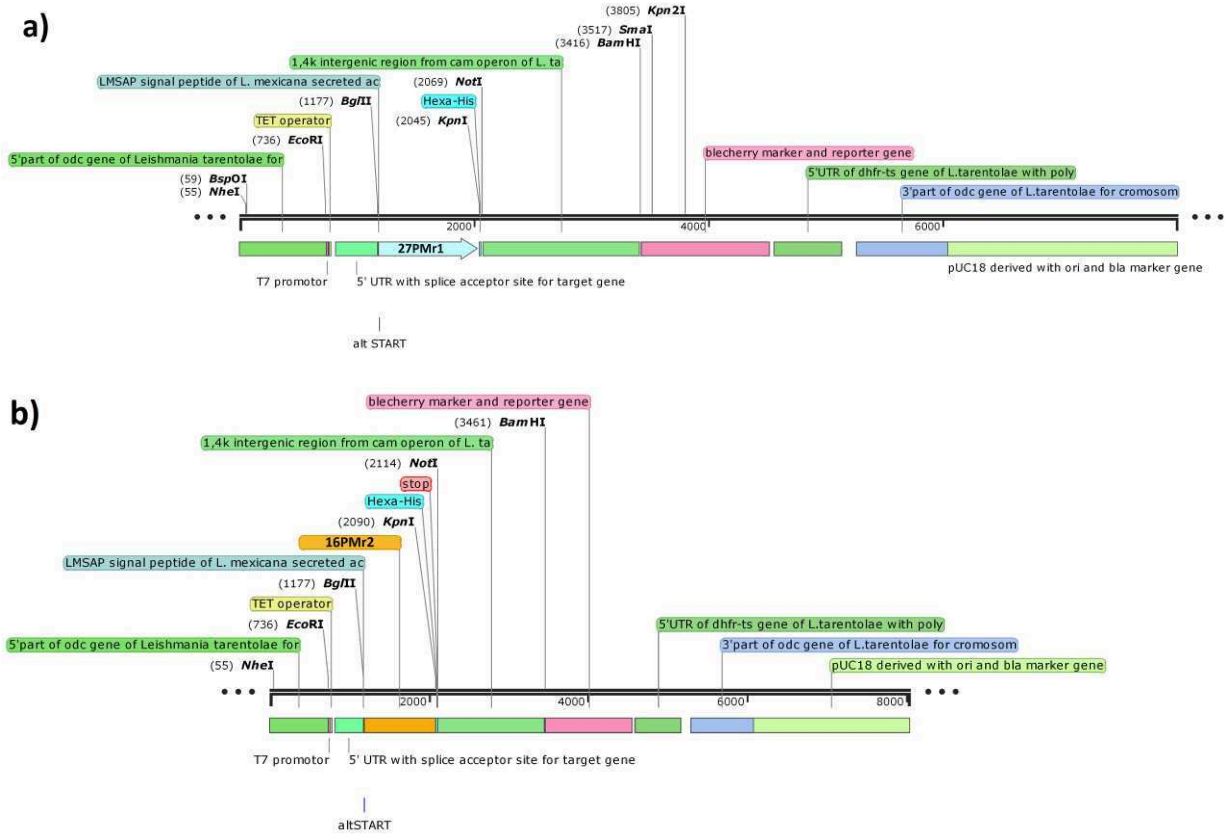


Figure 3.24 The plasmid maps of **a)** pLEXSY_I-blecherry3_27PMr1 and **b)** pLEXSY_I-blecherry3_16PMr2 with most relevant features and most common digestions sites depicted.

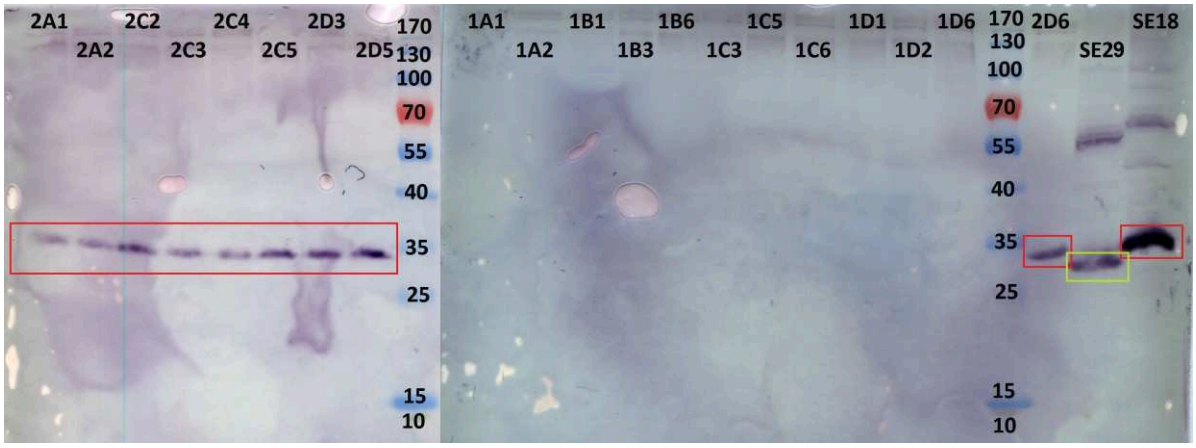


Figure 3.25 The WB membrane (stained with Anti PentaHis antibodies) of different LEXSY clones containing genes of 16PMr2H_6 (2A1-2D6, on the left) and 27PMr1H_6 (1A1-1D6, one the right) along with *E.coli* SE1 cells containing genes 29PMr1H_6 (SE29 on the image) and 18PMr2H_6 (SE18 on the image) within pSCodon1.2 plasmid (AIM). The red boxes depicting xPMr2H_6 construct proteins, while light green rectangle depicts xPMr1H_6. No detectable trace of 27PMr1H_6 protein registered within LEXSY clones. All samples were normalized to OD_{600}=1 within 1 ml sample volume.

Test revealed low but observable expression of 16PMr2 (lower than that of SE1 strain), while no 27PMr1 protein was detected in LEXSY.

At the same time we performed the *E.coli* comparative test of SE1, C41, C43 and Shuffle (New England Biolabs, USA) strains (all containing both PMr1 and PMr2 constructs within pSCodon1.2 plasmid).

	OD_{600}, AU						
Time, h	**SE1, PMr2**	**C41, PMr1**	**C41, PMr2**	**C43, PMr1**	**C43, PMr2**	**Shuffle, PMr1**	**Shuffle, PMr2**
0	0.1	0.1	0.1	0.1	0.1	0.1	0.1
2	0.35	0.25	0.29	0.31	0.40	0.40	0.35
5	0.4	2.1	2.1	2.2	2.4	2.0	1.4
7	0.4	2.4	2.4	2.8	2.5	2.7	2.5
9	0.4	2.6	2.6	2.9	2.9	3.2	3.1
10	0.5	2.6	2.7	2.9	3.0	3.2	3.3
20	2.4	3.8	3.4	4.6	4.2	5.9	7.0

Table 3.3 The OD_{600} over time of the cultures being tested. The IPTG induction with 1 mM IPTG was performed at OD ~0.4 (after taking 2 h-samples and OD measurements).

Comparison of the 20 h-samples with WB, despite interference of anomalously growing SE1 sample, showed that the protein content is highest for C41 and C43 strains. While the content of PMr2 in C41 and C43 strains seemed to be the same, in case of PMr1 C41 strain was preferable. Another notice is that both the PMr2 (in less extent) and PMr1 undergo the proteolysis.

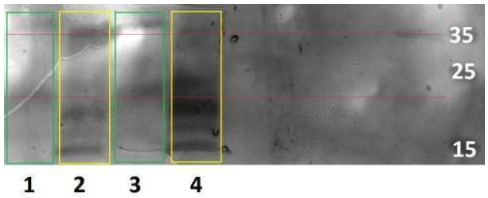


Figure 3.26The WB of C41 and C43 strains containing full-sized genes of PMr1 and PMr2. Samples: 1 - pSC-PMr2eoH6 C43, 2 - pSC-PMr1eoH6 C43, 3 - pSC-PMr2eoH6 C41, 4 - pSC-PMr1eoH6 C41. Despite poor image quality the strong proteolysis of PMr1 observed, while PMr2 is represented in two states (two lines corresponding to ~35 kDa and ~20 kDa; depicted with horizontal red lines).

The high proteolysis level seemed as another additional point into M18 and M29 (in PMr2 and PMr1 respectively) to be the alternative translation sites and thus these N-termini might be irrelevant to protein functioning. All the considerations above led to the plasmid DNA constructs pSC-18PMr2oeH6 and pSC-29PMr1eoH6 to be used with C41 expression strain.

The first expression trials led to a moderate expression yield of more than 2 mg/L of culture for both of rhodopsins ($OD_{induction}$=0.9, C_{IPTG}=1 mM, 12 h of expression stage). Despite high opsin expression level, we could estimate only the absorption spectra of $18PMr2H_6$ (with

maximum at ~530 nm). The samples of 29PMr1H_6 solubilized in DDM seemed to have also 2 peaks, but the retinal-corresponding peak seemed to be in the position corresponding to a free (non-bound) retinal (looking ahead, the same true also for full-sized PMr1 in DDM).

While performing the small-scale expression experiments, we noticed the overall independence of protein yield on the amount of harvested cells. This might be explained in terms of plasmid instability within C41 strain. During the cells grow and death ampicillin is being digested media (the ferment β-lactamase encoded within pSCodon1.2 plasmid is responsible for strain resistivity to ampicillin), which might lead to the C41 cells loss of pSCodon1.2 containing gene of protein of interest. Due to loss, it seems (by cells coloring) that only a fraction of cells maintain plasmid inside till the end of expression stage, while the rest don't.

To test this hypothesis we decided to add extra ampicillin to the medium while inducing the culture with IPTG. Despite decrease in the final cell mass being harvested, the protein yield increased. Despite no direct comparison was done, we empirically estimated (by OD_{600} of the culture increase rate in absence of ampicillin[k]) the approximate period of effective ampicillin concentration in medium to remain for 1h with constant culture OD_{600}=1. These observations leaded to a modified IPTG induction protocol.

Looking ahead, this extended protocol, unlike AIM or common IPTG induction, allowed to express full-sized PMr2H_6 purified rhodopsin with yield of up to 45mg from 6L of medium (7.5 mg/L of culture or 1 mg/g of cells harvested).

3.3.1.2. PMr1H_6 and PMr2H_6 solubilisation and affinity chromatography

The table data for PMr1H_6 and PMr2H_6 are provided in the Table 3.4.

As was mentioned before, the absorbance of PMr1/29PMr1 seemed to be unusual for rhodopsin proteins since retinal-correspondent peak was in the same region as non-bound (free) all-*trans* retinal.

The absorbance spectrum of PMr2/18PMr2 (identical) on the other hand typical to rhodopsin protein except being blue shifted (absorbance maximum ~470 nm; Figure 3.28).

[k] Usually observed by us C41 strain cells division (i.e. OD_{600} doubles) occurs each 35-40 min in absence of expression till OD_{600} 2-2.5.

Parameter	$PMr1H_6$/ $29PMr1H_6$	$PMr2H_6$/ $18PMr2H_6$
Isoelectric point	7.42/ 8.08	8.73/ 8.90
Charge at pH 8.0	-1.7/ 0.2	3.5/ 4.2
Weight	35.890 kDa/ 33.106 kDa	35.937 kDa/ 34.191 kDa
Absorbance maximum	N/A	470 nm/470 nm
Molar extinction coefficient	92460 $M^{-1}cm^{-1}$/ 92460 $M^{-1}cm^{-1}$	64720 $M^{-1}cm^{-1}$/ 64720 $M^{-1}cm^{-1}$

Table 3.4 Characteristic putative rhodopsins' values

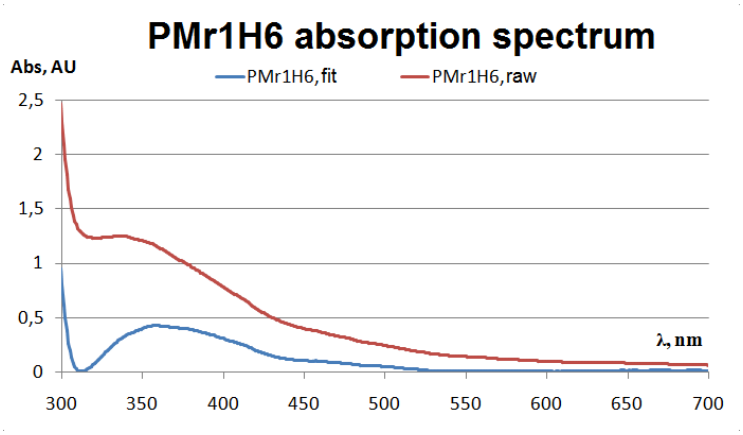


Figure 3.27 The absorbance spectrum of $PMr1oeH_6$ solubilized with DDM raw data (red). The "fit" curve is the result of Rayleigh scattering subtraction along with assumption of zero absorption at 310 nm.

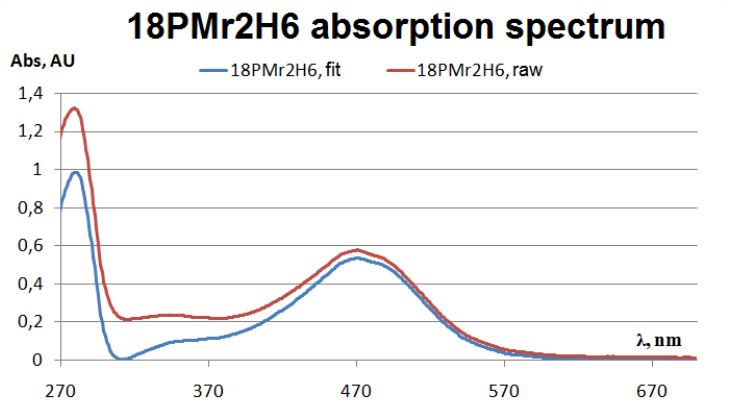


Figure 3.28 The absorbance spectrum of $18PMr2H_6$ construct in buffer 30T8.0, 300 mM NaCl, 0.5 mM EDTA, 2 mM 6AHA, 0.2%DDM. The fit done in the same manner as that of PMr1/PGr1.

Due to fact that truncated $18PMr2H_6$ protein constructs didn't demonstrate any functional activity (see 3.3.2.2) we will further describe procedure for purification of full-sized proteins and get back to truncated protein when it's relevant.

The purification procedure starts with culture cells harvesting and total membranes mixture preparation. The total membranes of both PMr1eoH_6 and PMr2H_6 were solubilised with 1% DDM in buffer 30T8.0, 300 mM NaCl, 5 µM all-*trans* retinal and cOmplete protease inhibitor (according to a manufacturer's instructions). The soluble fraction was separated and was further processed with affinity chromatography assay in the same manner as for PGr1H_6. The typical elution profile for PMr2H_6 construct is on the Figure 3.29.

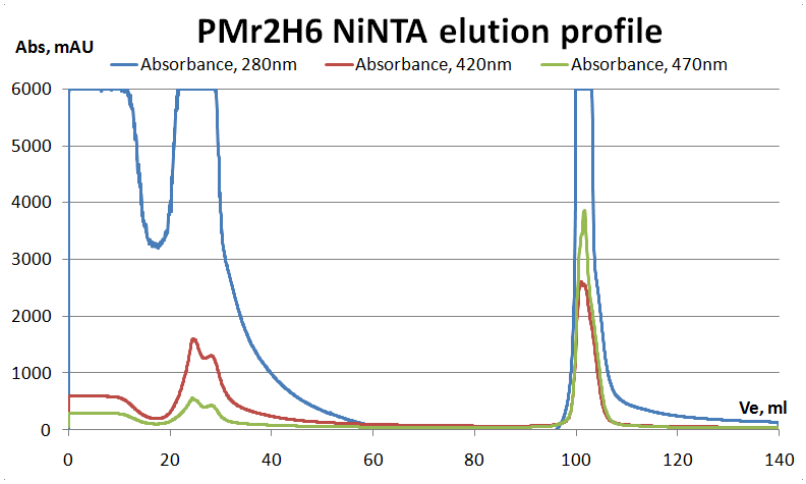


Figure 3.29 The NiNTA elution profile of PMr2H_6 (two buffers).

In the same manner as for PGr1, we added extra wavelength 420 nm to control the presence of specific contaminating protein[l].

The proteins bound to NiNTA resin column were washed with 30T8.0, 300 mM NaCl, 30 mM Imidazole, 0.2%DDM with 3 column volumes (90ml) and eluted with high concentration of imidazole (30T8.0, 300 mM NaCl, 300 mM Imidazole, 0.2%DDM[m]). The fractions corresponding to rhodopsin were collected (95-110 ml) and pooled to proceed with SEC.

3.3.1.3. PMr1H_6/PMr2H_6 size exclusion chromatography

Merged affinity chromatography fractions were divided to portions containing total up to 4mg of protein and these fractions were applied to SEC. The SEC column was pre-equilibrated with SEC buffer (30T8.0, 300 mM NaCl, 0.5 mM EDTA, 2 mM 6AHA and 0.1% DDM). The

[l] The PMr1eoH_6 rhodopsin construct elution profile at 280 nm had the very similar shape to that of PMr2H_6. But in the absence of distinguishable from that of retinal characteristic absorption wavelength in visible spectrum (470 nm in case of PMr2H_6) we had to analyze the eluted fractions with WB stained with PentaHis antibodies to confirm the presence of PGr1H_6 protein.

[m] Unlike PGr1, PMr1/PMr2 didn't tend to aggregate upon elution with 0.2%DDM concentration thus we could proceed with lower detergent concentrations on further steps.

SEC profiles of both rhodopsins are on the Figure 3.30. The PMr2H$_6$ SEC profile contains 2 regions. The 8-9 ml region corresponds to aggregates, while the peak at 10 ml corresponds to the PMr2eoH$_6$ homogeneous oligomeric state that by our estimations contains five to six (two trimers) protein molecules.

In contrast to PMr2, the PMr1H$_6$ SEC assay revealed high non-homogeneity of the protein collected.

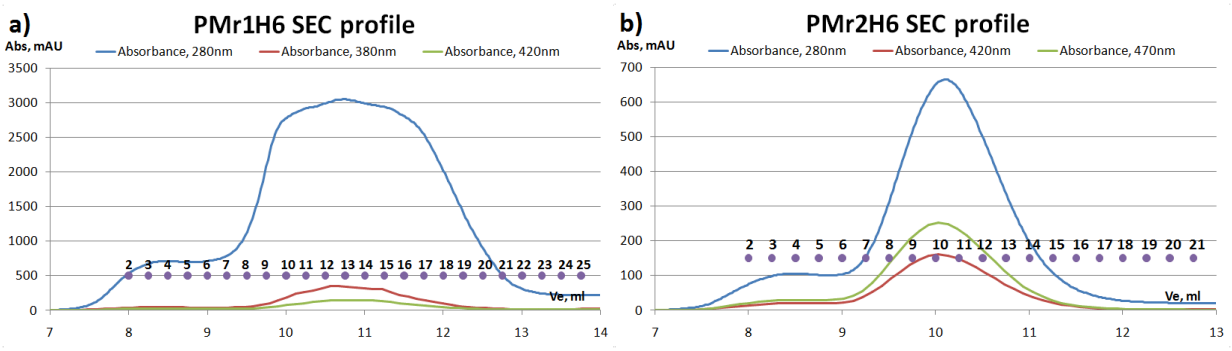


Figure 3.30 The SEC profiles of **a)** PMr1H$_6$ and **b)** PMr2H$_6$. The PMr2H$_6$.

The fractions corresponding to rhodopsins were collected (9-18 for PMr1eoH$_6$ and 8-13 for PMr2eoH$_6$).

3.3.2. Functional test of PMr1 and PMr2

The functional characterization efforts of PMr1H$_6$ neither *in vivo* (in SE1 and C41 strains) nor *in vitro* were unsuccessful. In addition, the absorbance spectrum of this rhodopsin also non-typical (with peaks corresponding to opsin and non-bound retinal). Taking into account these facts we concluded that despite opsin part is expressed well, the rhodopsin can't fold properly in E.coli to bind the retinal (while other expression systems didn't provide sufficient yield to perform characterization test necessary for rhodopsin proteins). Thus we proceeded only with PMr2.

3.3.2.1. The peak ratio determination of PMr2

Like for PGr1 protein, the PR of PMr2 should be estimated. Thus we denatured the PMr2H$_6$ sample in the same manner. The observed absorbance change present on Figure 3.31.

The ideal PR (see 3.2.2.1) in absence of retinal-corresponding absorbance at 390 nm was estimated to be ~0.7, while the ratio under given conditions (i.e. pH 8.0 and 300 mM NaCl)

should be ~1.4 (i.e. ε_{470}=46000 $M^{-1}cm^{-1}$). The sample of $PMr2H_6$ before denaturation had PR=1.8, which corresponds to 77% retinal content.

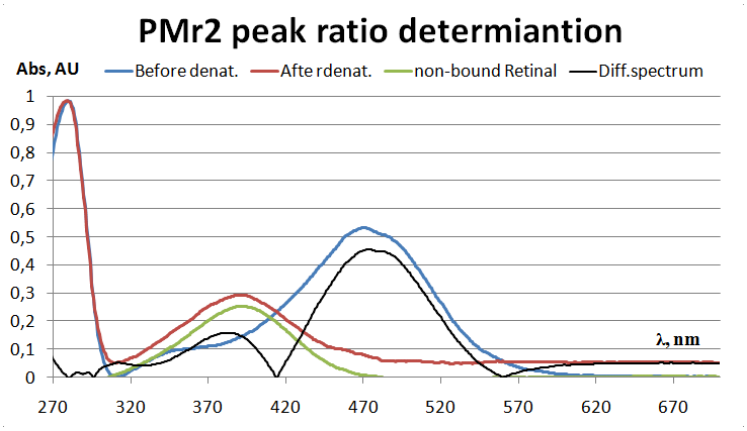


Figure 3.31 The absorbance spectra of $PMr2H_6$ before (blue) and after (red) denaturation with 2% SDS along with 10 μM of retinal (green). The difference spectra depicted with black curve. All spectra refined and normalized.

3.3.2.2. The 18 PMr2eoH6/PMr2eoH6 functional activity tests

The determination of functional activity started with $18PMr2H_6$ construct since it was first obtained in sufficient quantity. The activity was tested first on living *E.coli* SE1 and C41 strains by measuring pH shifts under illumination with light in presence of different ions (NaCl, KCl, KBr, $MgCl_2$, K_2SO_4, $NaNO_3$ and $CaCl_2$). Despite the high protein level in tested cells, there was no signal observed independently on presence or absence of TPP/CCCP and their combination. The test was repeated without success on the artificial membrane - $18PMr2H_6$ was reconstituted into asolectin liposomes (1 mg/ml $18PMr2H_6$, 1% asolectin, 200μm diameter). While preparing the liposomes, we decided to eliminate all the salts from the sample and noticed the significant absorbance maximum shift (~470 nm to ~530 nm; see Figure 3.32).

This shift, apparently, is due to rhodopsin-ion interaction. Since no other ions except Na^+ and Cl^- were in the mixture due to a thorough dialysis, we suggested that one of them interacts with the protein and could be transported. Since we didn't observe any active ion transport activity in our initial *in vivo* and *in vitro* tests, we assumed that either:

- PMr2 might be the channel and thus initial ion gradient should be made prior to light exposure;
- PMr2 is a pump but our modifications leaded to function loss;
- PMr2 is naturally not a functional rhodopsin.

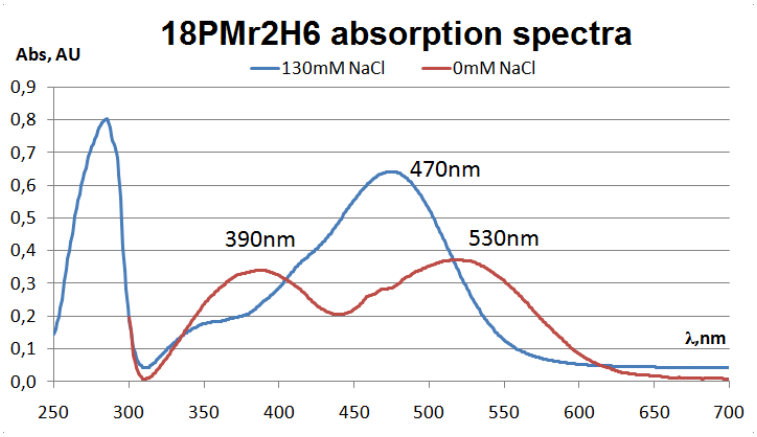


Figure 3.32 The ground spectrum shift of 18PMr2H$_6$ with and without presence of sodium chloride.

Despite gradient was supposed to be present in living cells test (cells were resuspended in 100 mM NaCl) and no signal observed, we decided to check if the first possible option is true by testing function activity in liposomes introducing the extra sodium chloride into liposomes mixture (200 mM NaC; making the outer salt concentration higher than inner one - 100 mM NaCl were used upon liposomes preparation) or 1.5× dilution of liposomes with water (decreasing the outer NaCl concentration to 66 mM). During the test we observed the very slow and permanent pH change in both absence and presence of illumination, which might be explained by diffusion, but not the rhodopsin activity.

Thus we produced the full-sized PMr2H$_6$ protein and reconstructed it into asolectin liposomes in the same manner as 18PMr2H$_6$ (without gradient of ions concentrations in- and outside of liposomes, i.e. initially in equilibrium state). The obtained results depicted on the Figure 3.33.

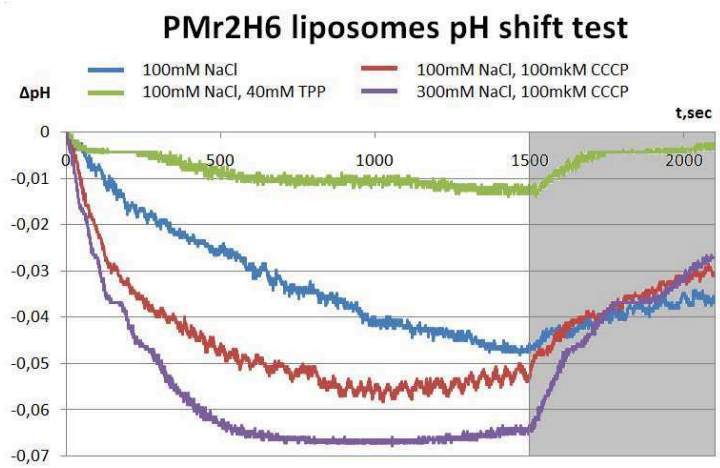


Figure 3.33 The pH shift upon illumination of 1% asolectin liposomes containing PMr2H$_6$ (1 mg/ml) without initial ion gradient. The grey region (1500-2100 sec) corresponds to light-off stage (system relaxation).

The pH change of sample without any ionophores added is apparently caused by the intrinsic proton permeability of the membrane. The signal growth upon addition of protonophore CCCP indicates that gradient of proton (being produced upon illumination in 1500 seconds) between outer space and inside of liposome is actually higher than we observed with passive intrinsic permeability. If the $PMr2H_6$ was a proton pump, we would observe the "drop" of both signals (with TPP and with CCCP) in comparison to sample without ionophore/protonophore. And if it was any type of light gated channel – we wouldn't see any signal at all. Thus we can state that PMr2 is an ion pump.

Further investigations didn't reveal any dependence of $PMr2H_6$ absorbance spectrum on the concentrations of sodium/potassium ions, but instead the one for Cl^-,F^-,Br^- and $NO3^-$ anions was observed. Which we think is sufficient proof of PMr2 being an anion pump.

This also might explain the reason of activity loss of truncated protein - according to the secondary structure prediction and computer modeling, the N-terminus contains a short helix, like that being reported for NpHR to respond for unidirectionality of anion transport (it was proposed to prevent the anion from rapid release from RSB region).

The other thing that should be mentioned and discussed is the protein orientation within liposome lipid bilayer. In our experiments we use asolectin - the soy bean lipids mixture (37% phosphatidylcholine, 29% phosphatidylethanolamine, 7% cardiolipin, 3% phosphatidylserine and 6% neutral lipids; the data given at [88], but apparently the content may vary due to the absence of strict content information from the manufacturer) that under physiological conditions (pH~7) presumably forms negatively charged liposomes. For different rhodopsins it was shown that in addition to the reconstitution method being applied, both, the protein and the lipid charges influence the protein orientation in the bilayer [89][88][90].

The experiments on the liposomes composition (and thus charge) performed on the model proteorhodopsin indicate the absence of significant vectorial pR orientation within overall neutral surfaces, while the protein found to be exposing the N-terminus out of the negatively charged liposomes [90][n]. Despite this finding, according to our observations for other rhodopsins, the typical orientation of rhodopsins function vectoriality in the neutral detergent-mediated asolectin liposomes prepared at neutral pH~7 is inside-out (i.e. reversed comparing to that in living cells; assuming common to all rhodopsins extracellular N-terminus topology, in our

[n] It should be mentioned, that in the described experiments authors perform reconstitution in presence of HEPES buffer salt at fixed pH 6.2.

experiments N-terminus is inside of liposomes). Even though the pumping vectoriality still should be confirmed with living cells/tissues experiments, we assume PMr2 to function as inward chloride pump.

3.3.2.3. BLM current measurements

In order to additionally confirm the pumping activity observed on liposomes samples, the new sample of dialyzed $PMr2H_6$ was reconstituted into asolectin liposomes in the same manner as we did before (1 mg/ml or rhodopsin, 1% asolectin, 200 nm liposomes diameter). The liposomes mixture then was tested with BLM assay in the manner described earlier ([79][6]). The measured photocurrents depicted on Figure 3.34 were obtained on the same black membrane and under the same temperature and buffer conditions (22°C, 20 mM HEPES, pH 7.4).

Prior to first measurement, the 1ml of buffer was added into both electrode volumes and 60 µl of liposomes mixture to the one side of membrane, while to the other the same volume of buffer was added to avoid the membrane destruction due to the liquid level difference pressure. The membrane capacitance was estimated to be 2.6 pF/mm^2.

After 15 min the system became stationary and the photocurrents reading was performed along with irradiating of setup with white light for 8 sec (black line). The small initial current I_0 (peak ~2 pA) was detected, but no stationary (I_∞) current was observed.

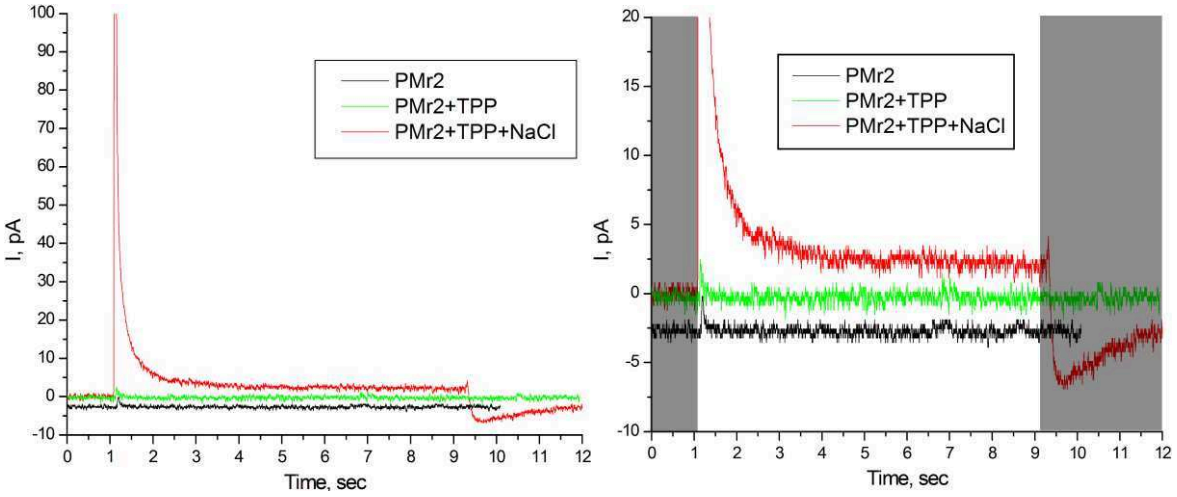


Figure 3.34 The photocurrent readings on BLM setup of PMr2-containing asolectin liposomes under different conditions. The I_0 peak (**left**) and enlarged steady state I_∞ (**right**) currents. The grey regions correspond to absence of illumination (illumination started at ~1 sec). On both images the current readings for PMr2 liposomes mixture depicted with black line; PMr2 liposomes after addition of 10 µM TPP - green line, PMr2 liposomes with 10 µM TPP, 60 mM NaCl - red line. All measurements were performed 15 min after addition of TPP/NaCl. Capacitance is 2.6 pF/mm^2

Next we proceeded with addition of 10 µM TPP, equilibrating the pressure in the same manner as with addition of liposomes to buffer. The photocurrent was recorded for the same 8 sec of illumination (green trace on Figure 3.34). After addition of TPP ionophore, the base level of current increased, but still no observable signal was detected (initial peak current I_0 ~2 pA).

Next we added 60 mM of NaCl and performed currents reading (red line). In the presence of both ionophore and sodium chloride we observed strong initial photocurrent of about 370 pA, that rapidly half-decreased in 27 ms and then slowly leveled (from maximum current value to a stationary current in 2.4 sec) to a quasi-stationary current of about 2.7 pA. After the light was off, the small negative reverse current ~6 pA was observed (it was leveled back to zero in terms of few seconds). The direction of both I_0 and I_∞ currents was the same among measurements on different membranes (the typical membrane capacitance was ~2 pF/mm^2; the pore diameter ca. 0.7mm).

The obtained data demonstrate expected appearance of chloride-dependent current in response to illumination.

3.3.2.4. The PMr2H$_6$ chloride binding constant

As was mentioned before while confirming the PMr2 functionality, chloride ion pumping activity was tested with spectroscopic methods. To do this, the PMr2H$_6$ protein sample, solubilized with DDM, was deeply dialyzed against 10 mM Na/K-Pi pH 7.0 phosphate buffer till the theoretical sodium chloride (sample initially contained 30T8.0, 300 mM NaCl, 0.5 mM EDTA, 2 mM 6AHA, 3%DDM) didn't drop into nanomolar concentrations.

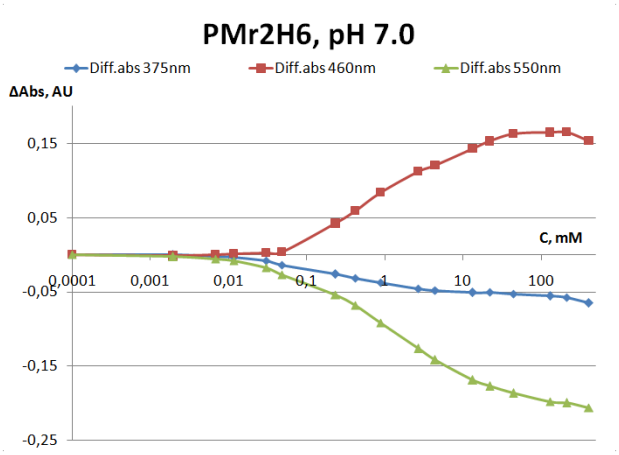


Figure 3.35 The dependence of diff. absorption of PMr2H$_6$ at 455 nm, 375 nm and 540 nm wavelengths on NaCl concentrations (17 concentration points).

The sample then was diluted in 10 mM Na/K-Pi pH 7.0 and the titration with sodium chloride was done along with absorbance spectra recording. The data present on Figure 3.35. For whole differential spectra see Appendix Figure 3.

The curves were fitted with sigmoid function and the calculated value of PMr2 chloride ion binding constant was estimated to be 0.9 mM. Interesting thought, such constant of truncated 18PMr2 rhodopsin was estimated to be 0.4 mM under the same conditions. This difference might be caused by absence of N-terminal domain. On the other hand, due to the logarithmic scale, such a difference might be neglected.

3.3.2.5. The flash-photolysis of PMr2

The kinetics of the rhodopsins is another important characteristics for both understanding of its mechanism and the optogenetic implications.

The photocycle of $PMr2H_6$ protein was measured in the same manner as PGr1. The obtained half-life time constants are depicted on the Figure 3.36, while the reconstructed spectra of intermediates are depicted in Figure 3.37.

The data for five well resolved intermediate states implies the low dependence of rate constants on the salt concentration – the relatively low dependencies are observed for K_A and K_B constants (A to B and B to C transfers respectively), while the rest transitions are quasi-independent. The recent studies on ClR and its mutants demonstrated, despite ClRs anion pumping functionality, the overall structure of active center similarity to that of KR2. Taking into account, that the sodium ions uptake and release proposed to occur during the first and last observed KR2 intermediates decays respectively, and the fact that the correspondent constants of PMr2 depend on the chloride concentrations implies similar anion transfer mechanism and thus the anion release seems to occurs during A→B, while uptake may occur during E→PMr2 (ground state).

The overall time of cycle vary depending on the temperature and changes from ~1 sec at 0°C to 60-80 ms at 50°C. The dependence of differential spectra of intermediates on salt concentration (at 20°C), as well as temperature dependencies at 0.5 M NaCl are given in Appendix (see Appendix Figure 1 and 2).

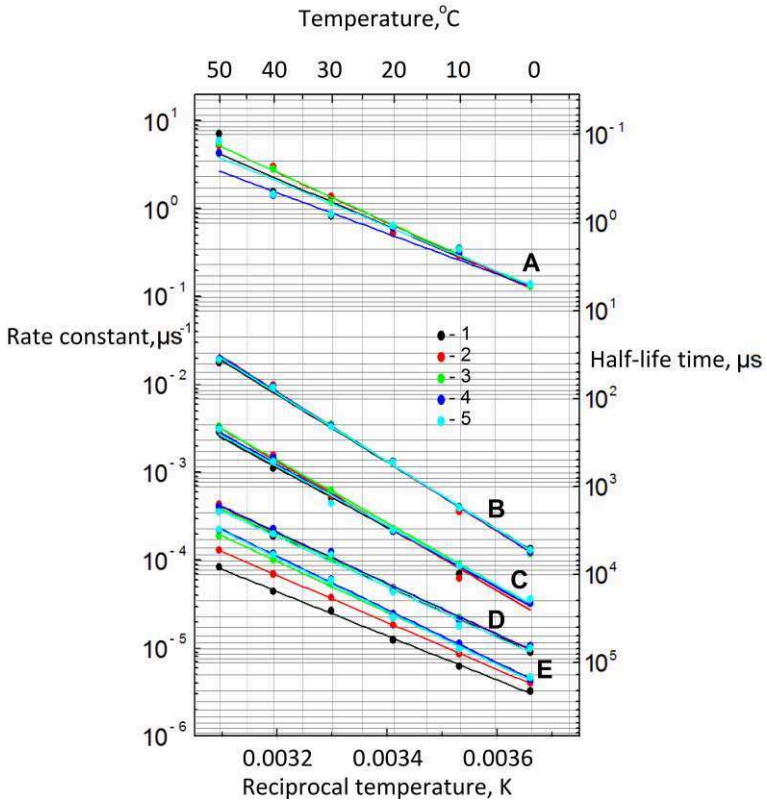


Figure 3.36 The $PMr2H_6$ intermediates half-life time and rate constants dependence on temperature and salt concentration. The intermediates are named A to E. The different colors depict different NaCl concentrations: 1(blue) - 0.1M, 2(red) - 0.2 M, 3(green) - 0.5 M, 4(blue) - 1 M, 5(light blue) - 2 M NaCl.

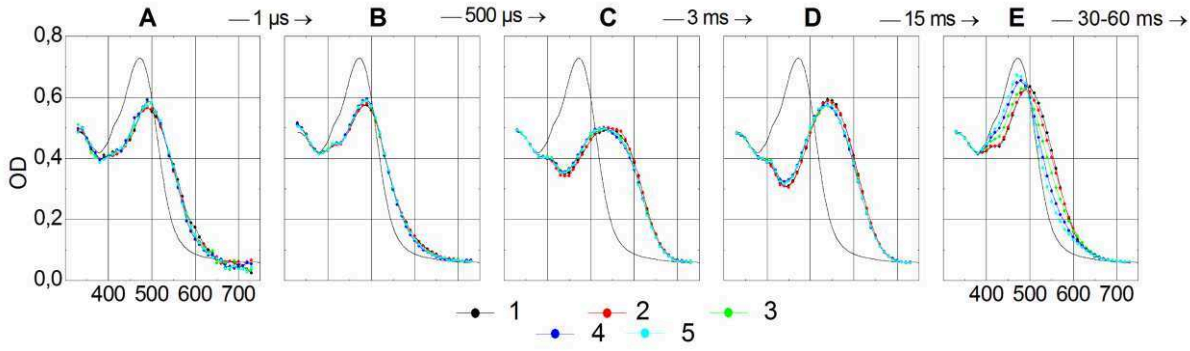


Figure 3.37 The reconstructed absorbance spectra of $PMr2H_6$ intermediates dependence on the NaCl concentrations. The different colors depict different NaCl concentrations: 1(black doted) - 0.1 M, 2(red) - 0.2 M, 3(green) - 0.5 M, 4(blue) - 1 M, 5(light blue) - 2 M NaCl. The ground spectrum depicted with thin black solid line.

3.3.3. Crystallisation of PMr2

The crystallization of PMr2 variants was performed in similar to PGr1 manner.

For initial crystallization conditions screenings the Cubic Phase I and Cubic Phase II precipitation solutions kits were applied. The protein for crystallization was purified as described before. The SEC fractions were taken and the absorbance spectra were measured to estimate the

peak ratio. Those fractions with PR <1.9 were pooled and concentrated using centrifugal filter with pore size of 10 kDa to a final protein concentration of 30-40 mg/ml. In all PMr2 crystallization trials the MO lipid was used with MO:protein = 1:2 ratio.

The screenings list presented in the table below:

Protein	$C_{protein}$ in phase, mg/ml	C_{DDM} came from protein, final %	Phase/Precipitate volumes, nl	Kit
$PMr2H_6$	20	4	150/800	CubicPhase I
$PMr2H_6$	20	4	100/800	CubicPhase II
$PMr2H_6$	17	4.5	150/500	CubicPhase I
$PMr2H_6$	17	4.5	150/500	CubicPhase II
$18PMr2H_6$	20	3	100/600	CubicPhase I
$18PMr2H_6$	20	3	100/600	CubicPhase II

Despite broad range of crystallization conditions used, no crystals were detected.

While the majority of HsHR/NpHR crystallization studies were performed with hanging drop vapor diffusion method/native membranes [91][65][10][8], the recently characterized ClR was crystallized using naonvolume *in meso* procedure, similar that in our disposal [69]. The methods applied to halorhodopsins differ significantly, but yet have one common and apparently key feature – the high Cl^- concentration. The Cubic Phase I kit doesn't contain any salt (the crystallization plate samples contain only the salt from protein buffer) and the Cubic Phase II kit contains 40 mM Cl^- (10 mM $MgCl_2$ and 10 mM $CaCl_2$), which seems to be insufficient (taking into account the 200-300 mM Cl^- concentration that was used in other studies; HsHR was reported to form crystals in presence of 3.3M KCl [65]).

In addition to chloride increase, the protein might be needed to be crystallized at low pH since at pH ~6 the additional peak corresponding to deprotonated RSB appears. That implies that two populations of protein emerge at higher pH reducing the effective crystal-forming protein concentration of the sample and making the protein in lipid phase less homogeneous.

References

[1] R. M. Bill *et al.*, “Overcoming barriers to membrane protein structure determination.,” *Nat. Biotechnol.*, vol. 29, no. 4, pp. 335–40, Apr. 2011.

[2] G. Nagel *et al.*, “Channelrhodopsin-1: a light-gated proton channel in green algae.,” *Science*, vol. 296, no. 5577, pp. 2395–8, Jun. 2002.

[3] G. Nagel *et al.*, “Channelrhodopsin-2, a directly light-gated cation-selective membrane channel.,” *Proc. Natl. Acad. Sci. U. S. A.*, vol. 100, no. 24, pp. 13940–5, Nov. 2003.

[4] S. Gao, J. Nagpal, M. W. Schneider, V. Kozjak-Pavlovic, G. Nagel, and A. Gottschalk, “Optogenetic manipulation of cGMP in cells and animals by the tightly light-regulated guanylyl-cyclase opsin CyclOp.,” *Nat. Commun.*, vol. 6, p. 8046, Sep. 2015.

[5] K. Inoue *et al.*, “A light-driven sodium ion pump in marine bacteria,” *Nat. Commun.*, vol. 4, p. 1678, Apr. 2013.

[6] I. Gushchin *et al.*, “Crystal structure of a light-driven sodium pump,” *Nat. Struct. Mol. Biol.*, vol. 22, no. 5, pp. 390–5, Apr. 2015.

[7] H. E. Kato *et al.*, “Structural basis for Na+ transport mechanism by a light-driven Na+ pump,” *Nature*, vol. 521, no. 7550, pp. 48–53, Apr. 2015.

[8] S. Kanada, Y. Takeguchi, M. Murakami, K. Ihara, and T. Kouyama, “Crystal Structures of an O-Like Blue Form and an Anion-Free Yellow Form of pharaonis Halorhodopsin,” *J. Mol. Biol.*, vol. 413, no. 1, pp. 162–176, 2011.

[9] M. Kolbe, H. Besir, L.-O. Essen, and D. Oesterhelt, “Structure of the Light-Driven Chloride Pump Halorhodopsin at 1.8 Å Resolution,” *Science (80-.).*, vol. 288, no. 5470, 2000.

[10] T. Kouyama, S. Kanada, Y. Takeguchi, A. Narusawa, M. Murakami, and K. Ihara, “Crystal structure of the light-driven chloride pump halorhodopsin from Natronomonas pharaonis.,” *J. Mol. Biol.*, vol. 396, no. 3, pp. 564–79, Feb. 2010.

[11] M. T. Facciotti, S. Rouhani, and R. M. Glaeser, “Crystal structures of bR(D85S) favor a model of bacteriorhodopsin as a hydroxyl-ion pump,” *FEBS Lett.*, vol. 564, no. 3, pp. 301–306, Apr. 2004.

[12] H. Luecke, “Atomic resolution structures of bacteriorhodopsin photocycle intermediates: the role of discrete water molecules in the function of this light-driven ion pump.,”

Biochim. Biophys. Acta, vol. 1460, no. 1, pp. 133–56, Aug. 2000.

[13] H. Kandori, "Ion-pumping microbial rhodopsins," *Front. Mol. Biosci.*, vol. 2, p. 52, Sep. 2015.

[14] J. P. Overington, B. Al-Lazikani, and A. L. Hopkins, "How many drug targets are there?," *Nat. Rev. Drug Discov.*, vol. 5, no. 12, pp. 993–6, Dec. 2006.

[15] M. Rask-Andersen, M. S. Almén, and H. B. Schiöth, "Trends in the exploitation of novel drug targets.," *Nat. Rev. Drug Discov.*, vol. 10, no. 8, pp. 579–90, Aug. 2011.

[16] H. Jhoti, A. R. Leach, C. A. Lepre, and J. M. Moore, "Structure-Based Drug Discovery," 2007. [Online]. Available: http://www.springerlink.com/content/h8257005k0601522/. [Accessed: 11-Feb-2016].

[17] A. B. Siemer, C. Ritter, M. Ernst, R. Riek, and B. H. Meier, "High-resolution solid-state NMR spectroscopy of the prion protein HET-s in its amyloid conformation.," *Angew. Chem. Int. Ed. Engl.*, vol. 44, no. 16, pp. 2441–4, Apr. 2005.

[18] L. Brocchieri and S. Karlin, "Protein length in eukaryotic and prokaryotic proteomes.," *Nucleic Acids Res.*, vol. 33, no. 10, pp. 3390–400, Jan. 2005.

[19] H. M. Berman *et al.*, "The Protein Data Bank.," *Nucleic Acids Res.*, vol. 28, no. 1, pp. 235–42, Jan. 2000.

[20] † Alberto Bartesaghi1,*, Alan Merk1,*, Soojay Banerjee1, Doreen Matthies1, Xiongwu Wu2, Jacqueline L. S. Milne1, Sriram Subramaniam1, "2.2 Å resolution cryo-EM structure of β-galactosidase in complex with a cell-permeant inhibitor," *Science (80-.).*, vol. Vol. 348, no. Issue 6239, pp. 1147–1151, 2015.

[21] "Method of the Year 2010," *Nat. Methods*, vol. 8, no. 1, pp. 1–1, Jan. 2011.

[22] News Staff, "Insights of the decade. Stepping away from the trees for a look at the forest. Introduction.," *Science*, vol. 330, no. 6011, pp. 1612–3, Dec. 2010.

[23] D. OESTERHELT and W. STOECKENIUS, "Rhodopsin-like Protein from the Purple Membrane of Halobacterium halobium," *Nature, Publ. online 29 Sept. 1971; | doi10.1038/10.1038/newbio233149a0*, vol. 233, no. 39, p. 149, 1971.

[24] A. E. BLAUROCK and W. STOECKENIUS, "Structure of the Purple Membrane," *Nature, Publ. online 29 Sept. 1971; | doi10.1038/10.1038/newbio233152a0*, vol. 233, no. 39, p. 152, 1971.

[25] D. M. Engelman and G. Zaccai, “Bacteriorhodopsin is an inside-out protein.,” *Proc. Natl. Acad. Sci. U. S. A.*, vol. 77, no. 10, pp. 5894–8, Oct. 1980.

[26] S. B. Hayward, D. A. Grano, R. M. Glaeser, and K. A. Fisher, “Molecular orientation of bacteriorhodopsin within the purple membrane of Halobacterium halobium.,” *Proc. Natl. Acad. Sci. U. S. A.*, vol. 75, no. 9, pp. 4320–4, Sep. 1978.

[27] R. Henderson and P. N. T. Unwin, “Three-dimensional model of purple membrane obtained by electron microscopy,” *Nature*, vol. 257, no. 5521, pp. 28–32, Sep. 1975.

[28] R. H. Lozier and W. Niederberger, “The photochemical cycle of bacteriorhodopsin.,” *Fed. Proc.*, vol. 36, no. 6, pp. 1805–9, May 1977.

[29] R. H. Lozier, W. Niederberger, R. A. Bogomolni, S. Hwang, and W. Stoeckenius, “Kinetics and stoichiometry of light-induced proton release and uptake from purple membrane fragments, Halobacterium halobium cell envelopes, and phospholipid vesicles containing oriented purple membrane,” *Biochim. Biophys. Acta - Bioenerg.*, vol. 440, no. 3, pp. 545–556, Sep. 1976.

[30] F. F. Litvin and S. P. Balashov, “[New intermediates in the photochemical transformation of rhodopsin].,” *Biofizika*, vol. 22, no. 6, pp. 1111–4.

[31] A. Matsuno-Yagi and Y. Mukohata, “Two possible roles of bacteriorhodopsin; a comparative study of strains of Halobacterium halobium differing in pigmentation,” *Biochem. Biophys. Res. Commun.*, vol. 78, no. 1, pp. 237–243, Sep. 1977.

[32] A. Matsuno-Yagi and Y. Mukohata, “ATP synthesis linked to light-dependent proton uptake in a red mutant strain of Halobacterium lacking bacteriorhodopsin,” *Arch. Biochem. Biophys.*, vol. 199, no. 1, pp. 297–303, Jan. 1980.

[33] R. V Greene and J. K. Lanyif, “Proton Movements in Response to a Light-driven Electrogenic Pump for Sodium Ions in Halobacterium halobium Membranes*,” vol. 254, no. 21, pp. 10986–10994, 1979.

[34] P. Hegemann, M. Steiner, and D. Oesterhelt, “Isolation and characterization of the retinal-binding component of halorhodopsin.,” *EMBO J.*, vol. 1, no. 10, pp. 1177–83, 1982.

[35] B. Schoberts and J. K. Lanyi, “Halorhodopsin Is a Light-driven Chloride Pump*,” *J. Biol. Chem.*, vol. 257, no. 17, pp. 10306–10313, 1982.

[36] R. A. Bogomolni and J. L. Spudich, “Identification of a third rhodopsin-like pigment in

phototactic Halobacterium halobium.," *Proc. Natl. Acad. Sci. U. S. A.*, vol. 79, no. 20, pp. 6250–4, Oct. 1982.

[37] J. L. Spudich and R. A. Bogomolni, "Mechanism of colour discrimination by a bacterial sensory rhodopsin.," *Nature*, vol. 312, no. 5994, pp. 509–13, 1984.

[38] P. Scherrer, K. McGinnis, and R. A. Bogomolni, "Biochemical and spectroscopic characterization of the blue-green photoreceptor in Halobacterium halobium.," *Proc. Natl. Acad. Sci. U. S. A.*, vol. 84, no. 2, pp. 402–6, Jan. 1987.

[39] H. Luecke, B. Schobert, H.-T. Richter, J.-P. Cartailler, and J. K. Lanyi, "Structure of bacteriorhodopsin at 1.55 Å resolution," *J. Mol. Biol.*, vol. 291, no. 4, pp. 899–911, Aug. 1999.

[40] J. Soppa, J. Duschl, and D. Oesterhelt, "Bacterioopsin, haloopsin, and sensory opsin I of the halobacterial isolate Halobacterium sp. strain SG1: three new members of a growing family.," *J. Bacteriol.*, vol. 175, no. 9, pp. 2720–6, May 1993.

[41] K. W. Foster and R. D. Smyth, "Light Antennas in phototactic algae.," *Microbiol. Rev.*, vol. 44, no. 4, pp. 572–630, Dec. 1980.

[42] K. W. Foster *et al.*, "A rhodopsin is the functional photoreceptor for phototaxis in the unicellular eukaryote Chlamydomonas.," *Nature*, vol. 311, no. 5988, pp. 756–9.

[43] P. Hegemann *et al.*, "From channelrhodopsins to optogenetics.," *EMBO Mol. Med.*, vol. 5, no. 2, pp. 173–6, Feb. 2013.

[44] F. Zhang *et al.*, "The Microbial Opsin Family of Optogenetic Tools," *Cell*, vol. 147, pp. 1446–1457, 2011.

[45] O. Yizhar, L. E. Fenno, T. J. Davidson, M. Mogri, and K. Deisseroth, "Optogenetics in Neural Systems," *Neuron*, vol. 71, no. 1, pp. 9–34, Jul. 2011.

[46] M. Müller, C. Bamann, E. Bamberg, and W. Kühlbrandt, "Projection Structure of Channelrhodopsin-2 at 6 Å Resolution by Electron Crystallography," *J. Mol. Biol.*, vol. 414, no. 1, pp. 86–95, Nov. 2011.

[47] H. E. Kato *et al.*, "Crystal structure of the channelrhodopsin light-gated cation channel," 2012.

[48] A. Inaguma *et al.*, "Chimeras of channelrhodopsin-1 and -2 from Chlamydomonas reinhardtii exhibit distinctive light-induced structural changes from channelrhodopsin-2.,"

J. Biol. Chem., vol. 290, no. 18, pp. 11623–34, May 2015.

[49] N. C. Klapoetke *et al.*, "Independent optical excitation of distinct neural populations," *Nat. Methods*, vol. 11, no. 3, pp. 338–346, Feb. 2014.

[50] J. Y. Lin, "A user's guide to channelrhodopsin variants: features, limitations and future developments," *Exp. Physiol.*, vol. 96, no. 1, pp. 19–25, Jan. 2011.

[51] 2 Joanna Mattis1,2,7, Kay M Tye1,7, Emily A Ferenczi1,2,7, Charu Ramakrishnan1, Daniel J O'Shea1,2, Rohit Prakash1 and 6 Lisa A Gunaydin1,2, Minsuk Hyun1, Lief E Fenno1,2, Viviana Gradinaru1,3, Ofer Yizhar1,4 & Karl Deisseroth1–3,5, "Principles for applying optogenetic tools derived from direct comparative analysis of microbial opsins."

[52] A. Berndt, S. Y. Lee, C. Ramakrishnan, and K. Deisseroth, "Structure-guided transformation of channelrhodopsin into a light-activated chloride channel.," *Science*, vol. 344, no. 6182, pp. 420–4, Apr. 2014.

[53] A. Berndt *et al.*, "Structural foundations of optogenetics: Determinants of channelrhodopsin ion selectivity.," *Proc. Natl. Acad. Sci. U. S. A.*, vol. 113, no. 4, 2016.

[54] E. G. Govorunova, O. A. Sineshchekov, R. Janz, X. Liu, and J. L. Spudich, "Natural light-gated anion channels: A family of microbial rhodopsins for advanced optogenetics," *Science (80-.).*, pp. 2–6, 2016.

[55] K. Inoue *et al.*, "A natural light-driven inward proton pump.," *Nat. Commun.*, vol. 7, p. 13415, Nov. 2016.

[56] K. Inoue *et al.*, "A light-driven sodium ion pump in marine bacteria.," *Nat. Commun.*, vol. 4, p. 1678, Jan. 2013.

[57] I. Gushchin *et al.*, "Crystal structure of a light-driven sodium pump," *Nat. Struct. Mol. Biol.*, no. April, 2015.

[58] E. Pastrana, "Optogenetics: controlling cell function with light," *Nat. Methods*, vol. 8, no. 1, pp. 24–25, Jan. 2011.

[59] D. Maclaurin, V. Venkatachalam, H. Lee, and A. E. Cohen, "Mechanism of voltage-sensitive fluorescence in a microbial rhodopsin.," *Proc. Natl. Acad. Sci. U. S. A.*, vol. 110, no. 15, pp. 5939–44, Apr. 2013.

[60] X. Han *et al.*, "A high-light sensitivity optical neural silencer: development and application to optogenetic control of non-human primate cortex.," *Front. Syst. Neurosci.*,

vol. 5, p. 18, 2011.

[61] J. K. Delaney, U. Schweiger, and S. Subramaniam, “Molecular mechanism of protein-retinal coupling in bacteriorhodopsin.,” *Proc. Natl. Acad. Sci. U. S. A.*, vol. 92, no. 24, pp. 11120–4, Nov. 1995.

[62] O. P. Ernst, D. T. Lodowski, M. Elstner, P. Hegemann, L. S. Brown, and H. Kandori, “Microbial and Animal Rhodopsins: Structures, Functions, and Molecular Mechanisms,” *Chem. Rev.*, vol. 114, no. 1, pp. 126–163, Jan. 2014.

[63] O. Kalisky, J. Feitelson, and M. Ottolenghi, “Photochemistry and fluorescence of bacteriorhodopsin excited in its 280-nm absorption band.,” *Biochemistry*, vol. 20, no. 1, pp. 205–9, Jan. 1981.

[64] S. P. Balashov, E. S. Imasheva, V. A. Boichenko, J. Antón, J. M. Wang, and J. K. Lanyi, “Xanthorhodopsin: a proton pump with a light-harvesting carotenoid antenna.,” *Science*, vol. 309, no. 5743, pp. 2061–4, Sep. 2005.

[65] W. Gmelin, K. Zeth, R. Efremov, J. Heberle, J. Tittor, and D. Oesterhelt, “The crystal structure of the L1 intermediate of halorhodopsin at 1.9 angstroms resolution.,” *Photochem. Photobiol.*, vol. 83, no. 2, pp. 369–77, 2007.

[66] J. Sasaki *et al.*, “Conversion of bacteriorhodopsin into a chloride ion pump.,” *Science*, vol. 269, no. 5220, pp. 73–5, Jul. 1995.

[67] J. B. Ames, J. Raap, J. Lugtenburg, and R. A. Mathies, “Resonance Raman study of halorhodopsin photocycle kinetics, chromophore structure, and chloride-pumping mechanism.,” *Biochemistry*, vol. 31, no. 50, pp. 12546–54, Dec. 1992.

[68] G. Váró, L. Zimányi, X. Fan, L. Sun, R. Needleman, and J. K. Lanyi, “Photocycle of halorhodopsin from Halobacterium salinarium.,” *Biophys. J.*, vol. 68, no. 5, pp. 2062–72, May 1995.

[69] K. Kim *et al.*, “Crystal structure and functional characterization of a light-driven chloride pump having an NTQ motif.,” *Nat. Commun.*, vol. 7, p. 12677, Aug. 2016.

[70] J.-H. Yoon, S.-J. Kang, S. Park, T.-K. Oh, and C. Jung-Hoon Yoon, “Reclassification of the three species of the genus Krokinobacter into the genus Dokdonia as Dokdonia genika comb. nov., Dokdonia diaphoros comb. nov. and Dokdonia eikasta comb. nov., and emended description of the genus Dokdonia Yoon et al. 2005.”

[71] H. Ono, K. Inoue, R. Abe-Yoshizumi, and H. Kandori, “FTIR Spectroscopy of a Light-Driven Compatible Sodium Ion-Proton Pumping Rhodopsin at 77 K,” *J. Phys. Chem. B*, vol. 118, no. 18, pp. 4784–4792, May 2014.

[72] I. Gushchin *et al.*, “Structure of the light-driven sodium pump KR2 and its implications for optogenetics,” *FEBS J.*, vol. 283, no. 7, pp. 1232–1238, Apr. 2016.

[73] K. Feldbauer, D. Zimmermann, V. Pintschovius, J. Spitz, C. Bamann, and E. Bamberg, “Channelrhodopsin-2 is a leaky proton pump.”

[74] C. T. Chung, S. L. Niemela, and R. H. Miller, “One-step preparation of competent Escherichia coli: transformation and storage of bacterial cells in the same solution.,” *Proc. Natl. Acad. Sci. U. S. A.*, vol. 86, no. 7, pp. 2172–5, Apr. 1989.

[75] F. W. Studier, “Protein production by auto-induction in high density shaking cultures.,” *Protein Expr. Purif.*, vol. 41, no. 1, pp. 207–34, May 2005.

[76] B.D.Hames, *Gel Electrophoresis of Proteins : A Practical Approach: A Practical Approach (Google eBook)*. 1998.

[77] Bollag D.M. and Edelstein S.J., *Protein methods*. 1991.

[78] T. K. Ritchie *et al.*, “Chapter Eleven – Reconstitution of Membrane Proteins in Phospholipid Bilayer Nanodiscs,” *Methods Enzymol.*, vol. 464, pp. 211–231, 2009.

[79] E. Bamberg, H.-J. Apell, N. A. Dencher, W. Sperling, H. Stieve, and P. Läuger, “Photocurrents generated by bacteriorhodopsin on planar bilayer membranes,” *Biophys. Struct. Mech.*, vol. 5, no. 4, pp. 277–292, Aug. 1979.

[80] “UniProt: the universal protein knowledgebase,” *Nucleic Acids Res.*, vol. 45, no. D1, pp. D158–D169, Jan. 2017.

[81] Y. Fukunaga, M. Kurahashi, Y. Sakiyama, M. Ohuchi, A. Yokota, and S. Harayama, “Phycisphaera mikurensis gen. nov., sp. nov., isolated from a marine alga, and proposal of Phycisphaeraceae fam. nov., Phycisphaerales ord. nov. and Phycisphaerae classis nov. in the phylum Planctomycetes.,” *J. Gen. Appl. Microbiol.*, vol. 55, no. 4, pp. 267–75, Aug. 2009.

[82] P. Simoneau, C. M. Li, S. Loechel, R. Wenzel, R. Herrmann, and P. C. Hu, “Codon reading scheme in Mycoplasma pneumoniae revealed by the analysis of the complete set of tRNA genes.,” *Nucleic Acids Res.*, vol. 21, no. 21, pp. 4967–74, Oct. 1993.

[83] M. Källberg *et al.*, “Template-based protein structure modeling using the RaptorX web server,” *Nat. Protoc.*, vol. 7, no. 8, pp. 1511–1522, Jul. 2012.

[84] I. Chizhov, G. Schmies, R. Seidel, J. R. Sydor, B. Lüttenberg, and M. Engelhard, “The photophobic receptor from Natronobacterium pharaonis: temperature and pH dependencies of the photocycle of sensory rhodopsin II.,” *Biophys. J.*, vol. 75, no. 2, pp. 999–1009, Aug. 1998.

[85] I. Chizhov, D. S. Chernavskii, M. Engelhard, K. H. Mueller, B. V Zubov, and B. Hess, “Spectrally silent transitions in the bacteriorhodopsin photocycle.,” *Biophys. J.*, vol. 71, no. 5, pp. 2329–2345, 1996.

[86] E. M. Landau and J. P. Rosenbusch, “Lipidic cubic phases: a novel concept for the crystallization of membrane proteins.,” *Proc. Natl. Acad. Sci. U. S. A.*, vol. 93, no. 25, pp. 14532–5, Dec. 1996.

[87] T. Nordahl Petersen, S. Brunak, G. von Heijne, and H. Nielsen, “SignalP 4.0: discriminating signal peptides from transmembrane regions,” 2011.

[88] M. J. (Milton J. Allen and International Symposium on Charge and Field Effects in Biosystems (3rd : 1991 : Virginia Commonwealth University), *Charge and field effects in biosystems--3*. Birkhäuser, 1992.

[89] K. Ihara and Y. Mukohata, “Proteoliposomes with right-side-out oriented purple membrane/bacteriorhodopsin require cations inside for proton pumping,” *FEBS Lett.*, vol. 240, no. 1–2, pp. 148–152, Nov. 1988.

[90] R. Tunuguntla, M. Bangar, K. Kim, P. Stroeve, C. M. Ajo-Franklin, and A. Noy, “Lipid Bilayer Composition Can Influence the Orientation of Proteorhodopsin in Artificial Membranes,” *Biophysj*, vol. 105, pp. 1388–1396, 2013.

[91] S. K. Chan *et al.*, “Crystal Structure of the 11- *cis* Isomer of *Pharaonis* Halorhodopsin: Structural Constraints on Interconversions among Different Isomeric States,” *Biochemistry*, vol. 55, no. 29, pp. 4092–4104, Jul. 2016.

[92] V. Gradinaru *et al.*, “Molecular and Cellular Approaches for Diversifying and Extending Optogenetics,” *Cell*, vol. 141, no. 1, pp. 154–165, 2010.

Appendix

PGr1 gene nucleotide sequence being used in this work:

ATGCCGCCGGGTTTTAGCTATGCAGAATGGAATGCAACCTATAATGCACTGTTTGGTATTGCAGCAA
TGGGTAGCGCAACCATCTTTTTTTGGCTGCAGCTGCCGAATGTTACCAAAAACTATCGTACCGCACTGAC
CATTACCGGTATTGTTACCCTGATTGCCACCTATCATTATATCCGCATTTTTAACAGTTGGAGCGAAGCATT
TACCGTTGCAAGCAAAGATGGTGGTGATTATACCGTGCAGCTGACAGGTGCACCGTTTAATGATGGTTAT
CGTTATGTTGATTGGCTGCTGACCGTTCCGCTGCTGCTGATTGAACTGATTCTGGTTATGAAACTGCCGC
AGGCAGAAACCGTTAATCTGAGCTGGAAACTGGGTCTGGCAAGCGCACTGATGGTTGCACTGGGTTAT
CCGGGTGAAATTCAAGAAGATCTGAGCGTTCGTTGGTTTTGGTGGTGTCTGAGCATGATTCCGTTTTGCT
ATGTTGTTTTTACCCTGGCAGTTGGTCTGGCAGAAGCAACCAGCAAACAGCCGAGTCCGGCAGCAGCA
AGCCTGGCCAGCGCAGCACGTTATCTGACCGTGCTGAGCTGGTGTACCTATCCGTTTGTTTATATGGTTA
AAAGCGTTGGCCTGGCAGGTCCTGCAGCAACCATGTATGAACAGGTTGGTTATAGCCTGGCCGATGTTC
TGGCAAAAGCCGTTTTTGGTGTTCTGATTTGGGCAATTGCAGCAGAAAAAAGCGCAGTTGAAGAAAGC
GGTAAACTGCTGCCGAAA

PMr1 gene nucleotide sequence being used in this work:

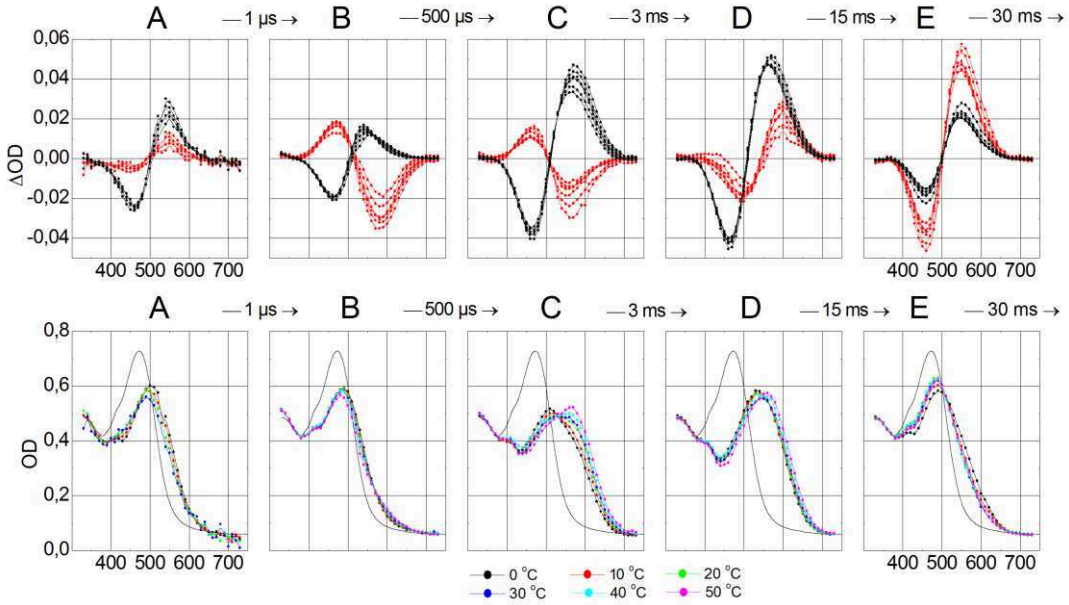
ATGCTGAGCAGCAGTCCGCTGCTGGCACAGGCACTGAGCGCAGCACCGCTGGCAGATGGTGAAA
GCGCAGTTAATCTGCATCACATGGCAAATTGGTTTGCATATACCCCGATGCAGTATCAGAGCGTTCTGCA
TGTTTTTACCCTGGGTTATGGTGTTTTTGCAGCAGCACTGGTTTTTTTCATTCTGACCCTGCGTAAAAGCC
ATGATCGTTTTCAGCTGAGCAGTGTTATTAGCTGTGTTGTTACCATTAGCGCAGGTCTGATTCTGTATCAT
CAGAGCAGCGTTTGGGAAAATGCCTTTGTTTTTAATGAAGCCACCGGTATGTATGAACGTATTGAAGGTC
GTCTGTTTAGCAATGGTTTTCGCTATATGAACTGGATGATTGATGTTCCGAATCTGCTGCTGAGTATGCTG
GTTCTGCTGCCTCTGGCAGGCGCAGCACGTAGCAATATTACCAAATGGGGTGCACAGTTTGTTGTTGCA
GGTCTGGTGATGGTTTTTTGTAGCTGGCTGGGTAGCTTTTGGGAACAGGGTCAGCATGTTGCCGGTCGT
GGCACCTTTTGGTTTTGGGTTAATTATCTGATTGGTTGGGTTGCCTATGTTTGGATTCTGGTTGTTGTTTG
GCAGGTTATTAATGCCGGTCTGGAAGTTCTGCCGGAACGTAGCGCAAAACTGCTGCGTACCATTCGCAC
CATTTTTCTGATTAGCTGGACCGTTTATGCCTTTACACTGGTTCAGCCGCTGTTTTGGTGGTCACCGGTTA
GCGTTGTTACCCGTCAGTTTCTGTTTACTCTGGCAGATATTACCAGCAAAGCAATTTATGGTGTGCTGCT
GGCCACCATTGGTTTCCAGCTGACCGATGAATTTGCAGCACGTGGTGAAAATCAGAGCAAACTGACCG
CAAGCGGTGAACCGGCACATGCCGAAGCA

PMr2 gene nucleotide sequence being used in this work:

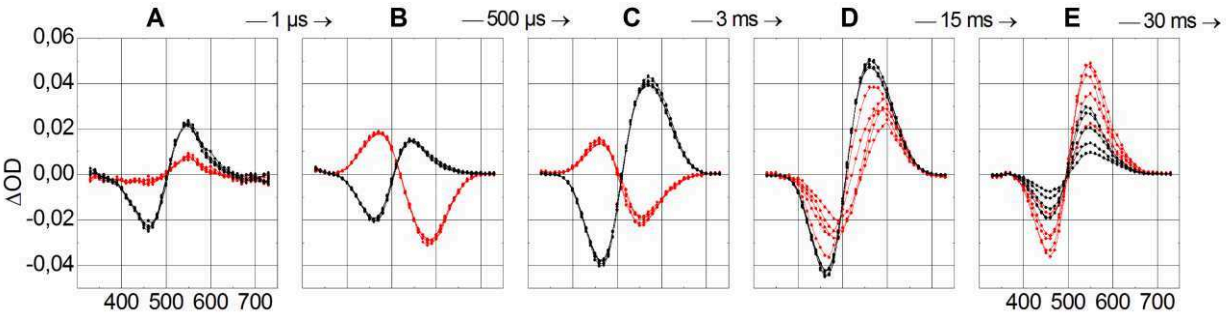
ATGCCGATTGCACTGACCACCCTGGCAGCAGTTGGTCAGCTGCATAATATGGAAAACTTTTTCAGC
TATACACCGGGTCAGCATTTTGCAATTAGCCAGATTCTGACCTTTGGTTATGGTTGTTTTCTGGCAAGCCT
GATCTATTTTCTGCTGACCCTGACCAGCATTCCGCCTCGTTATCGTCTGGCAGGTATTCTGAGCTGTTGTG
TTGCAGCAACCGCAGGTTTTATTCTGTATCATGAAACCCGTTATTGGCAGCAGACCTTTGTGTATGATAG
CCTGAGCGGTCTGTTTGTTCGTCGTCCGGATCAGATGTATAGCAATGGTTATCGTTATGTGAATTGGGCAA
TTACCGTTCCGCTGCTGCTGATGACCCTGATGGTTGTTATTCCGCTGGCACATGCAGCAAAACGTCAGA
AAGCAGCACGTCGTCTGGTTATTTTTGGTGTTAGCATGGTTTTTTGTAGCTGGGTGGGTGGTTTTTTTGA
AGCAGATGGTCATACCGAAGGTGGTAATCTGCTGGGTTTTTGGTTTAGTTATCTGCTGGGCTGGGTGTTT
TATGTTCTGCTGCTGATGCAGGTTTTTGCCGTTATTGGTGAAGGCCAGAAACATGTTAGCGCAGAAGCA
GGTAAACTGCTGCGTTGCCTGCTGGGTCTGTTTCTGGTTAGCTGGACCATTTATGCATTTGTGCTGCTGC
AGCCGCTGTTTTGGTGGTCACCGACCAGCGTTGTTGTTCGTCAGGCACTGTTTACCATTGCAGATGTTAG
CAGCAAAGCCGTTTATGGCATTCTGATGGGTCGTCTGGCCGTTCGTGTTGCCGATGGTAGCAGCGGTCT
GCCGAATGCATATCGTAGCCTGGCAAAAAGCCGTGAACAGACACATGCAAGCGGTGGTAGTGATGTTG
GTGTTCCGGCAGTGGAAACCCGTAATGAAGCACCGGCA

Time, min	After ind., h	Sample No.	0.1mM 0.8AU	0.2mM 0.8AU	0.5mM 0.8AU	After ind., h	Sample No.	0.1mM 1.0AU	0.2mM 1.0AU	0.5mM 1.0AU	After ind., h	Sample No.	0.1mM 1.2AU	0.2mM 1.2AU	0.5mM 1.2AU	After ind., h	Sample No.	0.1mM 1.5AU	0.2mM 1.5AU	0.5mM 1.5AU	After ind., h	Sample No.	0.1mM 2.5AU	0.2mM 2.5AU	0.5mM 2.5AU
0			0.200	0.200	0.200			0.200	0.200	0.200			0.200	0.200	0.200			0.200	0.200	0.200			0.200	0.200	0.200
60			0.293	0.293	0.293																				
120			0.385	0.385	0.385																				
210			0.698	0.698	0.698																				
232			0.744	0.744	0.744																				
240	0.0		0.800	0.800	0.800																				
252						4.2		0.993	0.993	0.993															
264													0.870	0.963	1.026										
289													0.984	1.084	1.134			1.022	1.068	1.082					
312	1.2	1	1.014	1.017	0.999	5.2	1	1.104	1.086	1.062	0.0		1.098	1.182	1.227				1.203						
325																			1.244						
336																			1.407						
345																5.8		1.338	1.395	1.383					
353																								1.435	
372	2.2	2	1.089	1.119	1.108	6.2	2	1.224	1.032	1.113	1.0	1	1.356	1.383	1.392										
405																6.8	1	1.653	1.680	1.608			1.796		
440	3.3	3	1.203	1.188	1.140	7.3	3	1.138	1.308	1.224	2.1	2	1.446	1.794	1.545	7.3	2	1.575	1.680	1.647			2.128		
462																							2.128		
505	4.4	4	1.372	1.264	1.320	8.4	4	1.512	1.452	1.312	3.2	3	1.732	1.696	1.816	8.4	3	1.872	1.984	1.988	0.0		2.508	2.320	2.612
615	6.3	5	1.440	1.332	1.398	10.3	5	1.596	1.596	1.456	5.1	4	1.784	1.784	1.840	10.3	4	1.948	1.980	1.964	1.8	1	2.788	2.496	2.704
670											6.0	5	1.780	1.748	1.844	11.2	5	1.952	2.000	1.956	2.8	2	2.820	2.508	2.744
1385	19.1	6	1.415	1.068	1.210	23.1	6	1.235	1.160	1.190	17.9	6	1.360	1.540	1.650	23.1	6	1.940	2.060	2.010	14.7	3	2.555	2.175	2.655

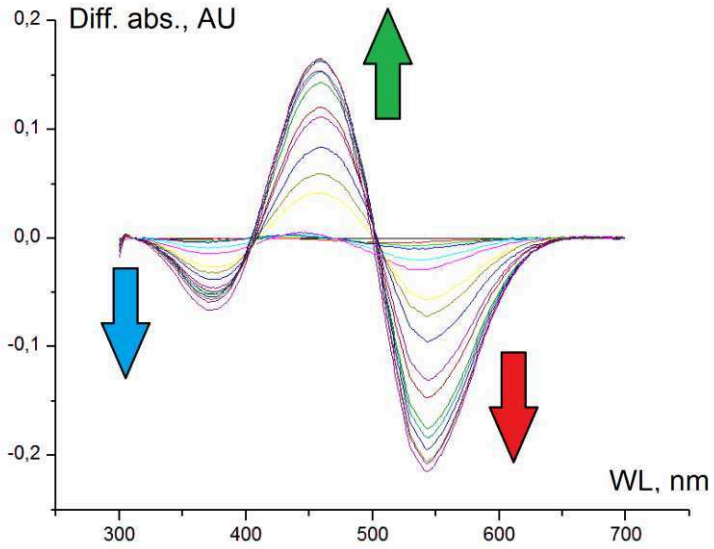
Appendix table 1. The OD_{600} data of the IPTG induced culture SE1 pSC-PGr1eoH6 strain samples (see 3.2.1, p.58). Blue boxes represent OD_{600} of IPTG injection. The orange boxes - the time/culture density when samples being taken.



Appendix Figure 1. The $PMr2H_6$ photocycle temperature dependence (0-50°C) in presence of 0.5 M NaCl. The intermediates are named A to E. After E state $PMr2H_6$ returns back to the ground state. The upper boxes represent amplitude spectra of five exponential components (in red) and corresponding difference spectra of the A-E intermediates vs. ground state spectrum of $PMr2H_6$ (black). Depicted time constants correspond to 20°C. In the lower row the derived absorption spectra of intermediates A-E are depicted. The ground spectrum of $PMr2H_6$ depicted with solid black line.



Appendix Figure 2. The $PMr2H_6$ NaCl concentration (0.1, 0.2, 0.5, 1, and 2 M of NaCl) dependence at 20°C. The intermediates are named A to E. After E state $PMr2H_6$ returns back to the ground state. The amplitude spectra of five exponential components depicted in red, while corresponding difference spectra of the A-E intermediates (in respect to ground spectrum of PMr2) depicted in black. The half-life time constants correspond to 0.5 M NaCl concentration.



Appendix Figure 3. The PMr2H6 differential absorbance spectra at pH 7.0, 20°C in presence of different NaCl concentrations (see 3.3.2.4). The arrows indicate the direction of absorbance change with NaCl concentration increase. The most of the difference observed at 375 nm (blue arrow), 460 nm (green arrow) and 550 nm (red arrow).

Acknowledgements

I am very grateful to Prof. Dr. Valentin Gordeliy for supervising this PhD project and for offering me the opportunity to work on this exciting project in the highly stimulating and encouraging atmosphere.

It would be hard to specify the people who helped the most, since I was working in a highly experienced team of investigators, where each person taught me lots of things not only in terms of experiments performance, but also in the way of thoughts that should be applied to the results of these experiments to make the right conclusions.

I highly appreciate the help of Dr. Taras Balandin and Dr. Oleksandr Volkov, who significantly helped me in caring out expression and purification experiments and taught me basics of molecular biology. I thank them very much for their support, for the constructive discussions and especially their questions that allowed me to get the right direction in my work. The special thanks should and was said to Alexander and Taras for the proofreading of the draft of this dissertation and their comments and remarks on this point.

I appreciate very much the help of my colleagues and, at the same time, friends in Research Centre Juelich: Anastasia Yuzhakova, Vitaly Shevchenko, Dr. Dmitry Bratanov, Christian Baeken, Aleksey Alekseev and Kirill Kovalev. Discussions with them helped me to see my mistakes and to reconsider some obtained results.

A significant part of this work was carried out in cooperation with the laboratory of membrane protein structural studies in IBS, Grenoble. All the *in meso* crystallization trials were done there, while the crystals diffraction was measured at ESRF with assistance of Igor Melnikov.

I'm also grateful to Dr. Thomas Gensch who helped me with performance of fluorescence life time determination measurements.

The help and the knowledge obtained from Dr. Igor Chizhov (Institute for Biophysical Chemistry, Hannover Medical School) upon time-resolved laser spectroscopy measurements and data treatment couldn't be overestimated. The work with him was a pleasure and brought incredible results. I do honestly hope to perform more experiments and discuss the results with Dr. Chizhov in the future.

I’m grateful to Prof. Dr. Dieter Willbold for the opportunity to work at and ICS-6 in Research Centre Jülich.

And finally I want to thank my parents and again to my brother. I thank them to have encouraged me all along these studies. I thank them for what they brought me, for their unconditional support and their belief in me.

Abstract

The proteins can be divided into the two major types in terms of the cell localization: membrane proteins and non-membrane proteins. Membrane proteins typically constitute about third of all proteins that cell expresses in a given moment and play important role in a cell's life. So, the membrane protein receptors mediate information flow from the environment into the cell modulating the cell mechanisms in response to the environmental changes. Another type of membrane proteins - the transport proteins - allow cells to communicate by means of signaling molecules and receive necessary nutrients from the environment.

The vast studies led to a new method being called the optogenetics. This new approach utilizes the light to control cells in a living tissue. The key elements of this method are the membrane light sensitive proteins that work as the "function switches". And the majority of such "switches" belongs to the rhodopsins. Unlike direct neuron excitation methods via electrodes, the optogenetic approach is less invasive. The rhodopsin gene is injected into the cell allowing latter to express the rhodopsin and to embed it into the membrane the same way as its endogenous proteins. After the injection cell becomes light-sensitive and can be manipulated just with the visible light impulses.

The rhodopsins are known for a while and estimated to consist of two major types: microbial rhodopsins (type I) and mammalian rhodopsins (type II). Despite the common name (rhodopsin, derived from Greek for "rose" and "sight"), mammalian rhodopsins significantly differ from those in microorganisms - they belong to a large class of proteins called GPCRs, while their microbial analogues don't. Due to the differences in mechanisms of function, microbial rhodopsins are simpler thus are more convenient to use in the neuroscience.

The optogenetics uses rhodopsins to investigate the cells' mechanisms and their interaction within the tissue. But each protein has its own characteristics and there's no ideal "instrument" for all the applications – each experiment requires the specific "tools" (rhodopsins) with different properties for optogenetic investigations. So, one experiment requires fast quenching of neuronal cells signaling thus having no particular requirements to a long-term behavior of the protein, while in the other experiment investigator may use rhodopsins with slow kinetics, but requires the moderately high steady-state signal during the long-term illumination. The large diversity of possible optogenetic applications requires the expansion of a "tool-kit", which in turn leads to a characterization of the new rhodopsins.

The most abundantly used rhodopsins in optogenetics are channels (ChRs, derived from channel rhodopsins). These channels provide a light-modulated passive transport of ions along the gradient, which leads to a neuronal membrane depolarization. The other proteins type being applied is microbial pumping rhodopsins (the sensory rhodopsins despite being reported to be successfully applied need further characterization). The microbial pumping rhodopsins can be divided into two major groups: cation pumps and anion pumps. The first includes sodium pumps and proton pumps. The optogenetic application of latter is still disputed due to their ability to directly change the pH, while first posses low selectivity/overall poor performance. Thus, halorhodopsins (anion pumping rhodopsins, HRs), despite the debates on their ability to hyperpolarize membrane beyond the physiological levels, are more common membrane repolarizating rhodopsins.

The main goal of this work was to expand the list of rhodopsins that might be used as the membrane repolarization tools in terms of optogenetic. The genes of non-characterised before rhodopsins were optimised and the optimal conditions for rhodopsins expression in *E.coli* expression system were estimated. The positive results of expression trials of these membrane proteins were as well demonstrated for relatively new LEXSY expression system.

The two new rhodopsins PGr1 and PMr2 were expressed in *E.coli* and characterised from kinetic point of view. The model of unidirectional transitions cycle was proposed. The functional activity of a novel anion pump with significantly shifted into the blue light region (in compare to the reported halorhodopsins) was demonstrated as well as the pumping activity of a new proton-pumping rhodopsin was proven.

Along with functional characterisation, the importance of few structural features of novel anion pump was shown. The crystals of proton pump were obtained and the crystallisation trials for both the proton pump and anion pump are still going.

Abstrakt

Proteine können in zwei Hauptarten der Zelllokalisation aufgeteilt werden: Membranproteine und Nicht-Membranproteine. Membranproteine machen etwa ein Drittel aller Proteine aus, die zu einer gegebenen Zeit in den Zellen exprimiert werden, und spielen eine wichtige Rolle im Leben einer Zelle. Membranproteinrezeptoren vermitteln den Informationsfluss von der äußeren Umgebung in die Zelle und modulieren somit die Zellmechanismen bei sich ändernden äußeren Bedingungen. Eine andere Art der Membranproteine – Transporter Proteine – ermöglicht es den Zellen mittels Signalmolekülen zu kommunizieren und so notwendige Nährstoffe aus der Umgebung zu erhalten.

Im Rahmen umfangreicher Studien wurde eine neue Methode namens Optogenetik entwickelt. Diese neue Herangehensweise ermöglicht es Zellen in lebendem Gewebe mittels Licht zu kontrollieren. Das Schlüsselelement dieser Methode sind lichtsensitive Membranproteine, die als Funktionsschalter dienen. Die Mehrheit dieser Schalter bilden die sogenannten Rhodopsine. Anders als die direkte Neuronen Anregung mit Elektroden ist die Optogenetik weniger invasiv. Das Rhodopsin-Gen wird dabei in die Zelle injiziert, die dann das Rhodopsin exprimiert und es auf dieselbe Art und Weise in die Zellmembran einbaut wie seine anderen endogenen Proteine. Nach erfolgter Injektion wird die Zelle selbst lichtsensitiv und kann mittels Lichtimpulsen manipuliert werden.

Rhodopsine werden im Allgemeinen in zwei Klassen unterteilt: die mikrobiellen Rhodopsine (type I) und die Säuger-Rhodopsine (type II). Trotz des gemeinsamen Namens unterscheiden sich Säuger-Rhodopsine in signifikanter Weise von den mikrobiellen Rhodopsinen. Sie gehören zu der großen Klasse der GPCR- Proteine, was nicht auf die mikrobiellen Rhodopsine zutrifft. Aufgrund von Unterschieden bei Funktionsmechanismen sind die einfacheren mikrobiellen Rhodopsine leichter in den Neurowissenschaften nutzbar.

Die Optogenetik nutzt Rhodopsine um Zellmechanismen und deren Interaktion mit dem Gewebe zu untersuchen. Aber jedes Protein hat seine eigenen Charakteristika und es gibt kein ideales „Instrument“ für alle Anwendungen. Jedes Experiment erfordert ein spezifisches „Tool“ (Rhodopsin) mit unterschiedlichen Eigenschaften für optogenetische Untersuchungen. Dies kann zum Beispiel ein schnelles Unterbinden einer zellulären Signaltransduktion sein, wobei es hier keine konkreten Anforderungen an das Langzeit-Verhalten des Proteins gibt. Ein anderes Experiment kann ein Rhodopsin mit vergleichsweise langsamen kinetischen Eigenschaften benutzen, das aber stationär starke Signale während langer Belichtungsphasen braucht. Die große

Diversität möglicher optogenetischer Anwendungen erfordert die Entwicklung eines „Tool-Kits“ mit dem die Charakterisierung neuer Rhodopsine einhergeht.

Die am häufigsten genutzten Rhodopsine in der Optogenetik sind Kanäle (ChRs, abgeleitet von Channel Rhodopsin). Diese Kanäle ermöglichen einen licht-modulierten, passiven Transport von Ionen entlang eines Gradienten, der zu einer Neuronen-Membran-Depolarisation führt. Der andere Proteintyp, der in der Optogenetik Anwendung findet, ist eine mikrobielle Rhodopsin-Pumpe (Sensor Rhodopsine benötigen trotz erfolgreicher Anwendung weitere Charakterisierungen). Die mikrobiellen Rhodopsin-Pumpen können in zwei Hauptgruppen unterteilt werden: Kationen- und Anionen-Pumpen. Zu der ersten Gruppe gehören Natrium – und Protonenpumpen. Die optogenetischen Anwendungen von Protonenpumpen werden aktuell noch diskutiert, da hier direkt Einfluss auf den pH-Wert genommen werden kann, wohingegen Natriumpumpen hier nur eine geringe Selektivität zeigen und insgesamt eine geringe Leistungsfähigkeit haben. Die Rhodopsine, die in der Regel für eine Membranrepolarisation genutzt werden sind Halorhodopsine (Anionenpumpen-Rhodopsine, HRs), obwohl deren Eigenschaften eine Hyperpolarisation an der Membran herbeizuführen weiterhin diskutiert wird.

Das Hauptziel dieser Arbeit war es die Liste an Rhodopsinen, die als Membran-Repolarisations-Tool in der Optogenetik in Frage kommen, zu erweitern. Die Gene vorher nicht charakterisierter Rhodopsine wurden optimiert und optimale Bedingungen für eine Rhodopsinexpression in *E.coli* Expressionssystemen wurden abgeschätzt. Positive Expressions-Ergebnisse dieser Membranproteine wurden auch in dem vergleichsweise neuen LEXSY-Expressionssystem gezeigt.

Zwei Rhodopsine (PGr1 und PMr2) wurden in *E.coli* exprimiert und kinetisch charakterisiert. Ein Modell mit einem einfach gerichteten Transitionskreis wurde vorgeschlagen. Die funktionale Aktivität einer neuen Anionpumpe mit einer signifikanten Verschiebung in den Blaulichtbereich (im Vergleich zu bekannten Halorhodopsinen) wurde demonstriert. Weiterhin wurde die Pumpaktivität einer neuen Rhodopsin-Protonenpumpe gezeigt.

Neben der funktionalen Charakterisierung wurde die Bedeutung einiger strukturellen Änderungen in der neuen Anionenpumpe gezeigt. Kristalle der Protonenpumpe konnten gewonnen werden und weitere Kristallisationsexperimente mit sowohl der Protonenpumpe als auch der Anionenpumpe werden aktuell durchgeführt.